PRACA DOKTORSKA

http://rcin.org.pl



Droplet microfluidics in biochemistry and in microbiology

Tomasz S. Kamiński

Advisor: Prof. dr hab. Piotr Garstecki

The dissertation was prepared within the International PhD Studies at the

Institute of Physical Chemistry of the Polish Academy of Sciences

ul. Kasprzaka 44/52, 01-224 Warsaw

Biblioteka Instytutu Chemii Fizycznej PAN

F-B.484/16

90000000192784

Warsaw, January 2016

A-21-7, A-21-10, K-g-160, K-g-161, K-g-176, K-f-137

http://rcin.org.pl

Instytut Chemii Fizycznej PAN
BIBLIOTEKA
B. 484/16

http://rcin.org.pl

Acknowledgements

First and foremost, I would like to express my gratitude to prof. Piotr Garstecki for giving me the opportunity to work in his laboratory and for introduction to the world of amazing microdroplet technologies. I also thank Piotr for advices, fruitful exchange of ideas, freedom and trust that were essential to tackle diverse and challenging research projects.

I am very grateful for brilliant researchers who were my co-workers during my doctoral projects:

- Magda Czekalska for her contribution in the droplet interface bilayers project.
- Sławek Jakieła for the fruitful collaboration in droplet microchemostat project and for the precious help in other experiments requiring automation.
- Laci Derzsi for his input and ideas in the projects concerning passive droplet microfluidics.

I would like to acknowledge foreign collaborators:

- prof. Douglas Weibel from University of Wisconsin Madison for the help with interpretation of results of microbiological experiments.
- prof. Hagan Bayley and dr Tanuj Sapra from Oxford University for hosting me in their laboratory and introduction to the techniques of droplet interface bilayers and electrophysiology.

My warmest thanks to the current and former members of the Group of Microfluidics and Complex Fluids and the Department of Soft Condensed Matter for their help and interesting scientific discussions. I especially thank Joanna Smyda, Paweł Dębski, Witek Postek, Piotr Korczyk, Łukasz Kozoń, Olgierd Cybulski, Adam Opalski, Tomek Kalwarczyk, Piotr Pawlicki and Bogdan Dąbrowski.

Thank you Magda for being a special person in my life, for your support and inspiration throughout last years.

Chciałbym szczególnie serdecznie podziękować moim Rodzicom za trud wychowania i edukacji oraz za wsparcie i wyrozumiałość w czasie moich studiów doktoranckich.

http://rcin.org.pl

Acknowledgments for funding

The research presented in this dissertation was supported by the following projects:

1) VENTURES/2012-10/4 *"New technologies for high-throughput screening of lipid bilayers and membrane proteins"* within VENTURES Programme of Foundation for Polish Science, co-financed by the European Union within the European Regional Development Fund, through the Innovative Economy Operational Programme (Measure 1.2 *"Strengthening the human resources potential of science"*).



2) Author obtained the funds for the preparation of the doctoral dissertation from the National Center for Science within the scholarship on the basis of the decision number DEC-2014/12/T/ST4/00649.



3) Author was supported by Foundation for Polish Science through START Stipend (twice: agreements no 47.2013 and 47.2014).



4) Author was supported by Ministry of Science and Higher Education through the scholarship for outstanding young researchers (agreement 0722/E-64/STYP/10/295).



http://rcin.org.pl

5) Research was co-funded by TEAM/2008-1/1 project *"Droplet Microfluidics: Fundamentals and Applications"* within TEAM Programme of Foundation for Polish Science, co-financed by the European Union within the European Regional Development Fund, through the Innovative Economy Operational Programme.

6) Research was co-funded by Starting Grant 279647 *"Microfluidic Combinatorial on Demand Systems: a Platform for High-Throughput Screening in Chemistry and Biotechnology"* financed by European Research Council.

7) This work was partially performed in the NanoFun laboratories co-financed by the ERDF Project POIG.02.02.00-00-025/09.

http://rcin.org.pl

List of publications and patent applications

Publications related to the topic of the dissertation:

1) **T. S. Kaminski**, S. Jakiela, M. Czekalska, W. Postek P. Garstecki. *Automated and rapid generation of libraries of nL droplets.* Lab on a Chip 2012, 12, 3995-4002 (IF_{2011}=5,670).
2) **T. S. Kaminski**, K. Churski, P. Garstecki. *Automated droplet microfluidic chips for biochemical assays* - chapter in: *Microdroplet technology and microfluidics: principles, components, and emerging applications in biology and chemistry*. Editors: P.Day, A. Manz, Y. Zhang. Springer 28 July 2012 ISBN: 978-1461432647.
3) S. Jakieła*, **T. S. Kamiński*** **(*equal contribution)**, O. Cybulski, D.B. Weibel, P. Garstecki. *Bacterial growth and adaptation in microdroplet chemostats*. Angewandte Chemie Int. Ed., 2013, 52, 8908-8911 (IF_{2012}=13,734).
4) M. Czekalska*, **T. S. Kaminski*** **(*equal contribution)**, S. Jakiela, K. T. Sapra, H. Bayley, P. Garstecki. *A droplet microfluidic system for sequential generation of lipid bilayers and transmembrane electrical recordings.* Lab On a Chip, 2015, 15, 541-548 (IF_{2013} = 5,748).
5) L. Derzsi*, **T. S. Kaminski*** **(*equal contribution)**, P. Garstecki. *Antibiograms in five pipetting steps: precise dilution assays in sub microliter volumes with a conventional pipette*. Submitted to Lab on a Chip, under review.
6) **T. S. Kaminski**, W. Postek, P.R. Debski P. Garstecki. *Droplet digital PCR with extended dynamic range.* In preparation.

Other publications:

7) S. Hou, N. Ziębacz, T. Kalwarczyk, **T. S. Kaminski**, S.A. Wieczorek, R. Holyst. *Influence of Nano-viscosity and Depletion Interactions on Cleavage of DNA by Enzymes in Glycerol and Poly(ethylene) Glycol Solutions: Qualitative Analysis*. Soft Matter, 2011, 7, 3092-3099 (IF_{2010}=4,457).
8) S. Hou, N. Ziębacz, S.A. Wieczorek, E. Kalwarczyk, V. Sashuk, T. Kalwarczyk, **T. S. Kaminski**, R. Holyst. *Formation and structure of PEI/DNA complexes: quantitative analysis.* Soft Matter, 2011, 7, 6967-6972 (IF_{2010}=4,457).
9) K. Churski, **T. S. Kaminski**, S. Jakiela, W. Kamysz, W.Baranska-Rybak, D. B. Weibel, P. Garstecki. *Rapid screening of antibiotic toxicity in an automated microdroplet system.* Lab On a Chip, 2012, 12, 1629 - 1637 (IF_{2011}=5,670).
10) S. Hou, S. A. Wieczorek, **T. S. Kaminski**, N. Ziebacz, M. Tabaka, N. A. Sorto, M. H. Foss, J. T. Shaw, M. Thanbichler, D. B. Weibel, R. Holyst, P. Garstecki. *Characterization of Caulobacter crescentus FtsZ using dynamic light scattering.* Journal of Biological Chemistry, 2012, 287, 23878-23886 (IF_{2011}=4,773).
11) S. Hou, L. Sun, S. A. Wieczorek, T. Kalwarczyk, **T. S. Kaminski**, R. Holyst. *Accurate determination of proportion of doubly labeled DNA in fluorescent DNA pool by*

http://rcin.org.pl

fluorescence correlation spectroscopy for quantitative biochemical assays. Biosensors and Bioelectronics 2014, 51, 8-15 (IF_{2013}=6,451).

12) S. Hou, M. Tabaka, L. Sun, P. Trochimczyk, **T. S. Kaminski**, T. Kalwarczyk, X. Zhang, R. Holyst. *A Flexible Fluorescence Correlation Spectroscopy Based Method for Quantification of the DNA Double Labeling Efficiency with Precision Control*. Laser Physics Letters, 2014, 11, 085602 (IF_{2013}= 2,964).
13) P. Debski, K. Gewartowski, M. Sulima, **T. S. Kaminski**, P. Garstecki. *Rational design of digital assays*. Analytical Chemistry, 2015, 87, 8203–8209 (IF_{2014}=5,636).
14) O. Scheler, **T. S. Kaminski**, A. Ruszczak, P. Garstecki. *Dodecylresorufin (C12R) outperforms resorufin in micro-droplet bacterial assays.* Submitted to Lab on a Chip, under review

International patents and patent applications:

1) K. Churski, P. Korczyk, **T. Kaminski**, S. Jakieła, M. Izydorzak, S. Makulska, P. Garstecki. *System and Method for Automated Generation and Handling of Liquid Mixtures.* US Patent no 9,132,396.
2) S. Jakieła, **T. Kaminski**, P. Garstecki. *Method for splitting droplets on demand in microfluidic junction.* Patent Application WO/2013/014215 published on 31 January 2013, US20140147908 A1 published 29 May 2014, EP2736640 A1 published on 4 June 2014.
3) Garstecki, P. Debski, M. Oszmaniec, **T. Kaminski**, A. Warchulski. *Method for performing quantification assays.* Patent Application WO/2013/072069 published on 23 May 2013.
4) S. Jakiela, **T. Kaminski**, P. Garstecki. *Verfahren zur Teilung von Tropfen an einer mikrofluidischen Kreuzung.* Swiss patent CH 705288 published on 13 September 2013.
5) P. Korczyk, L. Derzsi, **T. Kaminski**, S.Jakieła, P. Garstecki. *Microfluidic device for performing operations on microdroplets*. Patent Application WO/2013/160408 published on 31 November 2013.
6) S. Jakiela, **T. Kaminski**, K. Churski, P. Garstecki. *Verfahren zur Teilung von Tropfen an einer mikrofluidischen Kreuzung.* Patent CH 705287 published on 13 December 2013.
7) M. Czekalska, **T. Kamiński**, P. Garstecki. *Microfluidic system, in particular for automated generation of phospholipid bilayers and testing of membrane protein activity.* Finnish Patent granted on 15 December 2015.

Polish patents and patent applications:

8) K. Churski, **T. Kamiński**, S. Jakieła, M. Izydorzak, S. Makulska, P. Garstecki. *Układ do zasilania podukładu mikroprzepływowego płynami i odpowiedni podukład mikroprzepływowy.* Patent application P-393619 published on 11 January 2011.

http://rcin.org.pl

9) S. Jakieła, **T. Kamiński**, P. Garstecki. *Sposób dzielenia kropel na żądanie w złączu mikroprzepływowym.* Patent application P-395776 published on 27 July 2011.
10) S. Jakieła, **T. Kamiński**, P. Garstecki. *Sposób dzielenia kropel na żądanie w złączu mikroprzepływowym.* Patent application P-395777 published on 27 July 2011.
11) S. Jakieła, **T. Kamiński**, K. Churski, P. Garstecki. *Sposób dzielenia kropel na żądanie w złączu mikroprzepływowym.* Patent application P-395778 published on 27 July 2011.
12) **T. Kamiński**, P. Garstecki. *Sposób dzielenia kropel w złączu mikroprzepływowym i układ do dzielenia kropel w złączu mikroprzepływowym.* Patent application P-396493 published on 30 September 2011.
13) P. Dębski, **T. Kamiński**, P. Garstecki, A. Warchulski. *Sposób przeprowadzania cyfrowych oznaczeń analitycznych i diagnostycznych.* Patent application P-397026 published on 17 November 2011.
14) P. Dębski, M. Oszmaniec, **T. Kamiński**, P. Garstecki. *Sposób przeprowadzania cyfrowych oznaczeń analitycznych i diagnostycznych.* Patent application P-397027 published on 17 November 2011.
15) P. Dębski, M. Oszmaniec, **T. Kamiński**, P. Garstecki. *Sposób przeprowadzania cyfrowych oznaczeń analitycznych i diagnostycznych.* Patent application P-397028 published on 17 November 2011.
16) P. Korczyk, L. Derzsi, **T. Kamiński**, S. Jakieła, P. Garstecki. *Urządzenie mikroprzepływowe i układ mikroprzepływowy obejmujący jedno lub więcej urządzeń mikroprzepływowych.* Patent application P-397028 published on 26 April 2012.
17) **T. Kamiński**, M. Czekalska, P. Garstecki. *Mikroprzepływowy układ zwłaszcza do automatycznego tworzenia dwuwarstw fosfolipidowych o zmiennej i kontrolowanej wielkości oraz jego zastosowanie.* Patent application P-405819 published on 29 October 2013.
18) **T. Kamiński**, M. Czekalska, P. Garstecki. *Mikroprzepływowy układ zwłaszcza do automatycznego tworzenia dwuwarstw fosfolipidowych i badania aktywności białek błonowych.* Patent application P-410696 published on 31 December 2014.
19) S. Hou, L. Sun, S. A. Wieczorek, T. Kalwarczyk, **T. Kaminski**, R. Holyst. *Sposób wyznaczania wydajności podwójnego znakowania dwuniciowego DNA barwnikiem fluorescencyjnym z zastosowaniem spektroskopii korelacji fluorescencji oraz jego zastosowanie w analizie biochemicznej.* Polish Patent P-402764 granted on 9 December 2015.
20) M. Czekalska, **T. Kamiński**, P. Garstecki. *Mikroprzepływowy układ zwłaszcza do automatycznego tworzenia dwuwarstw fosfolipidowych i badania aktywności białek błonowych.* Polish Patent P-405321 granted on 10 December 2015.

http://rcin.org.pl

Contributions

Thesis comprises the experimental results of five research projects (each ended or will end with scientific article - published, submitted for revision or being under preparation. I am the first author or co-first author (one of two authors with equal contribution) of each of the five publications:

1) **T. S. Kaminski**, S. Jakiela, M. Czekalska, W. Postek P. Garstecki. *Automated and rapid generation of libraries of droplets.* Lab on a Chip, 2012, 12, 3995-4002.
   Main contribution: TK designed, conducted and analyzed the majority of the experiments, and significantly contributed to writing the drafts and final publication.

2) **S. Jakieła*, T. S. Kaminski* (*equal contribution)**, O. Cybulski, D.B. Weibel, P. Garstecki. *Bacterial growth and adaptation in microdroplet chemostats*. Angewandte Chemie Int. Ed., 2013, 52, 8908-8911.
   Main contribution: SJ was responsible for automation, development of the method of droplet splitting and design of a microfluidic chip. TK was responsible for biological aspects of the project and the optimization of the chemical composition of droplets. SJ and TK together interpreted results and wrote the manuscript.

3) **M. Czekalska*, T. S. Kaminski* (*equal contribution)**, S. Jakiela, K. T. Sapra, H. Bayley, P. Garstecki. *A droplet microfluidic system for sequential generation of lipid bilayers and transmembrane electrical recordings.* Lab On a Chip, 2015, 15, 541-548.
   Main contribution: MC and TK together conceived the idea for the project. TK developed the initial version of the system. MC optimized the architecture of microfluidic system and conducted electrophysiological experiments, under supervision of TK. MC and TK together analyzed and interpreted the results and wrote the manuscript.

http://rcin.org.pl

4) **L. Derzsi*, T. S. Kaminski* (*equal contribution)**, P. Garstecki. *Antibiograms in five pipetting steps: precise dilution assays in sub microliter volumes with a conventional pipette*. Submitted to *Lab on a Chip*, under review

   Main contribution: LD conceived the idea and developed the Meter&Store trap - the main module of the system. TK significantly improved the geometry of the M&S module, and developed the system for the most important aspect of the project, i.e. for compatibility with being operated with a standard pipette, performed characterization of the chip performance and carried out bacteria susceptibility tests. TK significantly contributed to writing the drafts and final publication.

5) **T. S. Kaminski**, W. Postek, P.R. Debski P. Garstecki. *Droplet digital PCR with extended dynamic range.* In preparation

   Main contribution: TK designed, conducted and analyzed the majority of the experiments.

All results included in this dissertation are presented with the consent of all of the co-authors.

All projects were conducted under guidance of prof. Piotr Garstecki – supervisor of my doctoral studies.

http://rcin.org.pl

List of symbols and abbreviations

c	concentration
Ca	capillary number
C_T	capacitance
$C(t)$	concentration of the rate limiting nutrient
D	diameter, dilution ratio
f	frequency
h	height
I_C	capacitive current
K_d	dissociation constant
K_M	substrate concentration that yields half of the maximum growth rate
k_{on}	association rate constant
k_{off}	dissociation rate constant
N	number
N_0	initial number of cells
N_{SAT}	stable cell density
p_c	pressure of continuous phase
p_d	pressure of dispersed phase
P_{open}	probability of open channel
Q	flow velocity
Q_c	flow velocity of continuous phase
Q_d	flow velocity of dispersed phase
U	characteristic velocity
t	time
T	time interval
w	weight
V	electric potential or volume
γ	surface tension
λ	wavelength or expected value of a Poisson random variable
μ	dynamic viscosity of the fluid
μ	growth rate of bacteria
μ_{MAX}	maximum growth rate
τ_{on}	time of inter-event interval
τ_{off}	mean residence time

http://rcin.org.pl

AC	alternating current
ABS	absorbance
6-FAM	6-carboxyfluorescein
α-HL	*alpha*-hemolysin
ATCC	American Type Culture Collection
BHQ1	black hole quencher
BLM	black lipid membranes
CCD	charge-coupled device
CFU	colony-forming unit
CNC	computer numerical control
CNV	copy number variation
CV	coefficient of variation
DIB	droplet interface bilayer
DOD	droplets on demand
DNA	deoxyribonucleic acid
dNTPs	deoxynucleoside triphosphates
dPCR	digital polymerase chain reaction
ddPCR	droplet digital polymerase chain reaction
qPCR	quantitative polymerase chain reaction
DPhPC	diphytanoylphosphatidylcholine
ELISA	enzyme-linked immunosorbent assay
EMV	electromagnetic valve
FCS	fluorescence correlation spectroscopy
FEP	fluorinated ethylene propylene
FF	flow focusing
γCD	gamma-cyclodextrin
GUV	giant unilamellar vesicle
hERG	human *Ether-à-go-go*-Related Gene
IC_{50}	half maximal inhibitory concentration
IVTT	*in vitro* transcription and translation
LB	lysogeny broth
LBK	potassium modified lysogeny broth
MHB	Mueller-Hinton broth

http://rcin.org.pl

MIC	minimum inhibitory concentration
MS	mass spectrometry
MW	molecular weight
PC	polycarbonate
PCR	polymerase chain reaction
PDMS	polydimethylsiloxane
PEG	polyethylene glycol
PFPE	perfluoropolyether
PIPES	piperazine-N,N′-bis(2-ethanesulfonic acid)
POCT	point-of-care testing
PTFE	polytetrafluoroethylene
RSD	relative standard deviation
RPM	revolutions per minute
SACT-1	*Saccharomyces cerevisiae* actin gene
SDS	sodium dodecyl sulfate
PAGE	polyacrylamide gel electrophoresis
Taq Pol	*Thermus aquaticus* polymerase
TRIMEB	heptakis(2,3,6-tri-*O*-metylo)-*β*-cyklodextrin
TRIS	tris(hydroxymethyl)aminomethane

http://rcin.org.pl

Contents

ACKNOWLEDGEMENTS 3
ACKNOWLEDGMENTS FOR FUNDING 4
LIST OF PUBLICATIONS AND PATENT APPLICATIONS 6
CONTRIBUTIONS 9
LIST OF SYMBOLS AND ABBREVIATIONS 11
CONTENTS 14
STRESZCZENIE (ABSTRACT IN POLISH) 18
ABSTRACT 20
1. INTRODUCTION 22
1.1 Microfluidic technologies 23
1.2 Droplet microfluidics 24
1.2.1 Manipulations with droplets in microfluidic chips. 26
1.2.1.1 Formation of droplets 26
1.2.1.2 Merging of droplets 28
1.2.1.3 Splitting 28
1.2.1.4 Incubation 28
1.2.1.5 Sorting 30
1.2.1.6 Detection 30
1.2.2 Control over the chemical compositions of droplets 31
1.2.2.1 Generation of microfluidic gradients 31
1.2.2.2 Droplet libraries 33
1.3 Application of droplet microfluidics in microbiological assays 34
1.3.1 Cell assays in droplet microfluidics 34
1.3.2 Analysis of bacterial susceptibility using droplet microfluidic devices 36
1.3.3 Long-term studies of bacterial growth and adaptation in microfluidic devices 37
1.4 Application of droplet microfluidics in biochemistry 38
1.4.1 Analysis of lipid bilayers and membrane proteins 38

http://rcin.org.pl

1.4.1.1 Formation of planar bilayers 39
1.4.1.2 DIBs in microfluidics 41
1.4.2 PCR 41
1.4.2.1 Introduction to PCR 41
1.4.2.2 Preparatory PCR in microdroplets 42
1.4.2.3 Quantitative PCR 43
1.4.2.4 Droplet digital PCR 44
2. MATERIALS 46
2.1 Oils and surfactants 47
2.2 Polymers – materials used for the fabrication of microfluidic chips 48
2.3 Materials for microbial experiments 48
2.3.1 Media for bacteria culture 48
2.3.2 Bacteria cells 49
2.3.3 Antibiotic solutions 49
2.3.4 Bacteria viability indicator 50
2.4 Protein expression and purification 50
2.5 PCR mixtures 50
2.6 DNA sequences 50
3. METHODS 51
3.1 Fabrication of microfluidic devices 52
3.1.1 PDMS chips 52
3.1.2 Polycarbonate chips 52
3.2 Control of flow 53
3.2.1 Control of flow with external valves 53
3.2.2 Control of flow with syringe pumps 54
3.3 Methods for manipulation of droplets 54
3.3.1 Robotic systems and aspiration of droplets from microwell plates 54
3.3.2 Manipulation of droplets using passive geometries 55

http://rcin.org.pl

3.3.2.1 Metering trap 55
3.3.2.2 Merging trap 56
3.4 Image analysis 57
3.5 UV-Vis measurement 58
3.6 Fluorescence measurement 58
3.6.1 Qualitative measurement of fluorescent gradient 58
3.6.2 Measurement of fluorescence using gel imaging system 59
3.6.3 High-throughput measurement of fluorescent droplets 59
3.7 Electrophysiological recordings 60
3.8 PCR thermocycling 60
4. RESULTS 61
4.1 Determination of MIC in five pipetting steps: precise dilution assays in submicroliter volumes with a conventional pipette 62
4.1.1 The Meter and Store (M&S) module 64
4.1.2 Passive microfluidic system for antibiotic susceptibility testing 66
4.1.3 The full procedure of preparation of a dilution series with a component at constant concentration 68
4.1.4 Serial dilution of a fluorescent sample 69
4.1.5 Determination of Minimum Inhibitory Concentration (MIC) of ampicillin 71
4.1.6 Summary 73
4.2 Studies of bacterial growth and adaptation in microdroplet chemostats 75
4.2.1 Microdroplet chemostat design 75
4.2.2 Microdroplet formation 75
4.2.3 Microdroplet incubation 77
4.2.4 Controlling microdroplet chemistry 77
4.2.5 *E. coli* growth in microdroplet chemostats 79
4.2.6 Cell growth in microchemostats containing antibiotics 82

http://rcin.org.pl

4.2.7 Monitoring the response of bacterial communities to stress 83
4.2.8 Summary 85
4.3 Automated microfluidic system for generation of lipid bilayers and screening of membrane protein activity 87
4.3.1 Microfluidic device 87
4.3.2 Operation of a chip 88
4.3.3 Characterization of the bilayer 89
4.3.4 α–hemolysin measurements 91
4.3.5 Screening experiment 93
4.3.6 Summary 96
4.4 Generation of libraries of nanoliter droplets and application of this technique for improved DNA quantification with digital PCR 98
4.4.1 Generation of droplet libraries 99
4.4.1.1 Optimization of the geometry of the FF-junction for generation of droplet libraries 99
4.4.1.2 Generation of exemplary libraries 103
4.4.2 Combining droplet libraries with digital PCR for quantification of high DNA concentrations 105
4.4.3 Summary 112
5. CONCLUSIONS AND PERSPECTIVES 114
5.1 General conclusions 115
5.2 Determination of MIC using passive microdroplet system based on the technology of passive traps 115
5.3 Microdroplet chemostats 117
5.4 Screening of model lipid membranes using droplet microfluidic systems. 118
5.5 Generation of droplet libraries and application of this technology for the improvement of droplet digital PCR 119
LITERATURE 120

Instytut Chemii Fizycznej PAN BIBLIOTEKA
http://rcin.org.pl

Streszczenie (Abstract in Polish)

Mikroprzepływy są nową dziedziną nauki mającą na celu i) badanie hydrodynamiki i własności płynów w mikroskali, oraz ii) projektowanie, wytwarzanie i integrację układów dla praktycznych zastosowań w chemii, biologii i inżynierii materiałowej. Jednofazowe układy mikroprzepływowe po raz pierwszy opracowano na początku lat 90. XX wieku, a systemy oparte na technologii mikrokropel pojawiły się 10 lat później – w 2001 roku. Od tamtej pory mikroprzepływy dwufazowe zostały wykorzystane w wielu wydajnych i unikalnych metodach badawczych na poziomie akademickim. Wiele z tych technologii zostało już wdrożonych jako komercyjne produkty i urządzenia w branży badań biochemicznych, diagnostyki medycznej czy też kosmetologii.

Pomimo znaczącego rozwoju dziedziny w okresie ostatnich 15 lat, wciąż istnieją bariery, które ograniczają dalsze zastosowania mikroprzepływów dwufazowych w biologii eksperymentalnej – szczególnie w biochemii i w mikrobiologii. Jednym z największym wyzwań jest opracowanie wydajnych metod niezależnej i elastycznej kontroli składu chemicznego, objętości oraz transportu mikrokropel w czasie reakcji w układzie mikrofluidycznym. Drugim ważnym celem badań jest rozwój technik pozwalających na pasywne operacje na mikrokroplach w autonomicznych układach mikroprzepływowych, które mogą być wykorzystane w diagnostyce pierwszego kontaktu w miejscu opieki nad pacjentem, gdzie nie ma dostępu do wyspecjalizowanej aparatury ani wyszkolonego personelu.

Projekty badawcze, których wyniki są zaprezentowane w tej rozprawie, wykorzystują nowe metody tworzenia kropel o zdefiniowanym składzie chemicznym poprzez i) zautomatyzowane techniki kontroli przepływu oraz za pomocą zewnętrznych zaworów elektromagnetycznych, ii) zastosowanie pułapek hydrodynamicznych do precyzyjnego odmierzania i unieruchamiania małych objętości cieczy oraz iii) zautomatyzowanym tworzeniu bibliotek nanolitrowych kropel. Na potrzeby badań w ramach tej rozprawy, niektóre z tych metod zostały opracowane od podstaw (biblioteki kropel), podczas gdy inne (automatyzacja, pułapki hydrodynamiczne) częściowo opierają się na wynikach wcześniejszych projektów realizowanych w Grupie Mikroprzepływów i Płynów Złożonych. Główna

http://rcin.org.pl

część rozprawy zawiera przykłady praktycznych zastosowań ww. metod w wybranych badaniach z zakresu biochemii oraz mikrobiologii.

Rozprawa składa się z 5 rozdziałów. Rozdział 1 zawiera przegląd literaturowy obejmujący wprowadzenie do mikroprzepływów jedno- i dwufazowych oraz opis obecnie najważniejszych zastosowań technologii mikrokropel w badaniach biomedycznych. Materiały i metody użyte w badaniach są opisane odpowiednio w rozdziałach 3 i 4, a wyniki eksperymentów są przedstawione w rozdziale 4. Ostatni, 5 rozdział zawiera ogólne podsumowanie oraz propozycje dalszych badań.

Wyniki eksperymentów są przedstawione w 4 podrozdziałach:

1. Technologia pasywnej kontroli przepływu za pomocą pułapek hydrodynamicznych została wykorzystana do prowadzenia oznaczeń lekooporności bakterii w autonomicznym układzie mikroprzepływowym.
2. Metoda kontrolowanego podziału kropel z wykorzystaniem zautomatyzowanych mikroprzepływów pozwoliła na długotrwałą hodowlę bakterii w chemostatach mikrokroplowych.
3. Synergistyczne połączenie automatyzacji i pasywnych geometrii pozwoliło na wydajne tworzenie dwuwarstw lipidowych na styku dwóch nanolitrowych wodnych kropel oraz umożliwiło wykonanie pomiarów aktywności pojedynczych białek błonowych.
4. Automatyzacja została wykorzystana w celu wydajnego tworzenie bibliotek nanolitrowych kropel o zdefiniowanym składzie chemicznym. Technologia bibliotek kropel w połączeniu z pasywnymi i aktywnymi metodami kontroli przepływu umożliwiła ilościowe oznaczenie wysokich stężeń DNA za pomocą kroplowego cyfrowego PCR.

http://rcin.org.pl

Abstract

Microfluidics is a new field of science focused on i) studying the hydrodynamics and the properties of fluids at the microscale and ii) designing, manufacturing and assembling devices for practical applications in chemistry, biology and material sciences. First demonstration of continuous-flow microfluidic devices dates back to the beginning of the 1990s. The microdroplet technology was first introduced 10 years later, in 2001. Since then, droplet microfluidics has been rapidly evolving with outstanding academic demonstrations of highly efficient technologies. A number of them has already been turned into commercial products for biomedical research, molecular diagnostics and cosmetic industry.

Despite substantial progress of the technology in the last 15 years, there are still technical barriers hindering further implementation of microdroplet technology to experimental biology – especially to biochemistry and microbiology. One of the most important challenges is in acquiring an independent and flexible control over the chemical composition, volume and location of multiple droplets over time. A second important goal that still requires substantial research is to provide methods of passive handling of droplets in autonomous microfluidic systems that might be used for point-of-care diagnostics, i.e. in settings that do not offer neither specialized infrastructure, nor trained personnel.

Research projects presented in this thesis required formation of droplets with arbitrarily set composition through i) liquid handling techniques based on automation and use of external electromagnetic valves, ii) improved hydrodynamic modules that precisely meters and stores a small portion of liquid, and iii) automated generation of libraries of nanoliter droplets. For the purpose of this dissertation, some methods were created from the scratch (droplet libraries), while others (passive traps, automation) are based on previous research carried out in the Group of Microfluidics and Complex Fluids. The main part of the dissertation comprises demonstrations of the utility of these droplet microfluidic methods for selected applications in biochemistry and in microbiology.

Thesis comprises five chapters. Chapter 1 provides an introduction to continuous-flow and biphasic microfluidics and describes the current state-of-the-art applications of microdroplet technologies in biomedical sciences.

http://rcin.org.pl

Chapters 2 and 3 comprise brief description of materials and methods used in the experimental studies. Chapter 4 contains experimental results. Finally, general conclusions and propositions of future research are presented in chapter 5.

The results of experimental studies are arranged into four sections:

1. Technique for passive fluid handling with hydrodynamic traps was used in an autonomous system for determination of microbial susceptibility to antibiotics.
2. Method of controlled droplet splitting with automated microfluidics was used for demonstration of a long-term cultivation of bacteria in microdroplet chemostats.
3. Synergistic combination of automated and passive geometries enables for efficient formation of lipid bilayers at the interface between a pair of nanoliter-sized aqueous droplets and measurements of the activity of single membrane proteins.
4. Automation was used for rapid generation of libraries of nanoliter droplets with predefined chemical compositions. Droplet libraries method, along with techniques for passive and active liquid handling enable for quantification of very high DNA concentrations using droplet digital PCR.

http://rcin.org.pl

1. INTRODUCTION

This chapter comprises a general introduction to microfluidics with a comparison between continuous-flow and microdroplet systems (section 1.1). Section 1.2 provides a description of the microfluidic toolbox for manipulation of droplets and presents current methods tackling the challenge of formation of droplets with controlled chemical composition. Second part of this chapter is devoted to presentation of applications of droplet microfluidics to selected experimental procedures in microbiology (section 1.3: antibiotic susceptibility testing and long-term studies of microbial populations) and in biochemistry (section 1.4: reconstitution of a model lipid membranes and PCR assay). These last two sections give an overview of traditional versions of aforementioned assays and their state-of-the-art realizations in microfluidic systems. Advantages and limitations of both macro- and microscale approaches to those experimental procedures are also highlighted in this chapter.

http://rcin.org.pl

1.1 Microfluidic technologies

Knowledge-based economies and societies constantly demand for faster, portable, compact and more efficient components and devices. The miniaturization is one of the signs of the general technological progress in high-tech industry comprising telecommunications, semiconductors, photonics, nanotechnology, robotics, biotechnology and artificial intelligence.[1] A model example is the miniaturization of integrated electronic circuits within the last 40 years. Since the introduction of the first microchip in 1971, the number of transistors integrated on a single unit has risen from 2.3 thousand[2] to 7.1 billion,[3] while the size of a single transistor was reduced from 10 μm to 22 nm.[2,3] The potential of miniaturization in other branches of high-tech industry is significant. The process of laboratory miniaturization, often called Lab on a Chip or Micro Total Analysis System begun ca. 25 years ago and nowadays this technology commences to play a significant role in biomedical research, diagnostics and pharmaceutical industry.[4] Microfluidics is the field of research intersecting physics, chemistry, biology, nanotechnology and engineering. The main interest of microfluidics is studying properties of fluids at the microscale and practical applications aiming to develop systems for high throughput screening, diagnostics and research in chemistry and biology. In the first years of the microfluidic era, research activities focused only on single-phase continuous-flow systems, which are based on the controlling of the flow of liquids in the networks of microfluidic channels with diameters ranging from a few micrometers to single millimeters. Small portions of liquids can be delivered to a chip in a specified order, mixed and incubated under various conditions. Flow is usually controlled by means of pneumatic microvalves or through the use of electrokinetic effects.[5–7] The breakthrough momentum for continuous-flow microfluidics was the development of the microfluidic large-scale integration[8] – a fluidic analogue of the technology routinely used in the semiconductor industry. The introduction of the fluidic multiplexer allowed for efficient and highly parallel manipulations of fluids with a minimal number of valves. The microfluidic large-scale integration was successfully commercialized and this technology found many application in biomedical sciences e.g. DNA analysis with PCR,[9,10] protein crystallization,[11–13] single-cell analysis[14,15] or even very challenging operations on subcellular structures such as isolation and haplotyping of single

http://rcin.org.pl

chromosomes.[16,17]However, for many applications single-phase microfluidics is less attractive due to several issues associated with continuous and laminar flow. Mixing is slow[18] and the control of the local concentration of reagents is challenging due to the Taylor-Aris dispersion.[18–20] Another problem is the adsorption of biomolecules and chemical compounds on the surface of microfluidic channels, formation of biofilms[21] and cytotoxicity of non-completely cured monomers released from the polymeric material of the chip.[22,23]

1.2 Droplet microfluidics

Droplet microfluidics, an alternative approach to continuous-flow microfluidics has been rapidly evolving during last 15 years. Microdroplet technology enables formation and analysis of a large number of discrete microvolumes of fluids. Microdroplets are submerged in immiscible continuous phase and they can be transported through the network of microfluidic channels without the risk of cross-contamination or dispersion of analytes. The volume of microdroplets ranges from picoliters to single microliters. The comparison between continuous-flow microfluidics and droplet microfluidics is shown in Table 1 and Fig. 1.

Continuous-flow microfluidics and droplet microfluidics are complementary technologies and the choice between them depends on the type and the aim of an experiment. Single-phase microfluidic chips are suitable for experiments needing complex detection, e.g. microscope imaging,[23–25] and for assays requiring the contact with a solid substrate e.g. *in vitro* cultivation of adherent mammalian cells.[23,26] Droplet microfluidics is the best choice for assays with simpler protocols of liquid handling but requiring large number of compartments e.g. directed evolution of enzymes[27–30] or determination of DNA concentration using digital PCR.[31–34] The technology of microdroplets on a chip has been following a step behind the continuous-flow microfluidics, since the latter method was introduced 10 years earlier. Until recently, more complex experimental protocols were not available on droplet microfluidic chips. Still, some of the operations are challenging, such as efficient formation of droplets with arbitrarily predefined chemical composition and further control of the reaction conditions over time.

http://rcin.org.pl

Feature:	**Continuous-flow microfluidics**	**Droplet microfluidics**
Mixing	Slow mixing, mainly through diffusion.	Rapid mixing (down to a few miliseconds) as a result of chaotic advection.[35,36]
Dispersion of analytes	Flow with the parabolic profile causes continuous change of concentration – the phenomenon called Taylor-Aris dispersion.[37,38]	The local concertation of reagents is stable in droplets that do not merge with each other thank to the presence of the surfactant on the liquid-liquid interface.[39]
Wetting	Liquid wets the surface of a microfluidic channel – this process results in several undesired phenomena, such as cross-contamination, swelling of the polymeric material and adsorption of chemical compounds on the surface of a microfluidic channel.	A sample is partitioned into droplets that are separated from the surface of a microfluidic channel by a thin film of the continuous phase.
Number of reactions	Up to a few thousands assays can be performed in a single microfluidic chip, but the control of reaction conditions is complicated.	Number of reaction is very high - practically limited to several millions of droplets.[28]
Actuation	Slow actuation – single operation usually requires a few seconds.	The majority of operations can be conducted very quickly and efficiently with the throughput exceeding 1kHz, e.g. droplet formation, sorting and detection.

Table 1 The comparison of main features of continuous flow microfluidics and droplet microfluidics.

http://rcin.org.pl

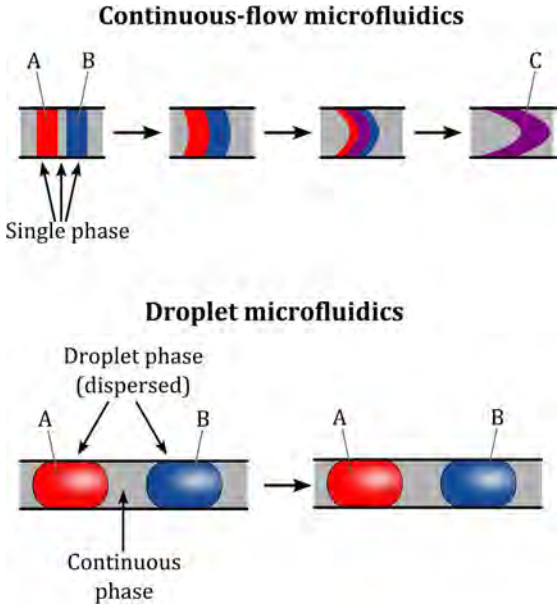


Fig. 1 A scheme depicting the main difference between continuous-flow and droplet microfluidics. Parabolic flow and Tayor-Aris dispersion[37,38] cause cross-contamination of two samples flowing through the channel. Two portion of liquids (A) and (B) are mixed with each other and eventually become (C). Radial diffusion is not presented on the scheme for the sake of simplicity. In the case of droplet microfluidics, the microvolumes of analytes are transported as discrete portions that do not contact with the surface of microfluidic channels and do not merge with each other. The scheme was created on the basis of the image published by Casadevall i Solvas and deMello.[19]

1.2.1 Manipulations with droplets in microfluidic chips.

1.2.1.1 Formation of droplets

Formation of droplets is the first and the most important step in any droplet microfluidic system. We distinguish three main geometries used for generation of droplets (Fig. 2): T-junction introduced by Thorsen *et al.*,[40] flow-focusing junction proposed by Anna *et al.*,[41] and co-flow geometry – most often composed of two co-axial capillaries.[42–44]

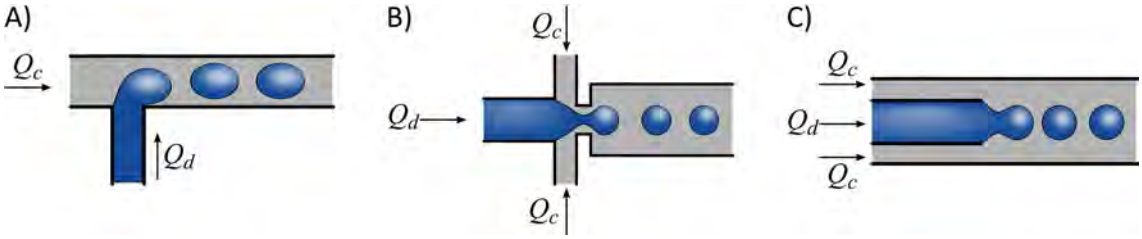


Fig. 2 A schematic diagram of different geometries used for formation of droplets: A) T-junction, B) flow-focusing junction, C) co-axial capillaries. The volume of generated droplets is defined by several factors, including flow velocities of dispersed phase (Q_d) and continuous phase (Q_c) and dimensions of microfluidic channels.

http://rcin.org.pl

The value of the capillary number defines the mechanism of droplet formation in co-axial capillaries, T-junction[45–48] and flow focusing junction.[49–51] The dimensionless capillary number represents the ratio of viscous shear stress to interfacial tension forces:

$$Ca = \frac{\mu U}{\gamma},$$

where:

μ – dynamic viscosity of the fluid (Pa · s)

U – characteristic velocity (m · s^{-1})

γ – surface tension (J · m^{-2})

At low values of capillary numbers ($Ca<10^{-2}$), formation of droplets is driven by interfacial effects and the process occurs according to the squeezing regime.[46,50] The tip of the fluid-to-be-dispersed advances to the junction and then blocks the flow of the continuous liquid (Fig. 3A). The upstream pressure increases, then squeezes and finally breaks the neck of fluid-to-be-dispersed. As a consequence a portion of the liquid is released as a droplet. The volume of droplet solely depends on the ratio of flow velocities of both immiscible phases. At higher values of capillary numbers, the shearing forces become predominant. Droplets are then formed according to dripping regime (Fig. 3B) – the fragmentation of a stream of fluid occurs before the fluid-to-be-dispersed blocks the junction. The rate of droplet formation is much higher than in the squeezing regime. In the jetting regime, very high flow rates lead to formation of a jet of fluid and droplets pinch-off downstream of the junction (Fig. 3C).

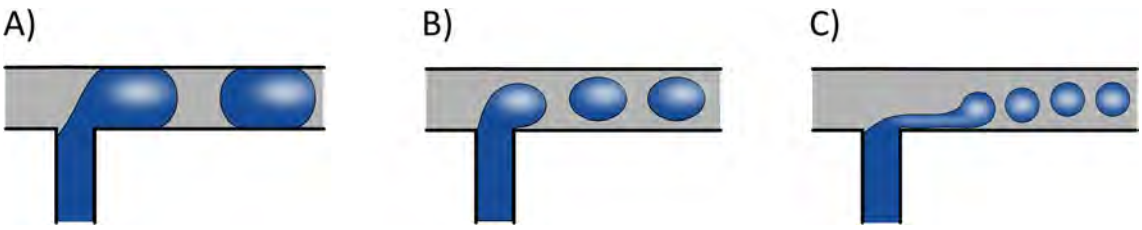


Fig. 3 A scheme depicting different regimes of droplet formation: (A) squeezing mechanism for low values of capillary number, (B) dripping regime occurring for intermediate values of *Ca* and (C) jetting regime typical for high values of capillary number.

http://rcin.org.pl

1.2.1.2 Merging of droplets

Stability of droplets is a crucial factor in various applications of droplet microfluidics. In some cases the coalescence (fusion) of droplets has to be prevented e.g. during formation of functional emulsions for industrial applications or storing of numerous droplet libraries for biological assays. Stability against coalescence is achieved by addition of appropriate surfactant to the continuous liquid or to the both phases.[39,31] On the other hand, in order to prepare reaction mixtures or add reagents during reaction, two or more droplets have to be merged. There are several passive approaches to coalescence of droplets - e.g. Bremond *et al.* and Niu *et al*. [52,53] developed microfluidic chambers in which droplets are squeezed and then fused due to expansion of the interface (Fig. 4a). Droplets stabilized by high concentration of surfactants have to be merged in an active way. The most common method of active coalescence is the use of an alternating electric field[54–56] (Fig. 4c, d). Other methods for droplet merging utilize surface acoustic waves (SAW)[57] or thermocapillary effects caused by a laser beam(Fig. 4b).[58]

1.2.1.3 Splitting

Splitting of droplets has been rarely used in droplet microfluidic systems. The main aim of droplet splitting is to improve the rate of generation of droplets[59] or to form densely packed emulsions.[60] Eastburn *et al.*[61] presented a microfluidic device that split droplets in order to remove the excess of lysis buffer before PCR reaction for a single-cell genetic analysis. T-junctions or Y-junctions, sometimes arranged in binary trees (Fig. 4e, g) are most commonly used for droplet splitting.

1.2.1.4 Incubation

On the contrary to the process of droplet formation, the time of incubation usually cannot be reduced in droplet microfluidic systems. Although there are some interesting exceptions, such as faster detection of single microbes confined in a tiny droplet, the duration of incubation mostly is determined by the chemical nature of assay and does not depend on the reaction volume. In the case of quick reactions, the incubation is occurring during the flow in a long channel until droplets reach the detection spot.[62] If more time is needed for the completion of a reaction, droplets can be transported in wide and shallow channels as a densely packed emulsion[63] (Fig. 4h). Droplets can be also locked in special geometries called *'dropspots'*[64] (Fig. 4i) or in an array of hydrodynamic traps[65,66] (Fig. 4j). Immobilization of droplets in

http://rcin.org.pl

static arrays provide a convenient way for microscope visualization. Very large assemblies of droplets (up to several of millions) are incubated off-chip (Fig. 4k) in tubings,[28] in syringes,[67] in Eppendorf tubes[32] or deposited in multi-well plates.[31] The off-chip incubation is also preferred in the case of specific reaction conditions e.g. thermocycling during PCR.[31,32]

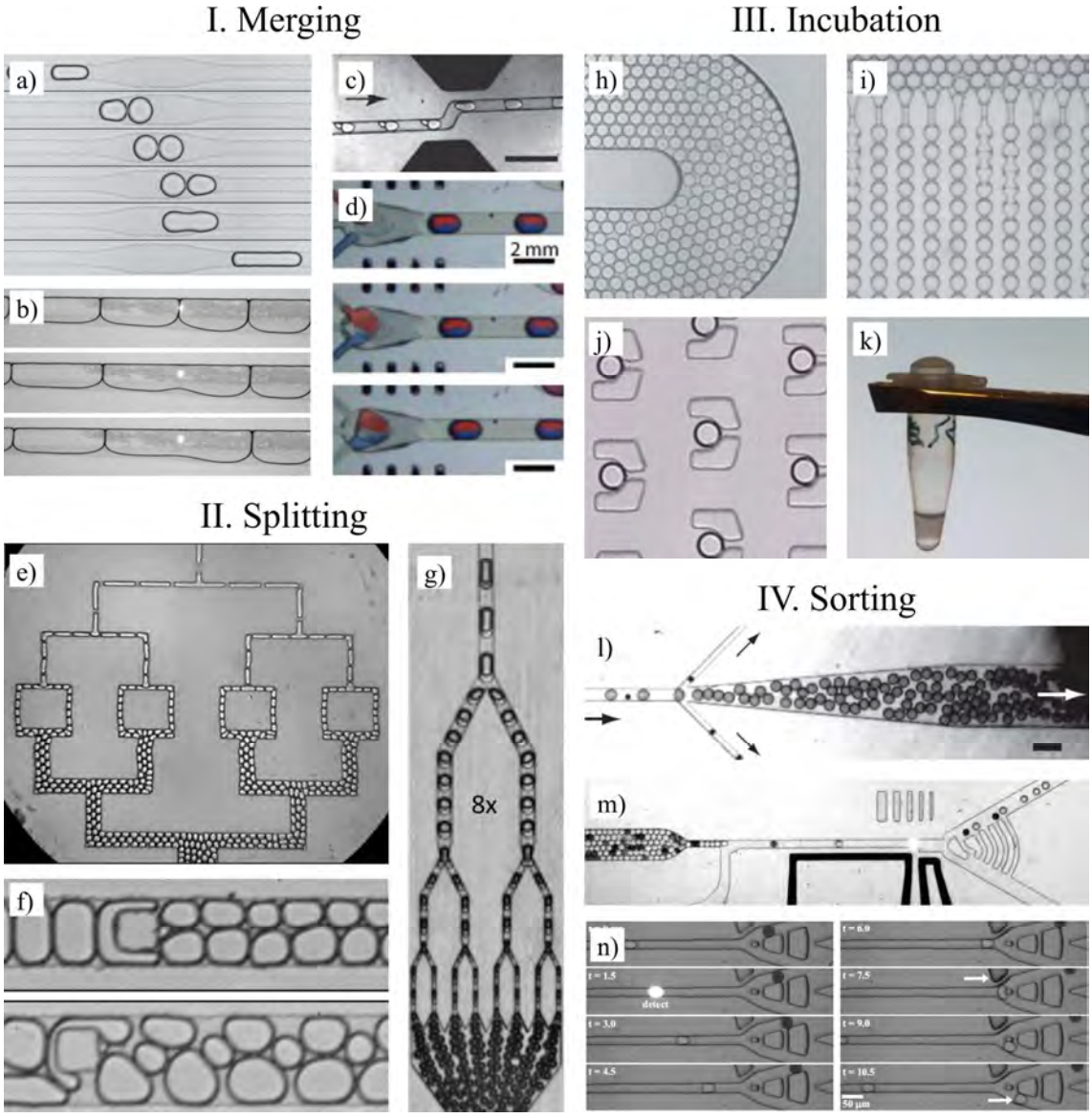


Fig. 4 Selected operations on droplets used in microfluidic systems:

I. Merging of droplets: a) passive fusion in a wide section of channel[52] b) active merging with the use of a laser beam,[58] c, d) coalescence of two[27] or more[55] droplets using an AC electric field.

II. Splitting: e) in series of T-junctions arranged in a binary tree,[68] f) with the use of an additional pillar located in the middle of a microfluidic channel[68] g) splitting of double emulsions in series of Y-junctions.[59]

III. Incubation: h) in wide channels,[69] i) in *dropspots*,[64] j) in an array of hydrodynamic traps[65] or k) off-chip in an Eppendorf tube

IV. Sorting: l) passive by droplet size[70] and active by fluorescence of droplets, using m) electric field[28] or n) pneumatic elements embedded on a chip.[71]

http://rcin.org.pl

1.2.1.5 Sorting

Sorting of drops can be executed in a passive or an active manner. The methods of passive sorting rely on a physical mechanism that distinguishes between selected properties of droplets e.g. size or electrophoretic conductivity. The process of sorting is usually performed in a microfluidic junction composed of one inlet channel and at least two outlet channels for collecting subpopulations of droplets. Mazutis *et al.*[70] presented a method of passive sorting by size (Fig. 4l). In another demonstration, Chabert *et al.*[72] proposed a sorting geometry for selection of droplets containing single cells. On the contrary to passive methods, active sorting uses an external force that modifies the route of flowing droplets and directs them to the desired outlet channels. There are number of stimuli that can be used to conduct active sorting: an electric field[28,73] (Fig. 4m), acoustic waves,[74] a laser beam[58] or mechanical forces generated by pneumatic[71] (Fig. 4n) or hydraulic[75] valving. Additionally, active sorting requires the feedback that triggers the operation of sorting when the measured value exceeds predefined threshold. Usually optical feedbacks based on CCD cameras or detectors of fluorescence are used in droplet microfluidic systems. The most efficient systems can sort droplets with throughput ranging from hundreds of Hz (pneumatic valves[71]) to several kHz (with an electric field[28,73] or acoustic waves[74]).

1.2.1.6 Detection

Measurement of the results of reactions in microdroplets is mainly based on optical methods. Fluorescence is the most universal detection technique due to high signal to noise ratio, short acquisition time and possibility of multiplexed measurement of up to several spectra simultaneously.[73,76,28] Larger submicroliter, slowly flowing droplets can be analyzed by UV-ViS spectroscopy.[56,77,78] The content of droplets can be also examined by more sophisticated optical methods such as Raman spectroscopy[79–81] or fluorescence correlation spectroscopy (FCS).[82] In automated systems, optical detectors are also used for droplet interrogation needed for feedback and synchronization. This task is usually realized by CCD cameras[77,83] or by photodiodes integrated on a chip.[78]

The second important approach used for the characterization of reactions in microdroplets is mass spectrometry (MS). Implementation of MS to droplet microfluidic systems was challenging due to the presence of the continuous phase,

http://rcin.org.pl

typically composed of mineral oils or fluorocarbons – liquids that strongly interfere with this detection technique. Problem was solved by extraction of the droplet content to continuous stream of aqueous liquid [84–86] or by replacement of the oil by air bubbles[87].

Electrochemical detection can be also used for read-out of reaction in droplets as an inexpensive alternative to optical methods or mass spectrometry. Electrochemical techniques are also compatible with non-transparent or opaque chips, expanding the choice of materials for microfabrication of microfluidic devices. In proof-of-concept demonstrations electrochemical sensors were used for quantification of NaCl concentration in droplets[88] and for amperometric studies of enzyme kinetics.[89]

1.2.2 Control over the chemical compositions of droplets

One of the main limitations of droplet microfluidics is the difficulty of generation of droplets with arbitrarily predefined chemical composition. The vast majority of the biochemical assays necessitates generation of concentration gradients of at least one component of the reaction e.g. inhibitor, drug or reaction substrate. On the other hand, many assays in high-throughput screening require that hundreds of thousands of distinct chemical compounds have to be tested with the lowest possible cost. Therefore, we can distinguish two main challenges for microdroplet technology: i) generation of gradients of reagents and ii) efficient testing of large numbers of various chemical compounds.

1.2.2.1 Generation of microfluidic gradients

There are two main approaches for generation of droplets with gradation of chemical composition: i) via active manipulation of flow velocities using pumps, valves and other external forces and ii) using passive techniques that are based on physical phenomena such as interfacial tension or gravity. A chemical gradient in droplets can be generated in active ways by varying the input flow rates of the constituent streams (Fig. 5A),[62] by drawing liquid from a chromatography column[90] or by formation of gradients in single-phase streams prior to droplet generation.[91,92] The latter approach was improved in a system[93] that exploits Taylor-Aris dispersion in a long capillary to create gradations of concentrations, that are subsequently segmented into picoliter drops (Fig. 5B). Another methods are based on merging

http://rcin.org.pl

droplets of different volumes[55,56] or use direct injection of portions of samples to already preformed droplets[94] (Fig. 5C). Most recently, Gielen *et al.* proposed a system[95] (Fig. 5E) generating a chemical gradient in a series of droplets by aspiration of liquid from a well which chemical composition was continuously changed due to injection of a sample.

In recent years, various techniques for passive operations on microdroplets have been developed - i.e. methods requiring programmable syringe pumps or other automated instrumentation for controlling the flow of liquid on a chip. Recent advances within this area include passive formation of monodisperse droplets[96–99] and techniques for subsequent operations on droplets. For example droplets can be passively merged in dedicated geometries such as pillar traps,[53,100] static arrays[101,102] or rails and anchors.[103,104] Passive microfluidics can be used for more complex operations such as formation of simple gradients in hydrodynamic traps[101,105,106] (Fig. 5D). However, passive methods are of low throughput and typically produce individually addressed compositions of droplets at Hz rates that are far too low for efficient screening. On the other hand, the passive methods can be implemented in autonomous devices dedicated to point-of-care testing (POCT).

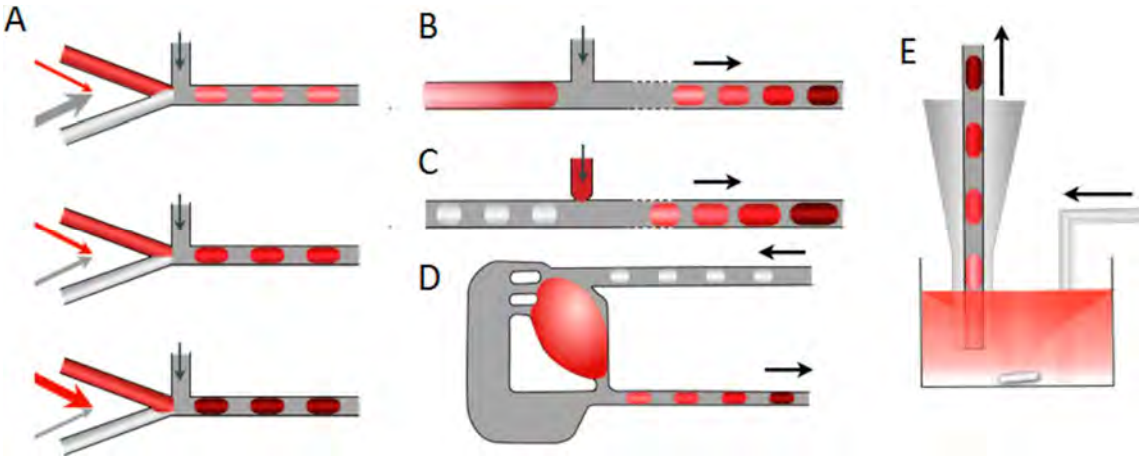


Fig. 5 A schematic presentation of various strategies for formation of gradients of chemical composition in series of droplets. A) A gradient with narrow dynamic range of concentrations can be generated by adjustment of the flow rates of two (or more) constituent single-phase liquid streams. B) A gradient in a continuous-flow stream is generated prior to segmentation of liquid into droplets. C) Control of chemical composition by injection of the sample to preformed droplets. D) Formation of a gradient by dilution of a large 'mother' droplet of sample locked in a hydrodynamic trap. E) Formation of droplets during aspiration of a sample which concentration is dynamically changed in a microliter well. Figure copied from the article published by Gielen *et al.*[95]

http://rcin.org.pl

1.2.2.2 Droplet libraries

Testing of a large number of various chemical compounds in a single microfluidic device is more challenging than generation of gradients of a single reagent. One issue to consider is the risk of cross-contamination. The other challenge is the difficulty of efficient transition from the format of multi-well plates into one-dimensional array of droplets.

It is possible to generate microdroplets comprising distinct chemical compositions from small samples deposited onto a chip,[56] by aspiration of micro-liter volumes of liquid from a microwell plate[100,107] or with a microfluidic slotted-vial array.[108,109] However, these methods are slow (up to a few Hz) and produce droplets that are too large for single molecule/cell studies that typically require small droplets (~pL or single nL). So far, the most efficient idea to tackle this challenge is the concept of droplet libraries[76,110,111] (Fig. 6) consisting of a large number of small (pL–nL) drops of identical, or nearly identical volumes and of different chemical compositions. A library is formed by mixing together distinct populations, each containing a multiplicity of identical droplets of same chemical composition. Formation of a library is labor- and time-intensive. For each chemical composition that is to be included in the library, a separate experiment is needed to split the liquid into a large set of monodisperse droplets (Fig. 6a). Then a large number of such sets needs to be mixed to produce the library. If the library contains a given number of different species, the droplets should be well mixed within the ensemble to guarantee that a part of the library contains the representation of each of the species. The droplets in the library are usually labeled with fluorescent dyes for unique identification of the chemistry encapsulated within each droplet. The encoding procedure is typically carried out as a preparatory step for the experiments on separate microfluidic device.[76,110,111] Then, in the experiment, each element of the random library can be merged with drops containing cells, molecules or other types of analytes (Fig. 6b). Decoding the content of droplets is done via multi-parameter detection: at least one of the measured values provides the information about the content of the droplet while other measurements provide the data for the particular study (Fig. 6d). Many experiments could benefit from simplification and automation of the process of generation of the libraries. For

http://rcin.org.pl

example, a droplet digital assay[31,60,112,113] could benefit from the ability to automatically form sets of drops containing different dilutions of a sample.[114,115]

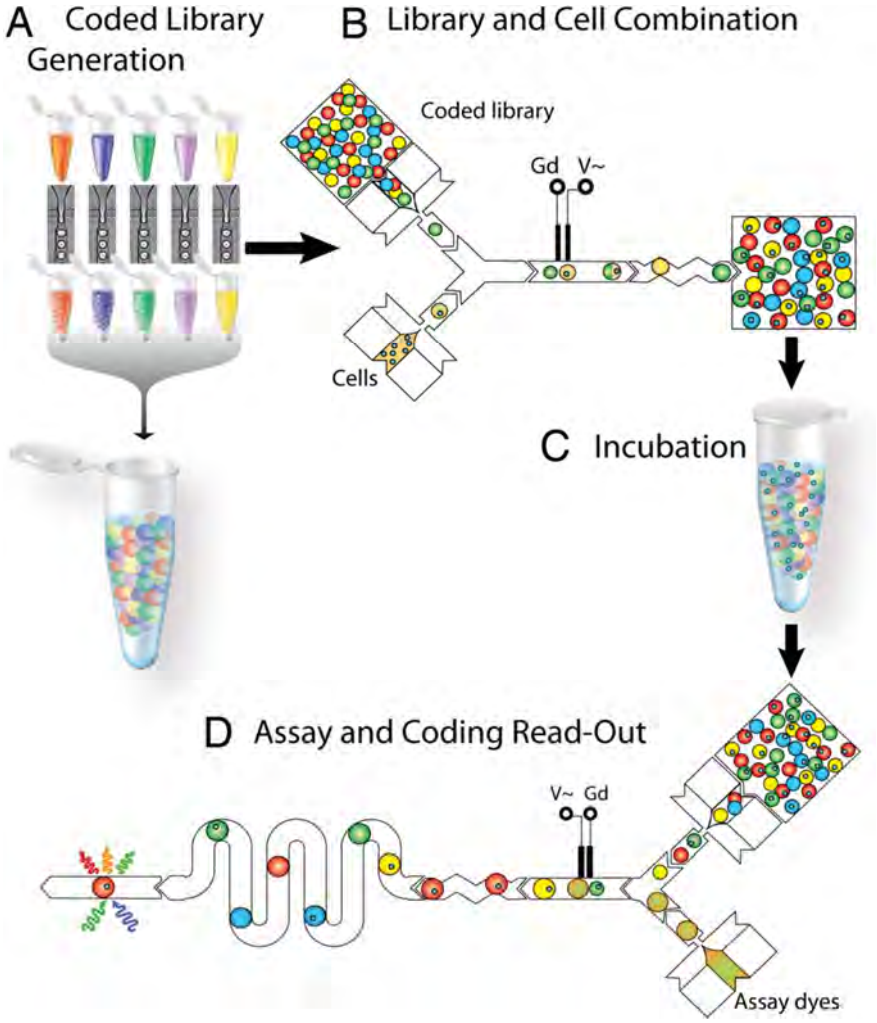


Fig. 6 A scheme depicting the idea of droplet libraries. A) Subsets of a library are formed prior to the main assay on separate microfluidic chips, then pooled together, mixed and stored e.g. in a tube. B) During the assay each library member is merged with one of the droplets containing analyte e.g. single cells. Next, emulsion is incubated (C) and then injected to the detection chip (D) for the multiparameter read-out of reaction results and decoding of the composition of each droplet. Figure copied from the article published by Brouzes *et al.*[76]

1.3 Application of droplet microfluidics in microbiological assays

1.3.1 Cell assays in droplet microfluidics

The first demonstration of analysis of cells encapsulated in aqueous droplets was presented by Joshua Lederberg nearly 60 years ago.[116,117] However, this experimental approach was not pursued further due to the lack of control over droplet formation, manipulation and interrogation. The development of droplet

http://rcin.org.pl

microfluidic systems within last 15 years opens new possibilities for quantitative biological studies at the level of small populations or even of single cells. Different types of organisms and cells were cultivated and studied in droplets, e.g. bacteria,[56,118–121] algae,[122] yeasts[123–125] or mammalian cells.[76,126] Various combinations of carrier fluids and surfactants were used for analysis of cells, but biologically inert fluorocarbons[126] seem to be the best existing group of liquids, thank to very low reactivity, high oxygen capacity and relatively low solubility of hydrophobic compounds in comparison to mineral oils. Encapsulation of single cells in microvolumes provides many advantages apart from the obvious reduction of consumption of reagents and samples. Stochastic confinement[119,127] of single cells in tiny compartments mimics high density populations and allows for studying signal processing among bacterial communities such as quorum sensing.[118,128,129] Confinement also facilitates the detection of chemical signals produced by a single organism due to rapid accumulation of products of cell metabolism.[127] This feature was used for faster detection of microbial pathogens.[119] Cultivation of single cells in droplets also introduces experimental challenges. For instance, the encapsulation of exactly single cells in majority of droplets is impossible due to Poisson distribution[130] – analogous process to compartmentalization of the reaction mixture during droplet digital PCR (described in section 1.4.2.4). In the best case, for low cell densities injected at the input, only small fraction of droplets contains single cells. In order to increase the efficiency of single cell encapsulation Chabert and Viovy[72] proposed to sort droplets and analyze only those containing single cells. Alternative methods based on inertial microfluidics were used for prearrangement of a stream of cell suspension prior to encapsulation, so that cells entered the droplet generating module at the frequency of droplet formation.[131,132] Another challenge, and one that has not yet been tackled, is the control over conditions of incubation over time e.g. dynamic changes of concentration of media components such as drugs, nutrients, ions, inhibitors, hormones and other stimuli. This problem is different from the process of gradient formation, described in section 1.2.2.1, because cell environment should be controlled independently both between the droplets, and within every droplet over time.

http://rcin.org.pl

1.3.2 Analysis of bacterial susceptibility using droplet microfluidic devices

Continuous-flow and droplet microfluidics in particular were extensively used as tools for the analysis of bacteria. We can distinguish four main applications of microdroplet technology in microbiology: i) studies of bacterial physiology[118,128,129,133] ii) selection of rare individuals for biotechnological and industrial applications[29,134,135] iii) faster detection and identification of pathogens[119,136] and iv) studies of bacterial susceptibility and antibiotic testing.[56,119,121] Due to limited length of the dissertation only antibiotic testing is described in this section, since this topic is closely related to one of the sections of experimental results.

Broth serial dilution and disk diffusion are the two universal and the most commonly used classical laboratory techniques for testing antimicrobial susceptibility and determining minimum inhibitory concentration (MIC).[137,138] The MIC value is defined as the lowest concentration of a chemical compound (e.g. antibiotic) that inhibits growth of bacteria. Classical methods are time- and labor-intensive and they require relatively large volumes of culture media. For example, the dilution technique needs preparation of 2-fold gradient of antibiotic in a series of separate tubes. Next, each tube is inoculated by microbial culture and finally all samples are incubated overnight to achieve sufficient cell density for bulk measurement. The workload of these methods can be reduced by the use of automated liquid handling robots. However, these instruments are expensive and not commonly available in laboratories.

Microfluidic devices are the alternative to classical methods of antibiotic susceptibility testing. Besides lower consumption of samples, the microbial growth rate is enhanced due to better oxygenation resulting from the high surface-to-volume ratio.[139] Several microfluidic devices were presented as systems capable of MIC determination, e.g.: by cultivation of bacteria in high aspect ratio microchannels,[139] by growth monitoring of bacteria trapped by dielectrophoretic forces[140] or immobilized in agarose-based 3D culture,[141] and by encapsulation of single cells in hydrogel microparticles.[142] However these methods are quite complex in terms of liquid handling and optical measurement of bacterial growth. What is more important, these new microfluidic techniques are quite distant from the standard and validated methodology – thus they require additional

http://rcin.org.pl

characterization and testing prior to implementation as devices for use in medical diagnostics. In one of the most interesting demonstrations, Cira *et al*. developed autonomous and self-loading PDMS chip[143] for determination of MIC. The device needs to be placed in vacuum and degassed prior to use. The degassed PDMS chip creates the slow flow of liquids that distributes bacterial suspension to chambers containing dried antibiotic. Despite obvious advantages, the device also possesses some limitations: the loading of the chip took ca. 100 minutes, which makes this operation much longer than preparing the serial dilution assay using classical approach (e.g by pipetting). Antibiotics solutions are pre-loaded into the chip and then dried before the assay – this operation creates a risk of biased and reduced antimicrobial activity due to degradation and adsorption of antibiotic compounds to the surface of PDMS.[144]

MIC can be also determined in droplet microfluidic devices, using series of plugs with gradually changing concentration of antibiotics.[56,119–121] However, as we mention in previous paragraphs, the generation of gradients in droplets is complicated operation requiring multiple pumps and valves. The ideal microfluidic system should be simple yet precise, cheap, disposable and autonomous – i.e. requiring minimal external instrumentation for generation of flow. Qualitative read-out should be performed by visual inspection.

1.3.3 Long-term studies of bacterial growth and adaptation in microfluidic devices

One of the main challenges of modern microbiology is the problem of evolution of antibiotic resistance among microbial pathogens.[145,146] Research in this field requires long-term studies of evolving bacteria. Continuous growth and observation of microbes is supported by a special type of bioreactor called chemostat. The introduction of the chemostat by Leo Szilard[147] was a milestone in the field of microbiology. Chemostats facilitate long-term culture of bacteria, yeast or algae by a continuous exchange of constant volume of fluid in order to maintain stable concentrations of cells and growth factors.[147–149] However, the consumption of large quantities of reagents and complicated operation limit the use of traditional chemostats.

Continuous-flow microfluidic versions of chemostats greatly reduce incubation volumes,[21,150–152] but these devices are limited by their complexity:

http://rcin.org.pl

the proportionality between the number of input/output controls and the number of microbioreactors hamper a large-scale parallelization. Additionally, single-phase microfluidic systems are prone to biofilm formation, which makes them either single use devices[151] or requiring additional washing steps to minimize cell adhesion.[21] Droplet microfluidics offers the unique solution to study microbial physiology or susceptibility to antibiotics. Recently, bacteria have been incubated in microdroplets in channels over short time intervals,[56,119,121,145] but sustained cell growth over dozens of generations in a series of fully addressable microdroplets is a much more challenging procedure comparing to droplet microfluidic systems for determination of the MIC).

1.4 Application of droplet microfluidics in biochemistry

1.4.1 Analysis of lipid bilayers and membrane proteins

Membrane proteins comprise 25% of the human proteome[153] composed of ca. 25 thousands proteins encoded by the genome. Examination of membrane proteins is a demanding task due to difficulties with their expression and purification. Moreover, often during the assay a membrane protein must be incorporated into artificial lipid bilayer or at least stabilized by surfactants. Screening of activity of ion channels is especially challenging but these proteins are targets for many potential drugs in treatment of channelopathies[154] – diseases resulting from impaired channel function, e.g. diabetes, hypertension, cardiac arrhythmia, cystic fibrosis and many other disfunctions.[154] The analysis of ion channel is mainly realized by precise electrophysiological measurements of ion currents flowing through the protein pore across the membrane. The main gold standard method is patch clamp[155,156] – an experimental technique used for recordings on target proteins over-expressed in live cell lines or on proteins incorporated into artificial membranes of lipid vesicles.[157,158] The patch-clamp method uses a micropipette with integrated electrode to enclose small patch of a membrane containing one or a few ion channels. Suction inside the micropipette is applied in order to create a seal[159] of resistance of around 10-100 gigaohms. The gigaohm seal reduces experimental noise and enables recordings of picoampere currents.[160] Unfortunately, patch clamp recordings are difficult to perform and this technique requires a skilled operator. High demand for the patch clamp technique

http://rcin.org.pl

in pharmaceutical sector led to automation and development of high throughput patch clamp platforms capable of acquisition of several thousand data points per day.[161,162] Improvement of the throughput of recordings resulted in a decrease of quality of measurements making them less useful. High-throughput patch clamp measurements do not provide much more information than IC_{50} values collected for a whole cell, and they are not as informative as recordings carried out on single ion channels.[163] Furthermore, there are significant cell-to-cell variations due to over-expression of the target proteins in selected cell lines.[164]

1.4.1.1 Formation of planar bilayers

A method of protein testing on *in vitro* assembled model lipid bilayers is an interesting alternative for patch clamp measurements, especially for detailed characterization of the physiology of membrane proteins and the kinetics of inhibition and molecular transport through protein nanopores. Currently, the most widely used approach for formation of artificial membranes is a method called black lipid membranes (BLM) suggested by Montal and Mueller in the 1960s and 1970s.[165–167] A lipid bilayer is formed over a Teflon aperture with a diameter in the range of 50-100 μm (Fig. 7A). The correctly reconstituted lipid bilayer caused the interference of the incident light and thus the membrane is visible as a black or gray spot in the microscope view. The main drawbacks of the BLM technique are the limited stability and the short lifetime of 5 nm-thick and delicate bilayer.[157,166] Formation of supported bilayers on a solid substrate[168,169] solves the problem of limited stability of a membrane (Fig. 7C). Unfortunately, supported bilayers suffer from undesired interactions of analyzed proteins and lipids with the solid support.[170]

Another widely used method of membrane reconstitution is performed via the use of large liposomes (called also giant unilamellar vesicles – GUVs). Solution containing GUVs is aspirated by a glass patch micropipette and then single vesicle breaks upon the contact with the tip of the micropipette.[158] The inlet of the micropipette is immediately blocked by newly formed lipid bilayer (Fig. 7B).

http://rcin.org.pl

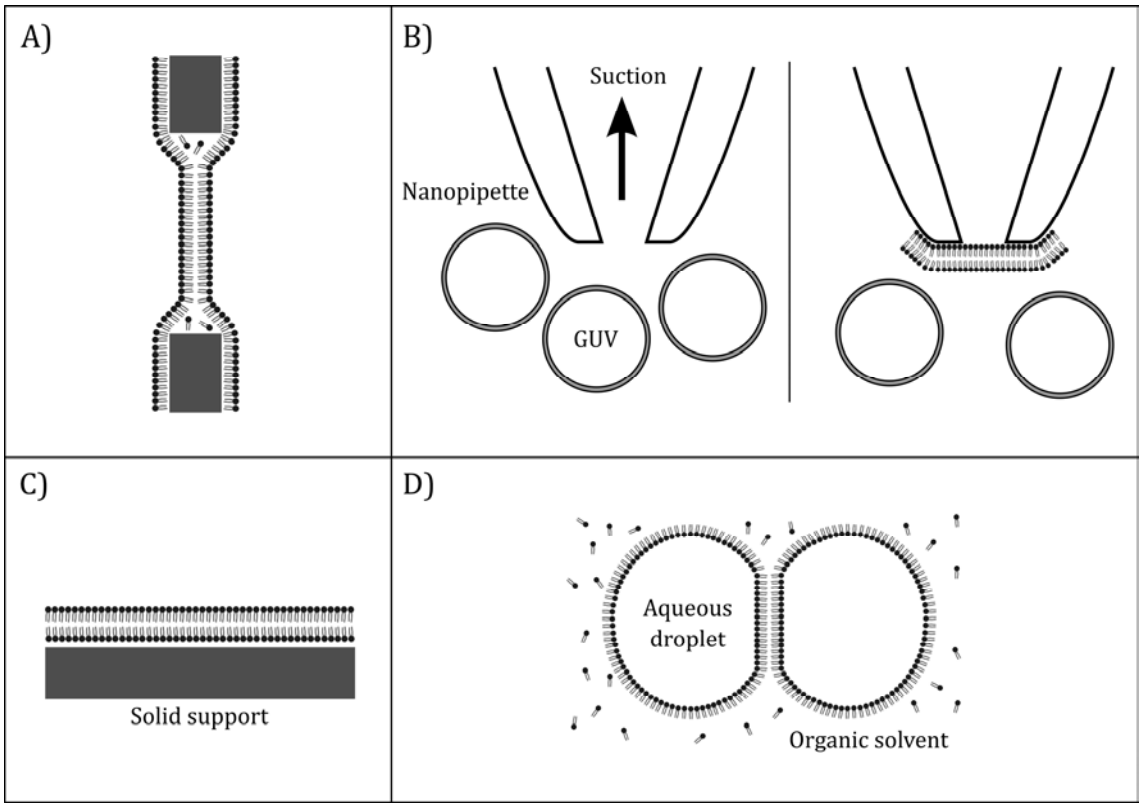


Fig. 7 A scheme presenting different experimental approaches for formation of a model lipid bilayer. A) A black lipid membrane formed over orifice in thin Teflon film B) A sketch depicting the process of formation of a bilayer by suction of GUVs to the patch pipette C) A model bilayer on a solid substrate D) Droplet interface bilayers. Lipid molecules and GUVs are not drawn to scale.

Lipid membranes can be also formed at the interface of two aqueous droplet submerged in oil with dissolved lipid molecules (Fig. 7D). This method called droplet interface bilayers (DIB) was presented for the first time in 1966 by Tsofina *et al.,*[171] but its development was not pursued further. In mid 2000s the method was rediscovered by research groups of prof. Bayley[172,173] and prof. Takeuchi.[174] The most important feature of DIBs is the exceptional stability that supports long-term measurements and minute, microliter consumption of samples. The method also enables formation of asymmetric bilayers (whose both leaflets have different chemical compositions) and droplet networks for power generation and light sensing.[172] The stability of the interface and the possibility to easily re-form the bilayer make the DIB method an attractive and robust strategy for implementation in inhibitor screening schemes.[172,175] Measurement of ion current through proteins embedded in DIBs can be executed by electrodes inserted into droplets. However, the DIB technique has not been yet commercialized, probably due to challenging handling and assembly of nanoliter droplets.

http://rcin.org.pl

1.4.1.2 DIBs in microfluidics

Droplet microfluidic seems to be perfectly suited for generation of droplet interface bilayers. Indeed, one of the pioneering demonstrations was carried out on a microfluidic chip. Funakoshi *et al.* presented a device[174] in which the bilayer was formed at the interface of two aqueous streams surrounded by an organic phase with dissolved lipid molecules. Formation of a functional membrane was followed by electrophysiological measurements of ion currents flowing through α-hemolysin nanopore[176] – a toxin from bacteria *Staphylococcus aureus*. Since then, the DIB method was used in various microfluidic platforms and proved to be useful in studies of other proteins, e.g. bacterial potassium channels,[177,178] eukaryotic mammalian menthol receptors[179,180] or hERG potassium channel.[181] So far, many microfluidic platforms have been developed for formation of DIBs.[177–180,182–193] All droplet microfluidic chips capable of electrophysiological measurements are single-use devices and they do not possess possibility of serial and automated formations of lipid bilayers. On the other hand, there are microfluidic systems in which up to several thousands of bilayers are formed simultaneously.[194–198] However, these systems rely solely on measurements of fluorescence that do not allow for detailed characterization of the function of the membrane proteins.

1.4.2 PCR

1.4.2.1 Introduction to PCR

Polymerase Chain Reaction (PCR) is one of the most important and the most widely used assays in molecular biology, biochemistry and medical diagnostics.[199–202] The reaction relies on *in vitro* amplification of a target region of DNA (often called amplicon) which length ranges from ca. one hundred to several thousand base pairs. Copies of amplicon are synthetized by thermostable enzymes – polymerases – originally isolated from thermophilic bacteria.[203,204] The reaction is usually conducted in dedicated devices - thermocyclers that provide rapid temperature changes needed for the execution of the assay. Very high specificity of PCR is ensured by a pair of primers – short DNA oligonucleotides that determine the length of the amplicon.

http://rcin.org.pl

Typical PCR consists of 30-45 cycles and each of them is composed of 3 steps conducted in different temperatures:

1. Denaturation – the hydrogen bonds in DNA are disrupted at 95 ^{o}C and the double stranded target is melted to two single strands.
2. Annealing – the primers bind to the 3' ends of each strands of the target sequence at temperature between 50 ^{o}C and 65 ^{o}C – depending on the length and the sequence of the primers.
3. Extension – polymerases bind to the primers and synthetize the complementary strand in 5' to 3' direction by condensation of free nucleotides (deoxynucleoside triphosphates - dNTPs) on the 3' end of the primer. This step is conducted at 72 ^{o}C in the case of the most commonly used Taq polymerase (an enzyme originally isolated from the bacterium *Thermus aquaticus*).

1.4.2.2 Preparatory PCR in microdroplets

Implementation of PCR in microdroplet format has been, so far, the biggest scientific and commercial success of droplet microfluidics. Performing PCR in microdroplets brings several unique advantages:

- Minute volumes and compartmentalization in thermostable emulsions allow for high-throughput operation and simultaneous execution of a reaction in thousands[31,112] or even millions[33,205] of droplet compartments.
- Each compartments might contain no more than one molecule of target DNA – this feature opens new possibilities of quantitative assays (see chapter 1.4.2.4).
- PCR can be executed on a single-cell level, thus providing a tool for profiling and analysis of heterogeneous tissues.[61,206]
- Droplets can be transported between zones of various temperatures[113,207] which results in the reduction of reaction time, since the operation of active cooling is not needed – on the contrary to classical PCR conducted in tubes or multi-well plates placed inside standard thermocyclers.

One of the first applications of droplet PCR was a preparatory amplification of DNA for second generation sequencing. This method, developed and commercialized by Raindance Technologies, allowed for non-biased amplification of multiple fragments of a genome. The technique is based on encapsulation of several

http://rcin.org.pl

thousand primer pairs in picoliter droplets, so that each droplet contains only one type (a single pair) of primers. Droplets with various primers pairs are next fused with drops containing genomic DNA and pooled together in a tube. There are several thousand different PCRs executed in a single tube, but in each droplet only one region of the genome is amplified, so there is no competition between various reactions. As a result, different regions of the genome are equally amplified. This method provides the unique preparatory step for sequencing of minute amounts of DNA isolated from rare cells e.g. subtypes of cancer tissue.

Another example of the droplet preparatory PCR is an isolation of single-cell genomes by the presence of a selected genomic feature e.g. mutation or polymorphism.[61,206] In this method, single cells are first encapsulated in droplets and then lysed. Next, PCR is performed and in the final step positive droplets (containing amplified target sequence) are sorted out for further analysis e.g. DNA sequencing.

1.4.2.3 Quantitative PCR

Quantitative reactions are currently the largest segment of PCR-based technologies, by the importance of applications and by the market value.[208] Quantitative PCR is a method used in research for the assessment of gene expression level[202,209] and in medical diagnostics for the detection of early stages of cancer[201,210] or infection[199,200,211] Quantitative PCR is also utilized for the evaluation of the progress of a disease and the efficiency of the therapy. Current golden standard is a real-time PCR (commonly called also qPCR)[212–214] that is based on the measurement of the increase of fluorescence intensity *'in real-time'* – in practice after each cycle. The fluorescent signal is generated by fluorogenic reporters released from sequence-specific molecular DNA probes or emitted by non-specific dyes intercalating into double stranded DNA.

The real-time PCR is widely used in research and medical diagnostics, however this technique poses several disadvantages and limitations:

- The amplification in PCR is an exponential process and absolute quantification is performed by comparison of the fluorescence intensity measured for a sample with the intensities measured for DNA reference standards of known concentration of a target sequence. This strategy provides limited precision

http://rcin.org.pl

(RSD is higher than 60% during quantitative measurement of DNA concentration[112]). The precision of real-time PCR can be further decreased by impurities present in a sample that inhibit polymerase and thus disturb exponential amplification.

- Due to exponential nature of the reaction, only two fold differences in amplification can be distinguished– consequently real-time PCR should not be used for comparison of similar DNA concentrations (within the same order of magnitude).
- The reaction cannot be used for detection and quantification of rare amplicons in a sample containing higher concentration of similar sequences. This phenomenon can be explained by non-specific binding of the primers to the background DNA. For example, mutated oncogenic DNA cannot be detected in early stages of cancer because DNA from cancer cells are rare, yet has similar sequence comparing to the wild-type DNA from health tissues.
- Measurement of fluorescence has to be sensitive, precise and integrated with thermocycling. Therefore, instruments for real-time PCR are bulky and expensive.

1.4.2.4 Droplet digital PCR

Restrictions of real-time PCR led to development and implementation of digital PCR: a new approach for quantification of nucleic acids. In digital PCR a sample is randomly partitioned into many subvolumes (compartments). Number of compartments should be much higher than concentration of DNA, so that according to Poisson distribution, each subvolume contains either '0' or '1' DNA molecule (Fig. 8). Next, classical PCR reaction is performed and in the final step qualitative endpoint measurement of fluorescence is conducted for each compartment. For measured value ***x*** defining the number of positive reactions and knowing number ***N*** of all compartments, the initial concentration of DNA can be calculated according to the following formula:

$$c = N \cdot \lambda = N \cdot \ln\left(\frac{N}{N-x}\right),$$

where $\boldsymbol{\lambda}$ defines the average number of DNA copies in each compartment before the reaction.

http://rcin.org.pl

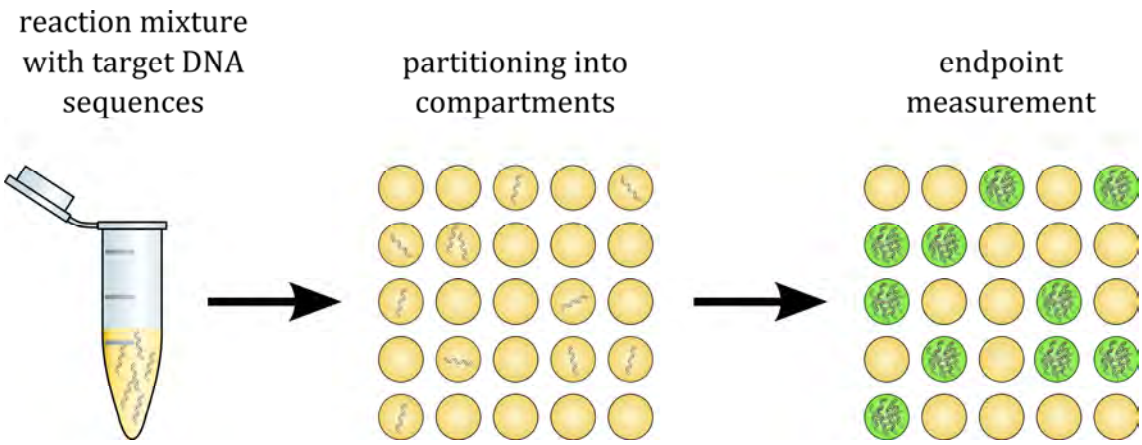


Fig. 8 A scheme with the overview of droplet digital PCR.

Digital PCR turned out to be a substantial improvement for the absolute quantification of DNA due to a 10-fold increase in precision comparing to real-time PCR.[112] Moreover, dPCR does not require preparation of a calibration curve and can be used for detection of rare amplicons.[32] Miniaturized multiwell plates,[215] Slipchips,[216,217] microcapillaries[218] and microfluidic chambers[9,10,219,220] were initially used as compartments in digital PCR, but currently single-phase platforms are being replaced by droplets. Using droplets is advantageous in terms of simplicity of generation of large number of compartments and ease of the high-throughput measurement. Fluorescence of droplets can be efficiently measured with kHz frequencies.[76,221] Droplet digital PCR was successfully commercialized by Bio-Rad[31,112] and Raindance Technologies.[33,205] Academic demonstrations proved that this technology can be useful for detection of mutation in oncogenes,[32] determination of viral load in a blood sample[217] and for analysis of genetic polymorphisms such as copy number variation (CNV).[31,222,223] The main restriction of the method is a challenging analysis of larger concentrations of DNA. Usually, a single sample is partitioned to up to 20 thousand droplets. Generation of millions of droplets is possible in some ddPCR instruments,[33] but this process is cost- and time-consuming. Moreover, droplet digital PCR is not compatible with simple devices for point of care (POC) diagnostics – an important segment of the PCR market.

http://rcin.org.pl

2. MATERIALS

This chapter provides a brief description of materials used for experiments presented in the dissertation. Section 2.1 presents details concerning various oils and surfactants used as a continuous phase. Next, the polymers used for fabrication of microfluidic devices are described (Section 2.2). The successive sections (2.3, 2.4, 2.5, 2.6) briefly report the other reagents and buffers used in biochemical and microbiological experiments.

http://rcin.org.pl

2.1 Oils and surfactants

- In section 4.1 describing the microfluidic system for determination of MIC, the continuous phase was composed of 50% (w/w) Novec HFE-7500, 49.6% (w/w) FC-40 (both acquired from 3M, United States) with 0.4% (w/w) perfluorooctanol (Alfa Aesar, Germany).
- In the project describing the process of bacterial adaptation in microdroplet chemostats (section 4.2) we used hexadecane (Alfa Aesar, Germany) with 0.4% (w/w) Span80 surfactant (Sigma Aldrich, Germany).
- For the formation of droplet interface bilayers (presented in section 4.3) we used mixture of oils containing phospholipid as a continuous phase. The oil mixture was prepared as follows: 200 mg of lipid 1,2-diphytanoyl-*sn*-glycero-3-phosphocholine - DPhPC (Avanti Polar Lipids, United States) was dissolved in 10 mL of chloroform (Chempur, Poland). The chloroform was evaporated under vacuum and the lipid film was re-solubilized in a mixture of 75% (v/v) hexadecane (Sigma Aldrich, Germany) and 25% (v/v) silicone oil AR20 (Sigma Aldrich, Germany).
- In the research presented in Section 4.4 entitled *Generation of libraries of nanoliter droplets and application of this technique for improved DNA quantification with digital PCR*, the following mixtures of liquids served as a continuous phase:
  - Paraffin oil Pionier 7467 (Hansen & Rosenthal KG, Germany) with 0.5% or 2% (w/w) Span 80 surfactant (Sigma-Aldrich, Germany) was used for experiments carried out in polycarbonate chips.
  - In case of PDMS chips we used perfluorocarbons HFE-7500 and FC-40 (both acquired from 3M, United States) with 0.5% or 3% (w/w) PFPE-PEG-PFPE surfactant. Triblock surfactant PFPE-PEG-PFPE is a copolymer composed of perfluoropolyether PFPE (Krytox FSH, DuPont, United States) with the average molecular weight of 7 kDa and of polyethylene glycol PEG (Sigma Aldrich, Germany) with the average MW of 600 Da. The chemical synthesis was conducted by Chemipan R&D Laboratories (Poland) according to the procedure described by Holtze *et al.*[39]

http://rcin.org.pl

- In the part of the dissertation describing droplet digital PCR (section 4.4.2), the commercial liquid *Oil for Probes* (Biorad, United States) served as a continuous phase.

2.2 Polymers – materials used for the fabrication of microfluidic chips

Two types of polymers were used for fabrication of microfluidic chips:

- Polycarbonate - PC (Macrolon®, Bayer, Germany) was used in the projects requiring automated control of flow with external valves. Stiffness of PC thermoplastic polymer enabled for precise and rapid control of flows "on demand" in methods for generation of nL droplet libraries, formation of lipid membranes and studying bacterial adaptation in microdroplet chemostats.
- Poli(dimetylosiloksan) - PDMS (Sylgard 184, Dow Chemicals, Unites States) – elastomer characterized by better optical properties than polycarbonate. After activation in plasma, PDMS can be easily bonded to a glass slide and the chip can be used for precise microscope measurements. The surface of PDMS can be efficiently modified with fluorosilanes[27,94,100] to become highly hydrophobic and next used for formation of aqueous droplets in biphasic microfluidic systems. PDMS is not compatible with most of mineral oils due to swelling,[224] but it can be used with fluorocarbon liquids.[224]

2.3 Materials for microbial experiments

2.3.1 Media for bacteria culture

In microbial experiments we used three types of rich media in liquid form:

- MHB - Mueller Hinton broth (Becton Dickinson, United States) – medium recommended for antibiotic susceptibility testing by Clinical and Laboratory Standards Institute.[137,138] The broth was autoclaved in 121 ^{o}C for 15 minutes.
- LB - Lysogeny broth (Becton Dickinson, United States) - LB consists of 0.5% (w/v) yeast extract (Becton Dickinson, United States), 1% (w/v) tryptone (Becton Dickinson, United States) and 1% sodium chloride (Sigma-Aldrich, Germany). We adjusted LB broth to pH=7 using a 1M solution of sodium hydroxide (POCH, Poland). The broth was autoclaved in 121 ^{o}C for 15 minutes.

http://rcin.org.pl

- LBK - Potassium modified lysogeny broth. LBK consists of 0.5% (w/v) yeast extract (Becton Dickinson, United States), 1% (w/v) tryptone (Becton Dickinson, United States), 0.64% potassium chloride (Sigma-Aldrich, Germany) and 100 mM of PIPES buffer (Sigma-Aldrich, Germany). We adjusted LBK broth to pH=7 using a 1 M solution of potassium hydroxide (POCH, Poland). PIPES buffer is unstable in higher temperature so we sterilized the medium by filtration with Nalgene® bottle-top sterile filters with pore size of 0.2 μm (Nalgene, United States).

2.3.2 Bacteria cells

As a model organism we used *E. coli* strain ATCC 25922, kindly provided by the research group of prof. Wojciech Kamysz from Medical University of Gdansk. We prepared stock solution of cells in LB broth containing 30% glycerol (Chempur, Poland) and froze the stocks at -80 ^{o}C. Before performing experiments, we streaked cells on LB agar plates and incubated them overnight. We picked individual colonies, used them to inoculate liquid broth (depending on the experiment: MH, LB or LBK), cultured cells at 37 ^{o}C and 200 RPM overnight, and transferred aliquots to fresh media and grew them until the absorbance reached the value of 0.1 at λ=600 nm. We diluted the culture 100x times (for antibiotic susceptibility testing – section 4.1) or 10x (for long-term cultivation of bacteria – section 4.2) in a fresh medium prior to transferring suspensions into microfluidic device.

2.3.3 Antibiotic solutions

We prepared antibiotic stocks prior to experiments. Chloramphenicol (Roth, Germany) was dissolved in 50% (v/v) aqueous solution of ethanol (POCH, Poland). Ampicillin (Sigma Aldrich, Germany) was dissolved in deionized water to concentration of 100 $g \cdot L^{-1}$. The concentrations of antibiotics in stocks were 500-1000x higher than the concentrations in medium injected to the microfluidic device. We sterilized antibiotic stock solution by filtration. Before each experiment, we diluted antibiotic stocks in liquid broth to the desired concentration and transferred the samples to the inlets of the device. The final concentration of antibiotic was subsequently obtained during the formation and merging of droplets on a chip.

http://rcin.org.pl

2.3.4 Bacteria viability indicator

We used resazurin sodium salt (Sigma-Aldrich, Germany) diluted in MH broth at a concentration of 44 μM as an indicator of cell viability. In order to maintain a constant concentration of resazurin in the incubation mixtures, we added the compound to all solutions introduced into the device with the exception of the suspension of bacteria.

2.4 Protein expression and purification

Alpha-hemolysin nanopore was provided in a frozen form by the group of prof. Hagan Bayley from Oxford University. Wild-type α-HL was expressed in *Staphylococcus aureus*, converted to a heptameric form with membranes from rabbit red blood cells and purified by preparative SDS polyacrylamide gel electrophoresis (SDS-PAGE) as described previously.[225] The stock solution (5 μg·mL^{-1}) was defrosted, kept on ice at all times and diluted 10 times in buffer immediately before introduction into the microfluidic chip. The buffer comprised 1 M KCl and 10 mM Tris–HCl with pH set to 7.0.

2.5 PCR mixtures

The PCR reaction solution consisted of 0.5 μL stock of each primer (at a concentration of 5 μM), 1 μL Taqman® probe (2.5 μM), 10 μL 2X ddPCR Supermix for Probes (Bio-Rad, United States), 2 μL SACT-1 sample at a given concentration and 6 μL of deionized water. Final concentration of each primer and probe was 250 nM.

2.6 DNA sequences

The amplified sequence was a fragment of the conservative gene SACT-1. The forward primer sequence AGAGTTGCCCCAGAAGAACA and the backward primer sequence TCTACGTTTCCATCCAAGCC were used. The sequence of the Taqman® probe was following: FAM-GACTGAAGCTCCAATGAACCC-BHQ1. The probe was labelled with the 6-carboxyfluorescein (6-FAM) dye on a 5’ end and with the black hole quencher (BHQ1) on a 3’ end. The custom synthesis of sequences were ordered from Institute of Biochemistry and Biophysics of Polish Academy of Sciences.

http://rcin.org.pl

3. METHODS

This chapter comprises a short description of procedures and techniques used in the experiments. These methods were developed previously in the Group of Microfluidics and Complex Fluids or by other research teams, however some of the protocols were optimized and improved for the specific purposes of experimental projects presented in this dissertation. Successive sections comprise the description of fabrication of microchips (3.1), tools used for flow control (3.2), methods for manipulation of droplets (3.3) and experimental strategies used for optical interrogation of drops (3.4, 3.5, 3.6). Last two sections present details concerning electrophysiological recordings (3.7) and conditions of thermocycling during PCR (3.8).

Besides these previously known techniques presented in this chapter, the newly developed methods are presented in chapter 4 as the part of the experimental results.

http://rcin.org.pl

3.1 Fabrication of microfluidic devices

3.1.1 PDMS chips

PDMS chips usually comprised a fluidic layer made of elastomer and a 1 mm-thick glass slide. In some devices, thin PDMS slab was used instead of the glass slide. Fabrication of the fluidic layer was as follows: in the first step we fabricated the polycarbonate molds in 5 mm plates of polycarbonate (Macrolon®, Bayer, Germany) using a CNC milling machine (MSG4025, Ergwind, Poland). Next, we poured PDMS (Sylgard 184, Dow Corning, United States) onto the PC chip and subsequently polymerized the mold at 70 ^{o}C for 2h. In the following step, we silanized the PDMS mold during 3h under 10 mbar pressure with vapors of tridecafluoro-1,1,2,2,-tetrahydrooctyl-1-trichlorosilane (Alfa Aesar, Germany). PDMS negative masters were cleaned and used for molding of the positive PDMS replicas that were subsequently bonded with the glass slide by exposing both parts to 30s of O_2 plasma and assembling them together. In the next step, we performed a hydrophobic modification of microfluidic channels by filing the chip with Novec 1720 liquid (3M, United States) for 10 minutes. Next we blew out Novec 1720 with compressed air and let the rest of the fluid evaporate in room temperature. In order to preserve modification, we baked the chip at 135 ^{o}C for 1 h. The microfluidic devices used for formation of libraries of nL droplets were modified by other commercially available liquid called Aquapel (PPG Industries, United States).

3.1.2 Polycarbonate chips

We fabricated polycarbonate chips in 5 mm-thick plates (Macrolon®, Bayer, Germany) using a CNC milling machine (MSG4025, Ergwind, Poland). The milled plates were thermally bonded to flat 2 mm-thick plates by compressing them together in a custom made hydraulic press (for 30 min, at 130 °C and 0.2 MPa). We created the world-to-device interface using 21 gauge needles (~ 4 cm, O.D. 0.82 mm, I.D. 0.65 mm, Fishman Corporation, United States) that were inserted to the inlets and outlets of microfluidic devices. We connected the needles to resistive steel capillaries (O.D. 400 μm, I.D. 205 μm, length 200 cm, Mifam, Poland) extending from the valves using short segments of Tygon® tubing (~ 2 cm, O.D. 0.91 mm, I.D. 0.25 mm, Ismatec, Switzerland).

http://rcin.org.pl

3.2 Control of flow

3.2.1 Control of flow with external valves

Custom written Lab View script controlled external valves (V165, equipped with Z070D coils, Sirai, Italy) via a card NI PCIE-6321 (National Instruments, United States). The valves controlled the flow of oil from pressurized reservoirs (Fig. 9). Oil was pumped from a reservoir, through a polyurethane tubing (I. D. 6mm), then through the valves, the steel capillaries and onto the chip. All aqueous samples were deposited on the chip into long storage channels directly from sterile glass syringes equipped with sample lock termination (model 1750 SL, Hamilton, United States). Once the liquids were deposited on the chip, the flow of oil pushed the samples into the network of fluidic channels. We controlled the pressure applied to the oil reservoirs using manual regulators (Bosch Rexroth PR1-RGP, Germany) and monitored the pressure using digital manometers (AZ 82100, AZ Instruments, Taiwan). Generation of droplets was aided with an edge-detection algorithm to track the process of microdroplet formation and controlled the volume to an accuracy of ~0.3%.[77,83] Merging of droplets was facilitated by using an electrocoalescence mechanism[54,226] by applying AC electric field (500 V, 200 Hz).

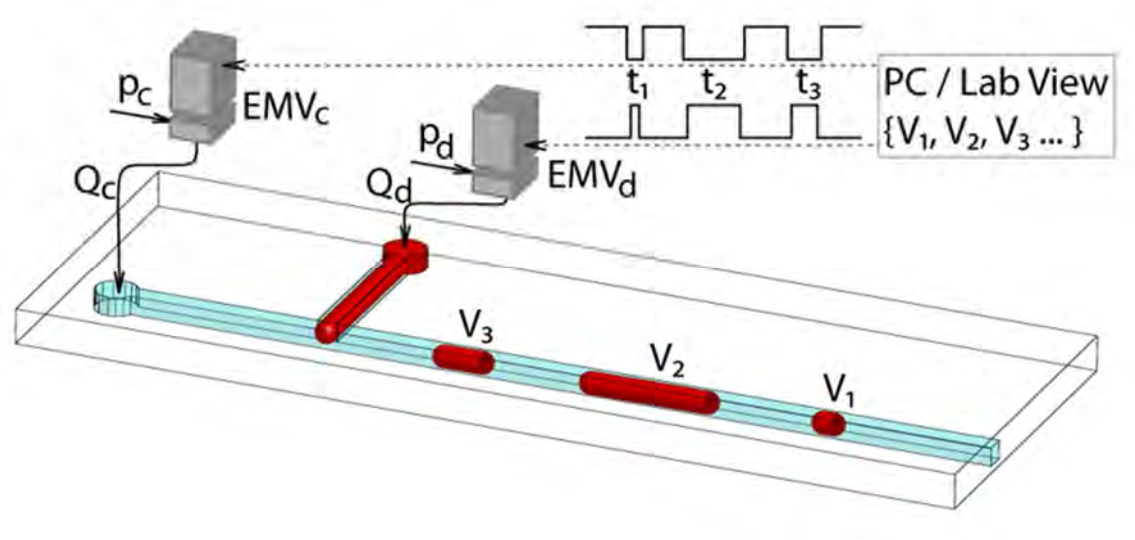


Fig. 9 A schematic illustration of the generation of droplets on demand (DOD) using a system equipped with two electromagnetic valves for the control of the flow. One valve (marked as EMV_c) controls the continuous liquid (drawn from reservoir maintained under the pressure p_c) while other valve (EMV_d) controls the dispersed (droplet) phase (p_d). In our experiments the droplet phase was deposited on a chip in order to avoid passing the fluid through the valve. Image taken from the article published by Churski *et al.*[55]

http://rcin.org.pl

3.2.2 Control of flow with syringe pumps

We used programmable syringe pumps (Nemesys, Cetoni, Germany) as the source of flow. The liquids were delivered using glass syringes (Series Gastight 1000 and 1700, model RN, Hamilton, United States) of the following volumes: 0.25, 0.5, 1.0, 2.5 and 5 mL. The syringes were connected with the chip by PTFE tubings (O.D. 0.9 mm, I.D. 0.4 mm, Bola Bohlender, Germany).

3.3 Methods for manipulation of droplets

3.3.1 Robotic systems and aspiration of droplets from microwell plates

We prepared the sequence of microliter droplets using the automated positioning system (Rotaxys, Cetoni, Germany) coupled with the precise syringe pump (Nemesys, Cetoni, Germany). Droplets were formed inside 0.8 mm diameter fluorinated ethylene propylene (FEP) tubing (Bola Bohlender, Germany) by alternating the aspiration of portions of aqueous samples and oil from a standard 96-well plate (Fig. 10). In order to increase the precision of aspiration we placed a short section of PTFE tubing (Bola Bohlender, Germany) of inner diameter of 300 μm at the end of the 800 μm tubing. Smaller droplets (less than 0.5 μL) were aspirated to PTFE tubing (I.D. 0.3 mm, O.D. 0.6 mm, Bola Bohlender, Germany).

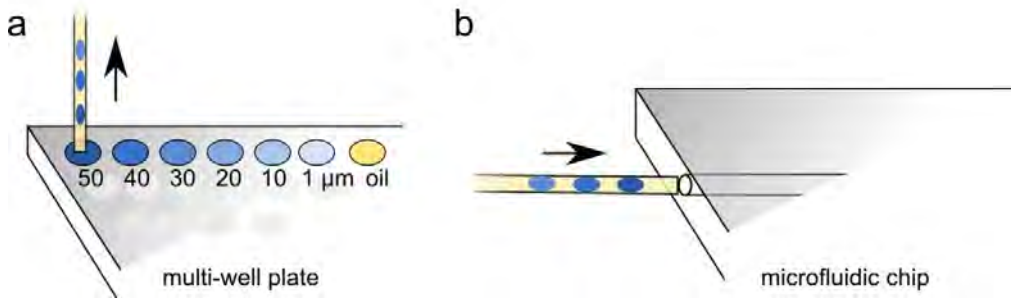


Fig. 10 A schematic illustration depicting the operation of aspiration of droplets from a multi-well plate using the precise syringe pump (Nemesys, Cetoni, Germany) and the positioning system (Rotaxys, Cetoni, Germany). In this example the sequence of droplets containing various concentrations of inhibitors (1 – 50 μm) was stored inside the tubing and introduced onto the chip by applying the flow from the syringe.

We checked experimentally for the potential of cross-contamination between the microliter samples during aspiration from a multi-well plate. In the experiment we prepared sequences of droplets of pure water separated by drops with a set of fluorescein solutions (Sigma Aldrich, Germany) of concentrations ranging from 1 nM

http://rcin.org.pl

to 100 μM. The results (Fig. 11) do not show cross-contamination exceeding the level of 0.1% - even for very high concentration of fluorescein.

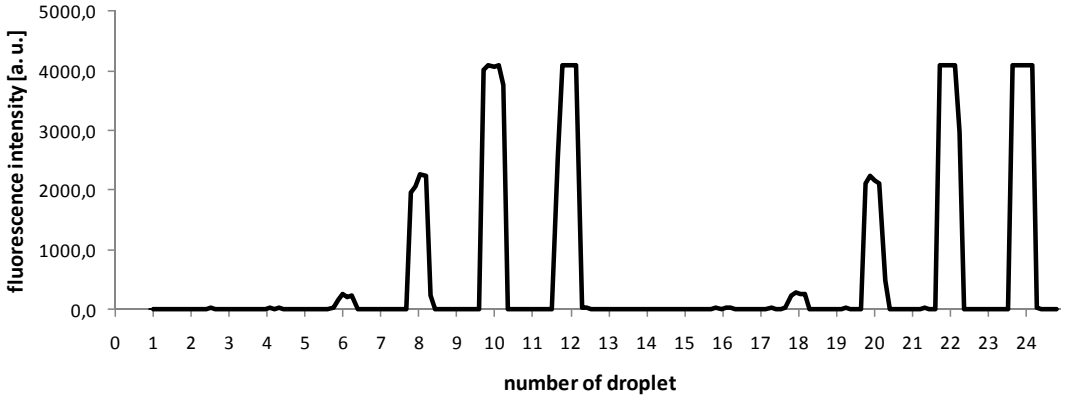


Fig. 11 Intensity of fluorescence from a sequence of 24 droplets aspirated from a multiwall plate. The sequence comprised patterns of 12 droplets: odd droplets contained neat water and even droplets contained aqueous solutions of fluorescein at gradually increasing concentrations: 1 nM; 10 nM; 100 nM; 1 μM; 10μM; 100 μM. We did not observe any fluorescence from the clean droplets and from droplets with concentration of dye lower than 100 nM. Water droplet no 11 which is placed between droplet with highest concentration (no 10 and 12), also does not show fluorescence above the limit of detection for the instrument settings used in the experiment (corresponding to concentration of 100 nM). This suggests that the level of cross contamination is lower than 0.1%. The level of signal from droplet containing 10 μM and 100 μM is equal due to saturation of the detector.

3.3.2 Manipulation of droplets using passive geometries

Some of operations on droplets were carried out using passive modules that can precisely generate micro- and nanoliter droplets and next fuse them, split them and control their position on a chip. The first design of hydrodynamic traps was developed and published by Korczyk *et al.*[105] For the purpose of some of the experiments presented in this dissertation, we improved and modified versions of two passive geometries: the metering and merging traps.

3.3.2.1 Metering trap

The metering trap is presented in a Fig. 12. The length of the metering trap is determined by two bypasses – narrower side sections of the channel that are milled to 25-30% of the depth of the main channel (Fig. 12a). At the terminus of the trap there is an obstacle in the form of a barrier in the main channel that extends upwards to 70-75% of the channel height i.e. the upper surface of the barrier is on the same level as the bottom of the bypasses. A droplet shorter than a trap is locked inside the trap because the flow through the barrier would require unfavorable expansion of

http://rcin.org.pl

the interface and thus increase of the Laplace pressure which is proportional to the sum of the principal curvatures of the droplet. When a droplet longer than the trap reaches the barrier, the rear part of the droplet blocks the entrance to the bypasses. Consequently, the continuous phase cannot flow by the droplet efficiently and pushes the droplet forward until the rear of the droplet aligns with the entrance to the metering trap. At that moment continuous liquid begins to flow around the droplet via the bypasses and the droplet stops. Subsequently the Rayleigh–Plateau instability causes the breakup of the liquid neck at the front barrier, leaving a precisely metered volume of the droplet locked in the metering trap (Fig. 12b).

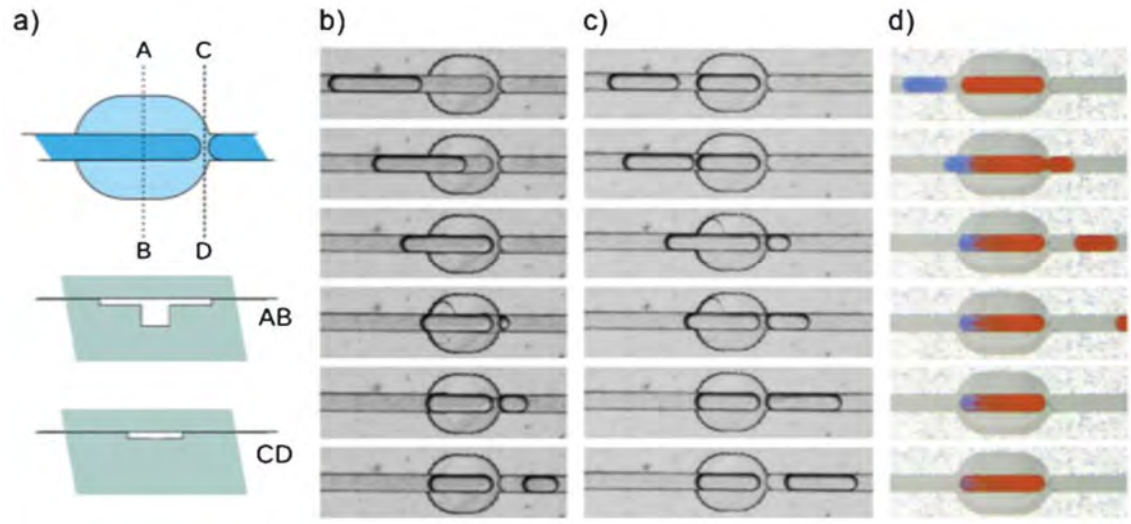


Fig. 12 A scheme depicting the geometry and functionality of the metering trap. a) Architecture of the trap. b) Micrographs illustrating the process of spitting of a droplet longer than a trap. This operation results in metering of the well-defined volume locked in the trap. c-d) Micrographs depicting the process of mass exchange during the flow of the droplet through filled trap. Two droplet fuse, then the excessive volume is released and finally the content of the trap is mixed by the diffusion and convention caused by the flow of the oil. Figure copied from the article published by Korczyk *et al.*[105]

3.3.2.2 Merging trap

The main function of the merging trap is fusion of two droplets, provided that the first droplet is shorter than the length of the trap. The merging trap comprises similar bypasses and obstacle at the terminus of the trap (Fig. 13). However, unlike to the metering trap the obstacle is in the form of side intrusions, not the continuous barrier. Consequently, the squeezed droplet is less deformed and more stable against breakup during the flow through the trap (Fig. 13b). A droplet shorter than the trap is locked in a similar way as in the metering trap (Fig. 13c). Using these

http://rcin.org.pl

properties we can perform the fusion of two droplets – first, short droplet is locked, then another one enters the trap and both droplets merge. If merged droplet is longer than the trap then it is pushed by the oil and leaves the trap without a breakup (Fig. 13c).

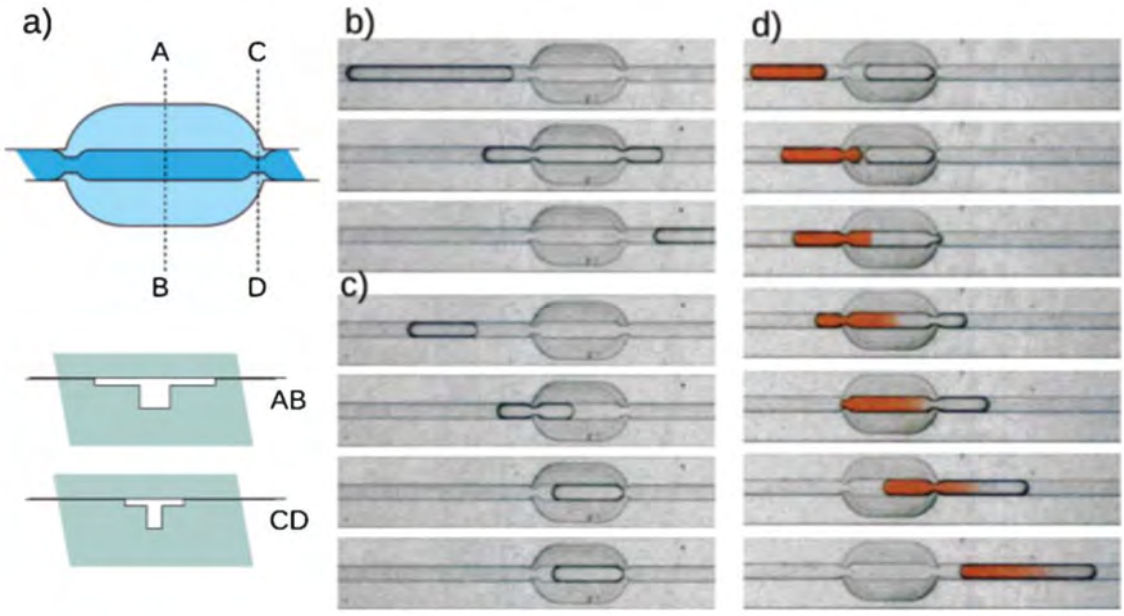


Fig. 13 A scheme depicting the geometry and functionality of the merging trap. a) Architecture of the trap. Micrographs illustrating b) flow of a droplet longer than and c) locking of a shorter droplet. d) Micrographs depicting the fusion of two droplets. Figure copied from the article published by Korczyk *et al* [105]

3.4 Image analysis

The purpose of image analysis was to measure the volume of each droplet generated in a flow focusing junction in the course of splitting of large plug for the generation of droplet libraries (section 4.4). We used ImageJ freeware software (National Institutes of Health, United States) to analyze the video acquired with at high frequency (3 000 fps, shutter set at 0.02 ms) by Fastcam 1024PCI high speed imaging system (Photron, Japan) coupled with SMZ 800 stereomicroscope (Nikon, Japan). In order to quantify the distribution of the volumes of daughter droplets we measured the surface area of the projection of each droplet immediately after the formation in the FF-junction. The outlet of the FF-junction had a height of 100 mm and droplets were slightly squeezed between the top and the bottom wall of the channel. For the sake of simplicity of calculations, we assumed that every droplet has circular planar cross-section. For the purpose of judging the tightness of

http://rcin.org.pl

distribution of the volume of the droplets we used the disc model described previously.[51,227] Briefly, the surface area can be recalculated to the volume by the following formula:

$$v = \frac{\pi}{12}[2D^3 - (D-h)^2 \cdot (2D+h)],$$

where D is the diameter of a disc (droplet) and h is the height of the channel.

3.5 UV-Vis measurement

Microfluidic device for cultivation of bacteria in microdroplet chemostats (section 4.2) contained waveguides (UM22-400, Thorlabs, United States) positioned perpendicularly to the channel that enabled us to record light passing through the droplet with the USB2000+ spectrophotometer (Ocean Optics, United States). The full spectra were acquired at 500 Hz using an optical path (through the droplet) of 5 mm. To monitor the cell density in the microdroplet chemostats, we recorded absorbance at λ=600 nm. Due to the high speed of the signal acquisition by the spectrophotometer we were able to record at least 70 spectra for each droplet as it flowed through the optical path, yielding 0.2% variability in measurements of optical density of microchemostats.

3.6 Fluorescence measurement

3.6.1 Qualitative measurement of fluorescent gradient

We used confocal microscope Nikon A1-R (Japan) in order to assess the quality of the gradient in a series of droplets. We used 10 μM rhodamine 110 (Sigma Aldrich, Germany) dissolved in a reaction mixture. The ratio of values of fluorescence intensity signals at 488 nm wavelength for two successive droplets indicated the dilution ratio. We repeated the measurement for all measured droplets. In order to collect the values of fluorescence intensities over nearly 3 orders of magnitude, we set the laser power so that the fluorescence intensity of the first droplet is just below the limit of the dynamic range of the detector of the microscope. Then we measured the fluorescence intensities of the first 7 droplets. Then we set the laser power so that the 6th droplet in the sequence had a fluorescence intensity just below the limit of the dynamic range of the microscope. We then measured fluorescence intensities of droplets no. 6 to 12. Next, we combined the data from both measurements by proportionality based on the overlapping data for droplets 6 and 7. Values of fluorescence were subtracted by the auto-fluorescence of droplet without

http://rcin.org.pl

rhodamine. Concentrations of rhodamine 110 higher than 10 μM did not give linear response of the fluorescent signal. For concentration smaller than 10 nM the experimental noise and dye photobleaching considerably influenced the measured fluorescence. In practice, 2-fold decreasing fluorescence of 10 to 12 droplets can be measured using this approach.

3.6.2 Measurement of fluorescence using gel imaging system

In order to measure results of antibiogram assay we performed the readout of the fluorescence signal using Gel Doc XR System (Bio-Rad, United States). We excite fluorescence of droplets using UV light passing through XcitaBlue Convertion Screen (Bio-Rad, United States). The emission filter enable for acquisition of signal in the range of wavelengths between 460 and 700 nm. Image analysis and signal quantification was performed with Image Lab™ software (Bio-Rad, United States).

3.6.3 High-throughput measurement of fluorescent droplets

We used confocal microscope Nikon A1-R (Japan) for high throughput measurement of fluorescence in each droplet flowing through the detection spot (Fig. 14). We used the 488 nm argon laser for excitation and we collected the fluorescent signal at a wavelength range of 500-550 nm. We set the microscope to the resonant mode with line scan that enabled us to collect the fluorescent signals with ca. 15 kHz. Each data point used for further analysis an average of 8 acquired signals.

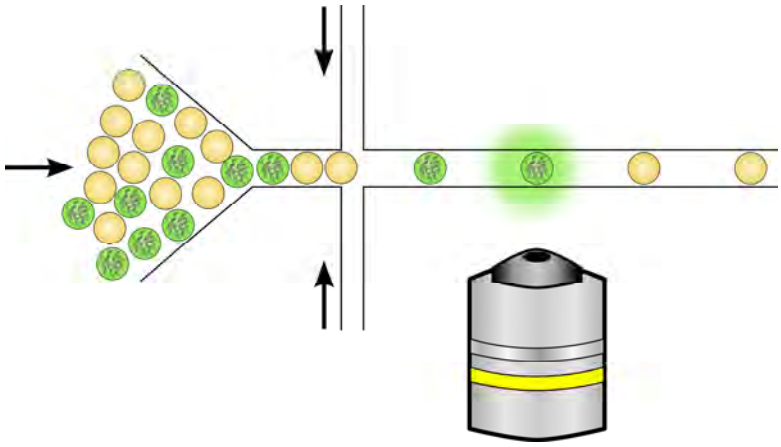


Fig. 14. A schematic illustration presenting experimental approach for high-throughput measurement of fluorescence in nanoliter droplets. Arrows indicate direction of the flow of oil.

http://rcin.org.pl

3.7 Electrophysiological recordings

For electrochemical measurements we used Ag/AgCl electrodes, prepared as follows: pieces of 100 μm-wide silver wire (Sigma Aldrich, Germany) were treated overnight (12 h) with sodium hypochlorite solution (Sigma Aldrich, Germany). The tips of the electrodes were submerged in melted agarose (1% w/v, Roth, Germany) diluted in 1 M KCl and 10 mM Tris-HCl (pH 7.0) buffer (both acquired from Sigma Aldrich, Germany). The AgCl and agarose coatings allowed for sufficient wetting and electrical connectivity when the chip was tested intensively over a period of 3 weeks.

We used Axopatch200B patch-clamp amplifier (Molecular Devices, United States) for recording of the electrical current, which was acquired with a 1 kHz low-pass Bessel filter at a sampling rate of 10 kHz. The electrical recordings were post-filtered with a 400 Hz Gaussian filter for the analysis of single channel and measurements of capacitive current. We also used 100 Hz filter for preparation of displays. The analysis of electric current traces was performed in Clampfit 10.3 software (Molecular Devices, United States).

3.8 PCR thermocycling

Prior to PCR, the reaction mixture was placed in 96-well PCR plates (Eppendorf, Germany) or 0.2 ml PCR tubes (Eppendorf, Germany). PCR was carried out using TC-5000 thermocycler (Techne, Great Britain). We set the following reaction protocol: 10-minute initial enzyme activation in 95^{o}C, followed by 40 cycles of 30-second denaturation at 94 ^{o}C and 60-second annealing/extension in 55^{o}C. After the last cycle, the final extension was applied for 10 minutes in 98 ^{o}C and the plate was cooled down to 4 ^{o}C.

http://rcin.org.pl

4. RESULTS

The results are arranged in four sections.

The first section (4.1) of this chapter provides description of the passive microfluidic system for generation of serial dilutions and execution of a protocol for antibiotic susceptibility testing while being operated only with manual pipettes.

The automated systems for cultivation of microorganisms in tens to hundreds of microdroplet chemostats in parallel and over extended periods of time is presented in section 4.2.

Section 4.3 presents the system that synergistically combine automated microfluidics and the technology of passive hydrodynamics traps for screening of membrane protein activity. The automated microfluidic device presented here is capable of formation of a lipid bilayer at the interface between two aqueous microdroplets submerged in oil and current measurements at the level of single protein nanopore incorporated into the membrane.

Finally, in section 4.4 the technology of automated droplet libraries is presented. This technique, along with active liquid handling with syringe pumps and methods of passive hydrodynamic traps can be applied for determination of high DNA loads using droplet digital PCR.

http://rcin.org.pl

4.1 Determination of MIC in five pipetting steps: precise dilution assays in submicroliter volumes with a conventional pipette.

In this section we demonstrate a microfluidic system that passively automates a common laboratory liquid handling protocol. The system reduces the number of manual pipetting steps to a minimum required to deliver the sample and reagents. The technique offers precision in handling nano-liter volumes while not requiring neither skill nor precision in using a common pipetting tool to operate the microfluidic chip.

Vast majority of chemical, biochemical and microbial assays use liquids. A large fraction of these tests are commonly executed manually via multiple pipetting steps. For example an antimicrobial assay that determines the MIC (minimum inhibitory concentration) of an antibiotic against a given bacterial sample is performed by growing bacteria in a range of dilutions of an antibiotic. Preparation of this assay requires a large number of pipetting steps, equal to a multiple of the number of dilutions.[137,138] For example, in order to prepare 11 dilutions the technician must perform at least 33 manual pipetting actions (Fig. 15a). Many sites, both in the rich and in the developing countries, do not have access to commercial automated systems. A viable question arises if it is possible to design disposable microfluidic chips that would minimize the number of manual operations while maintaining at least the precision and flexibility of standard protocols (Fig. 15b).

We demonstrate a microfluidic chip for standard microbial susceptibility testing. Execution of the test with our chip requires just five pipetting steps: three for the deposition of aqueous solutions: bacterial culture, antibiotic solution and pure broth. The final two operations are required to drive the flow in the chip: the first one for metering of equal volumes of bacterial culture and the second for metering the subvolumes of pure medium broth and for diluting the antibiotic. In the final step the droplets containing bacteria autonomously merge with droplets comprising gradually decreasing concentration of the antibiotic.

http://rcin.org.pl

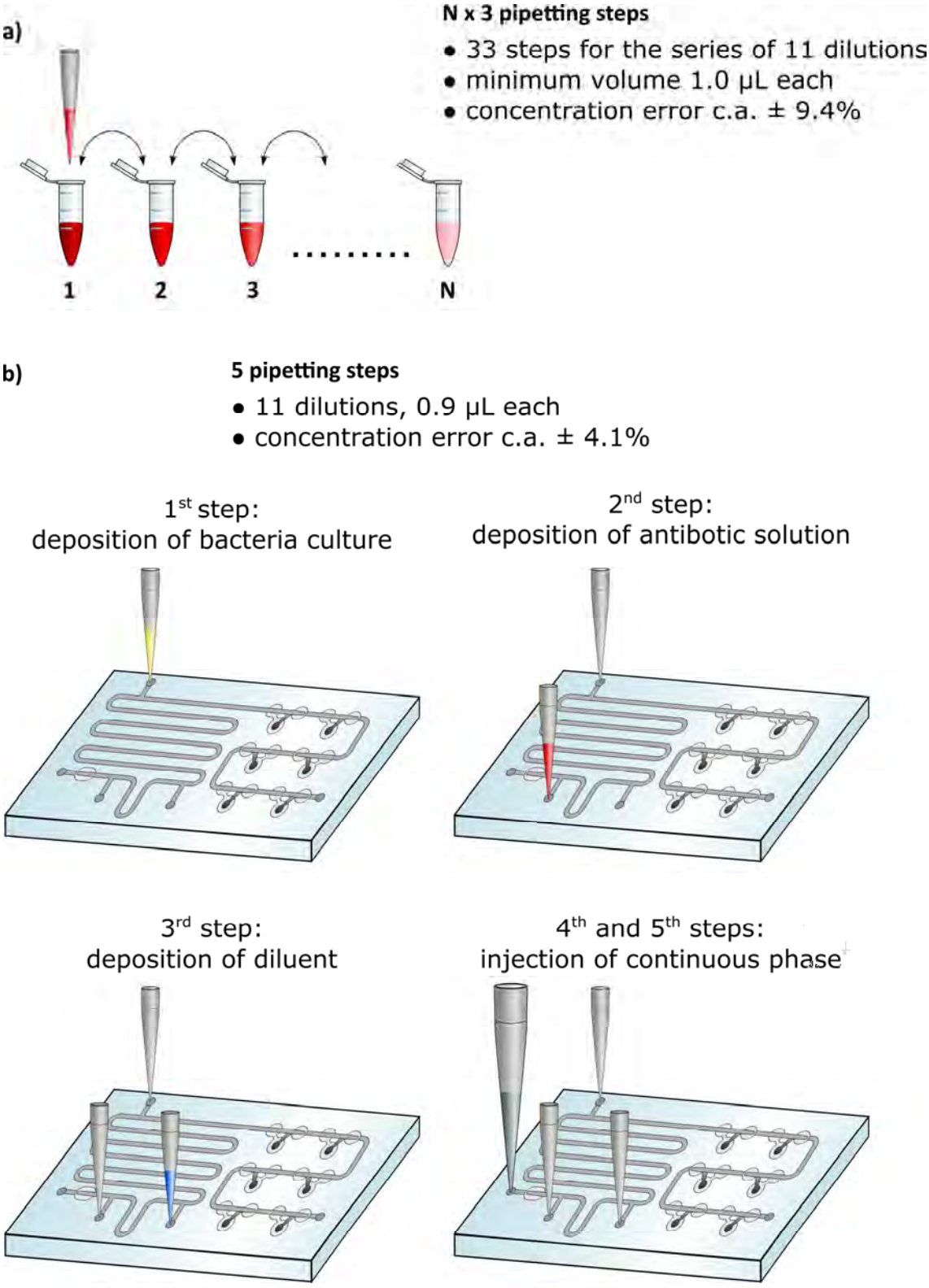


Fig. 15 The comparison of a classical way of testing the antibiotic susceptibility with dilution in a passive droplet microfluidic device. A) The *'golden standard'* method requires 3N pipetting steps: aliquoting of pure broth in each tube, dilution of antibiotic, addition of bacteria liquid culture. B) The microfluidic device requires 5 pipetting steps, regardless of the total number of dilutions.

http://rcin.org.pl

4.1.1 The Meter and Store (M&S) module

The functionality of the device is based on the unique geometries of hydrodynamic traps that passively meter, merge, route and lock nanoliter droplets. The basic functional unit of our system is a Meter&Store module (Fig. 16).

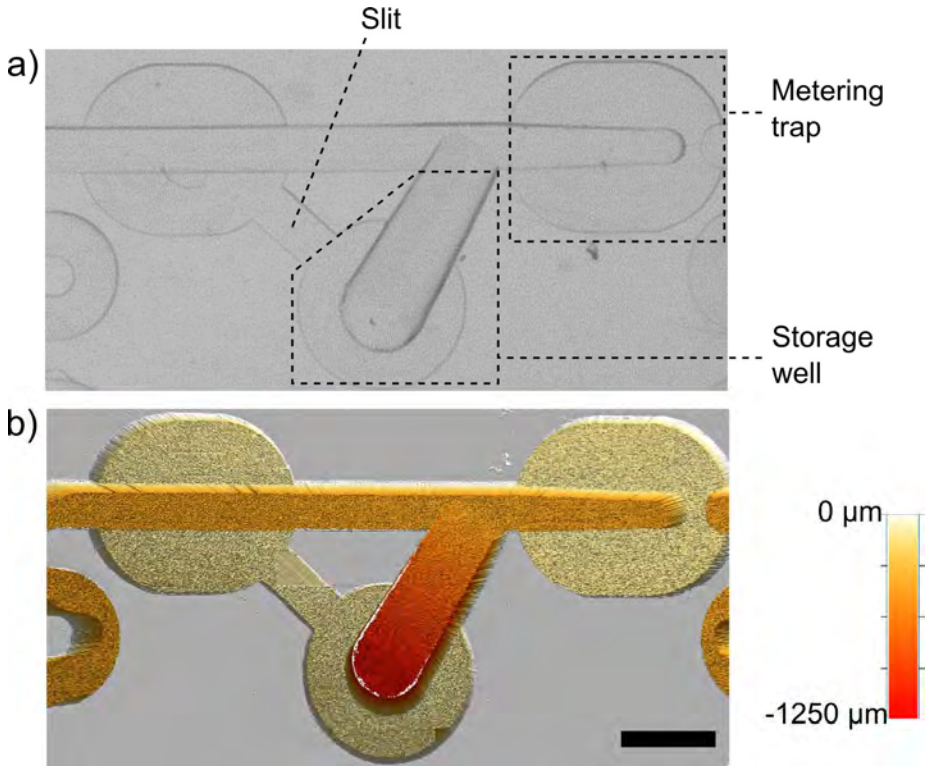


Fig. 16 A single unit of the Meter&Store module. A) Snapshot of the module that comprises the metering trap with narrowed front, the storage chamber connected with the slit to the main channel. B) Image from the optical profilometer (Brücker ContourGT-K, Germany) showing the 3D geometry of the module. Scale bar is 1mm.

Each of these units serves as an autonomous droplet handling module that precisely meters the droplet phase into a pre-defined volume, allows for exchange of the trapped droplet in a dilution scheme, and after switching the flow off, stores the metered aliquot in the side chamber. The unit comprises a metering trap[105] that is able to precisely meter a tiny volume of a liquid. (Fig. 16a) The general design and functionality of the metering trap is described in methods section 3.3.2. In the system presented here, we used the enlarged trap (channels 500x500 µm) with modified geometry. Comparing to the basic architecture of the metering module,[105] here the trap comprises progressively narrowing main channel from 500 µm at the entrance to a width of 375 µm at the terminus that aligns with the barrier. The 25% reduction of the width of the main channel produces a higher curvature of the interface at the front of the droplet than at its rear. When the flow is stopped the

http://rcin.org.pl

droplet minimizes its surface energy by leaving the trap in reverse direction. Another modification is the addition of the storage well (Fig. 16) that is gradually widening and deepening away from the main channel. When the flow is stopped, the droplet metered in the trap starts to flow spontaneously towards the storage well within ~30s due to the action of the capillary pressure (higher at the front of the droplet than at its rear). The storage chamber has the second connector (marked as 'slit' in Fig. 16a) with the main channel. This slit allows for drainage of the side chamber when a droplet flows into it.

Fig. 17 shows the process of formation of a gradient in two successive M&S modules. In the first step a large yellow plug of 0.01% (w/w) solution of tartrazine (Sigma Aldrich, Germany) representing the *sample* is metered into micro-aliquots of tightly predefined volume in the successive metering traps (Fig. 17a-c). Next, the flow of oil is halted and the newly formed droplets of sample are derailed to the storage wells (Fig. 17d). We use the term *sample* as an equivalent of a stable component of the assay - e.g. bacterial suspension. In the following step, two plugs are injected into the system. First, a large blue plug of 0.001% (w/w) resazurin (Sigma Aldrich, Germany), represents the *diluent* and the second smaller (red) plug of 0.05% (w/w) Congo Red (POCH, Poland) models the *reagent* – e.g. an antibiotic. As the large blue plug flows through the M&S units, it is portioned into the micro-aliquots in the metering traps (Fig. 17e). As we do not stop the flow of oil, these droplets do not flow back into the store chambers, but are immediately merged with the reagent plug that has a larger volume than metering trap. The reagent plug merges with the droplet of diluent locked in the metering trap and pushes out a plug that has a volume equal to the initial volume of the reagent, yet is composed of both the reagent and the diluent liquids. The droplet comprising both solutions flows in the winding channel towards the next M&S units and its content is mixed by convection.[228] The operation of dilution is repeated in the successive ten M&S modules. In the final step, the flow of continuous phase is switched-off again and the droplets of diluted reagent are derailed to the storage well (Fig. 17g). There, they merge with already locked sample droplets (Fig. 17h). This step initiates the reaction.

http://rcin.org.pl

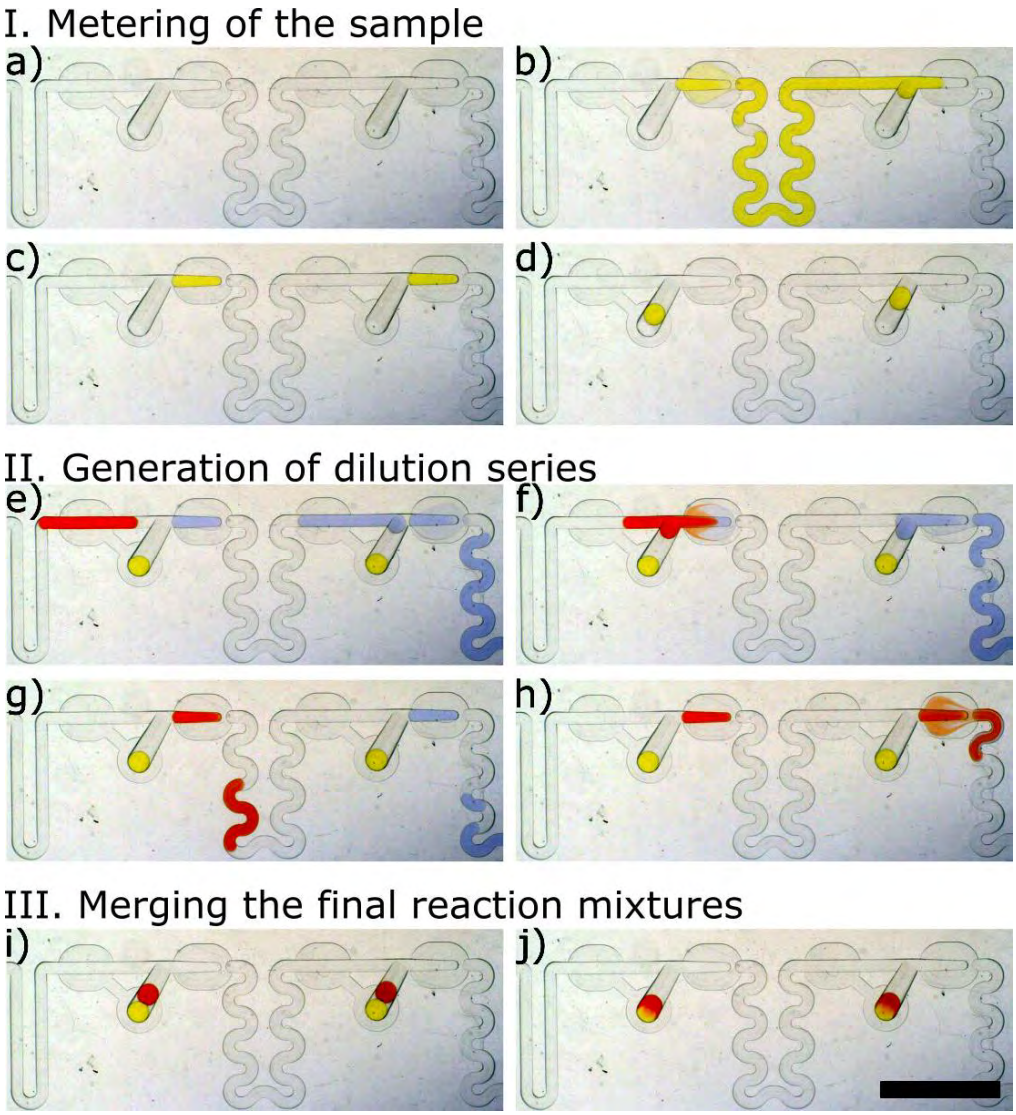


Fig. 17. Two subsequent Meter&Store modules handling module. Micrographs a) through j) illustrate the metering, dilution and storage of microdroplets in side chambers: a) empty modules filled with continuous phase, b, c) metering of the sub-volume of the first sample – stable component of the assay, d) derailing of the droplets with first component to the storage chamber, e-h) metering the second component (buffer) and dilution of the sample. Derailing i) of droplets with diluted sample to the storage well and j) merging with the first component. Scale bar is 5 mm.

4.1.2 Passive microfluidic system for antibiotic susceptibility testing.

Fig. 18a shows the micrograph of the microfluidic chip. We highlighted three functionally distinct sections: (1) for deposition of the liquid samples, (2) for transport of plugs along a delay channel, and the dilution section (3) for formation of the gradation of concentrations and for storing the mixtures for subsequent analysis. Dilution section comprises 11 serially connected Meter&Store units.

http://rcin.org.pl

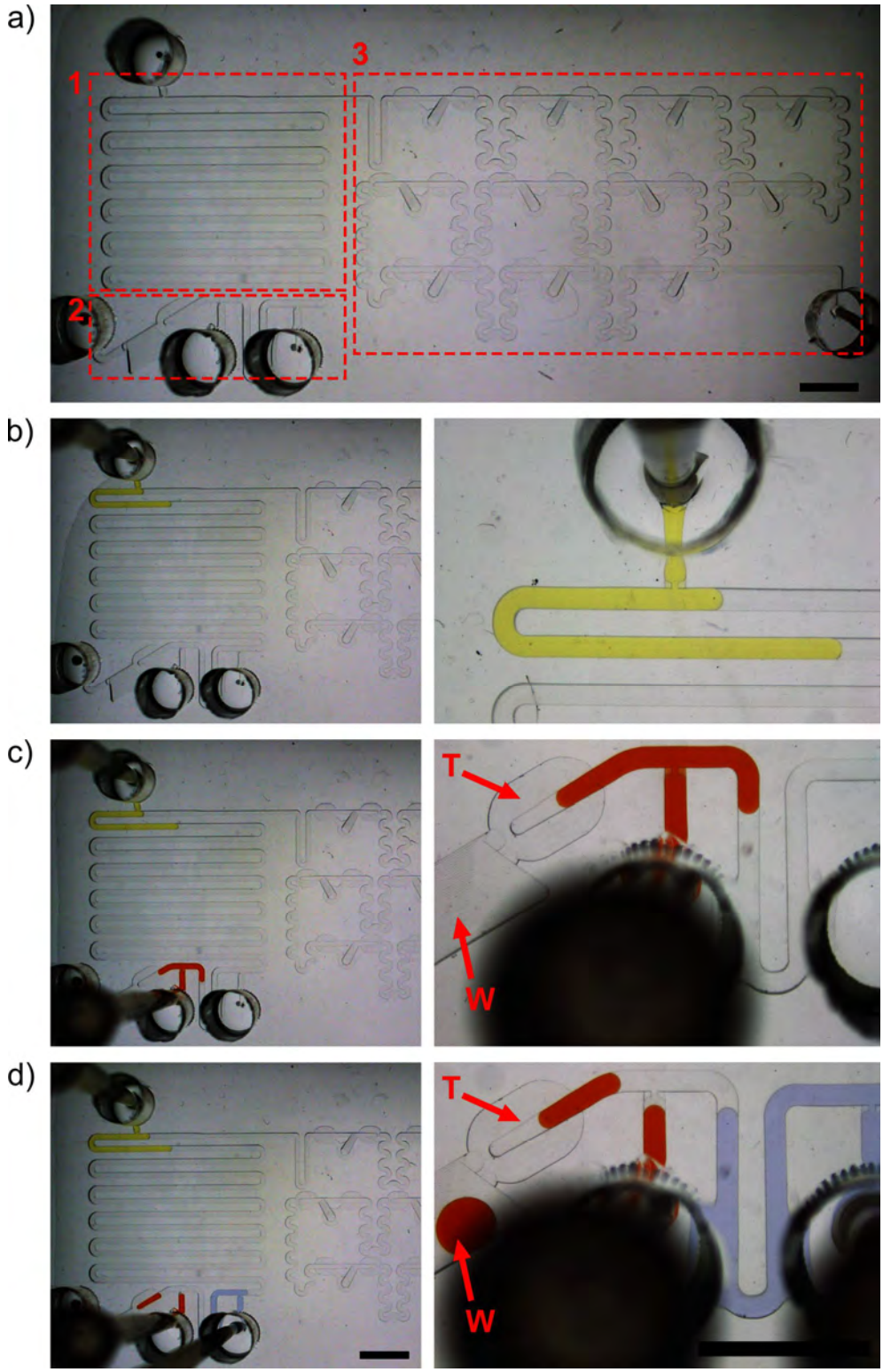


Fig. 18 a) Microfluidic chip comprising 3 parts – module (1) for deposition of a sample to-be-diluted (e.g. antibiotic solution) and buffer (e.g. pure broth), delay channel (2) with inlet for deposition of an another reagent (e.g. bacterial culture) which concentration will be stable in each droplet. The main part (3) comprises 11 Meter&Store modules for generation of gradient. b-d) Snapshots depicting the depositions of the subsequent portions of liquids. Letter 'T' indicates the metering trap and letter 'W' indicates the waste reservoir. Scale bar is 5 mm.

http://rcin.org.pl

The chip comprises three layers, all fabricated in PDMS (Fig. 19): a bottom (flat) slab, an intermediate fluidic layer and an upper thick slab with through-holes that serve as wells for oil and prevents injection of bubbles during deposition of samples from the pipette. The fluidic functionality of the chip can be captured by a chip made of a single injection molded part (comprising the wells and ports for deposition of the samples on the top side and the fluidic channels on the bottom) laminated with a plastic foil from the bottom.

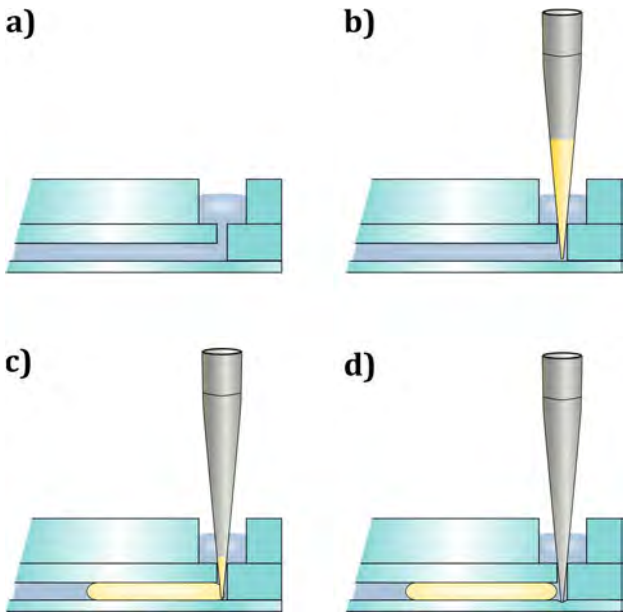


Fig. 19 A scheme depicting process of deposition of a sample into microfluidic channel with an automatic pipette.

4.1.3 The full procedure of preparation of a dilution series with a component at constant concentration.

We start the experiment with the system filled with the continuous liquid. We then deposit the sequence of three plugs comprising solutions of different dyes on the chip (Fig. 18b-d) using a simple automatic pipette (Brand Transferpette S, volume range 0.5-10 µL, Germany). First, we deposit a large (9 µL) plug (Fig. 18b) representing the *sample*. Then we inject the second 4.5 µL plug comprising the *reagent* (Fig. 18c) and finally a 9 µL plug modeling the *buffer* (Fig. 18d).

During the deposition of the *buffer* solution, the much higher hydrodynamic resistance towards the dilution section (to the right) forces the reagent-plug to flow through the metering trap located on the left side of the deposition module (the trap is indicated with the letter 'T' in Fig. 18c-d). This additional metering trap has twice the volume of the metering traps in the dilution section and meters a droplet

http://rcin.org.pl

containing 900 nL of the *reagent*. The excess reagent liquid is locked away in a deep on-chip waste container (indicated with the letter 'W' in Fig. 18).

After deposition of each specimen, each pipette tip is pressed against the bottom of the inlet channel and released from the pipette (Fig. 19). The diameter of inlets in the PDMS chip are smaller than the outer diameter of the terminus of the pipette tip, allowing us to seal the port.

In the next step, we inject 100 μL of the continuous phase liquid (solution of fluorocarbon fluids) into the chip at a constant flow rate of ca. 9 $mL \cdot h^{-1}$. For this purpose we use and electronic hand dispenser Multipette Xstream with 0.1 mL Combitip, (both from Eppendorf, Germany). As a result, the yellow plug of tartrazine solution is pushed to the dilution section for metering of portions of *sample* while the two other plugs (*buffer* and *reagent*) flow along the delay channel. Next we remove the oil tip from the inlet and this operation generates additional transient back-pressure that speeds up the derailing of the *sample* droplets into the side chambers. This action takes up to a few seconds. Next, we inject another 100 μL of the continuous phase into the chip via the same inlet. The flow generated in the second step pushes the *buffer* and the *reagent* through the network to generate the gradation of concentration of the *reagent* in the M&S modules. Finally, the dispenser tip is removed and droplets with gradually decreasing concentration of the reagent are derailed to the storage well. They merge with the portions of the sample within a few seconds.

4.1.4 Serial dilution of a fluorescent sample

We prepared the gradient in the same way as described above, but as a sample we used 10μM rhodamine 110 (Sigma Aldrich, Germany) dissolved in Mueller-Hinton (MH) broth (BD Biosciences, United States). The pure MH broth served as the sample (not diluted in the experiment) and also as the dilution buffer. Fig. 20 shows stable values of dilution ratios between 11 successive droplets and the decrease in fluorescence.

The results are averaged between 7 independent executions of the whole experiment. The averaged dilution ratio equals 1.68 ± 0.07 (RSD 4.1%). The dilution ratio is not the same as the ratio (equaling 2) of the volumes of the reagent plug (900 nL) and of the droplet of diluent aliquoted in the Meter&Store unit (450 nL). The

http://rcin.org.pl

difference roots in the observation that when a plug of reagent (or a mixture of reagent with diluent) flows into a metering trap that locks a droplet of pure diluent, not all of the diluent liquid is flushed forward. The fact that the dilution ratio does not follow straightforward from the ratio of volumes necessities calibration of any new geometry of the chip. Most importantly, however, the system generates reproducibly the same dilution ratio in all of the M&S units in the series and within a broad spectrum of the rates of flow of the continuous liquid, ranging from 5 $\mu L \cdot h^{-1}$ to 16 $\mu L \cdot h^{-1}$.

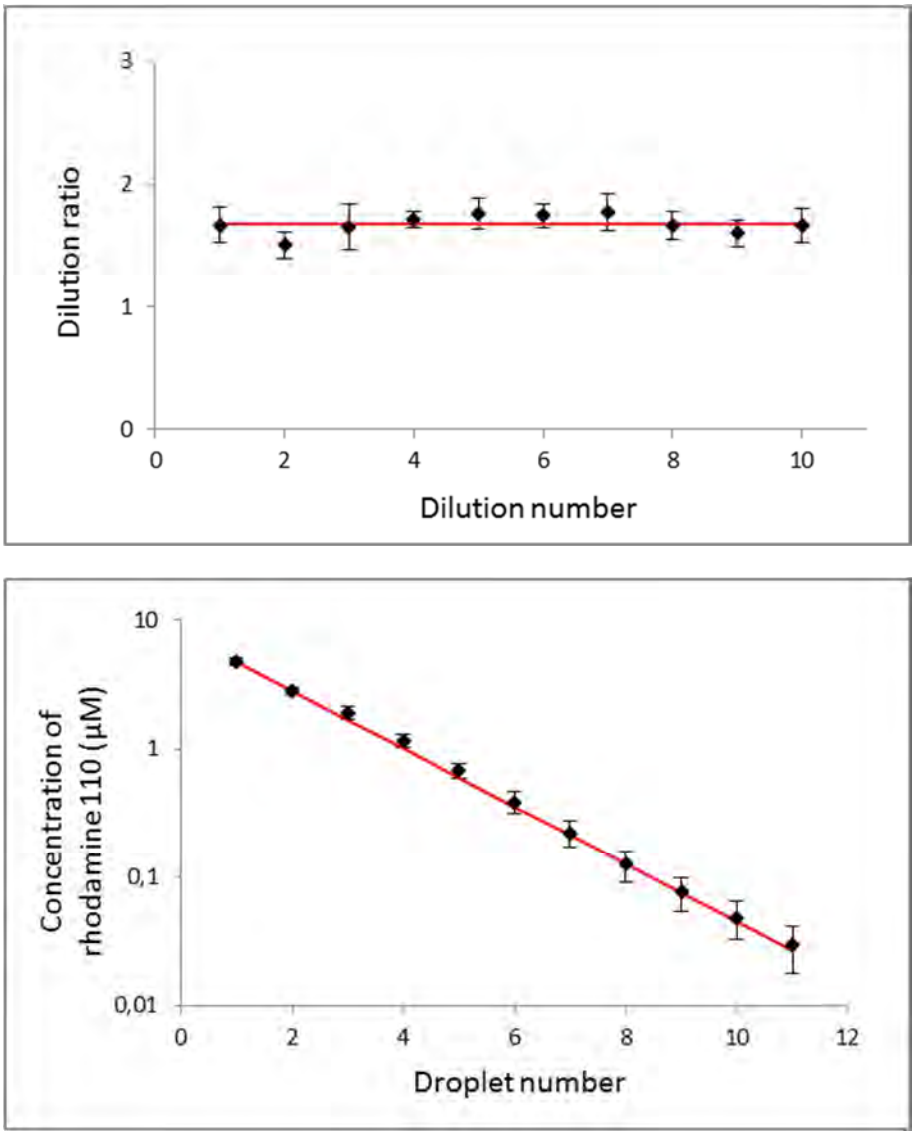


Fig. 20 Result of measurements of the fluorescence intensity of the droplets after the dilutions. The error bars represent standard deviation (n=7). Red line represents averaged dilution ratio (upper plot) and expected decrease of concentration in successive droplets (lower plot).

http://rcin.org.pl

We compared the level of reproducibility of the microfluidic generation of gradient with the precision and accuracy of a classical automatic pipette. We used the values[229] describing technical features of Eppendorf Research® plus pipette – a comparable device to Brand Transferpette S® used in this study. The pipette doses 0.5 µL aliquots of liquid with the inaccuracy of ±8.0% and imprecision of ±5.0%. These values can be recalculated to the relative standard deviation of ±9.4% that is significantly higher than the RSD of dilution in our microfluidic system. Two components (bacterial culture and solution of an antibiotic) are needed for an antibiogram assay, so the minimum reaction volume is ca. 1.0±0.1 µL.

We can distinguish two sources of variation in the microfluidic system: extrinsic (or user-dependent) and intrinsic resulting from imperfections of the dimensions of channels and traps. The main reason of the user-dependent variation is low precision of metering of the sample (Fig. 18d). During this operation fluid is pushed by the manual pipette, so the fluctuations of flow rate might be much higher than during the use of an electronic dispenser that drives the oil through the system. The dilution ratio also varied between successive traps on the same chip (RSD between 5.5% and 10.0%). This intrinsic variation might be explained by the limited precision of micromilling – for example depths of the main channel inside the traps differed by up to 3%. Variations in the dimensions of the trap structures might introduce additional errors during gradient formation. Other, more precise method of fabrication should completely alleviate this source of intrinsic error. Fabrication of tilted channels with soft lithography is challenging, but possible.[97] The structures that we propose are also fully compatible with precision injection molding.

4.1.5 Determination of Minimum Inhibitory Concentration (MIC) of ampicillin

In a model use of our system we deposited 3 plugs of MH broth – 1st with bacteria (density of 10^6 CFU·mL^{-1}), 2nd with an ampicillin (concentration 200 mg·L^{-1}) and 3rd with the pure medium for dilution of the antibiotic. Antibiotic solution and pure medium contained the same concentration of viability indicator – 88 µM of the resazurin sodium salt dye (Sigma Aldrich, Germany) which is converted to highly fluorescent resorufin in a presence of viable bacteria.

http://rcin.org.pl

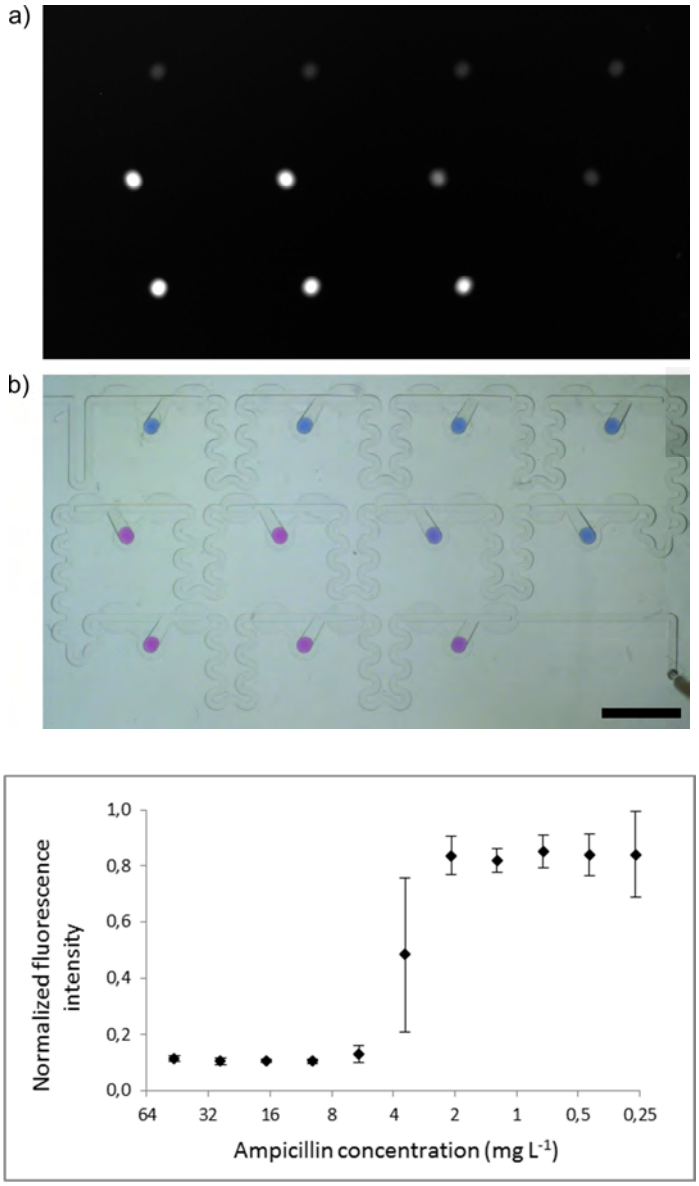


Fig. 21 Results of an antibiogram assay for ampicillin against ATCC 25922. Snapshots from a) fluorescent gel imager and b) conventional camera depicting conversion of resazurin to resorufin across the droplets locked dilution module after 5h of incubation in 37 °C. Scale bar is 5mm. Each point on the MIC plot is an average of 5 experiments and the error bars show the standard deviation for the set (n=5).

We generated droplets with the same concentration of bacteria and resazurin but with decreasing concentration of antibiotic in consecutive droplets. Importantly, bacteria contacted only the already-diluted solutions of the antibiotic, just as in a classic antibiotic susceptibility test. The chemical composition of final droplets was the following: 44 μM of the resazurin sodium salt dye, *E.coli* cells at the density of $5x10^5$ CFU·mL^{-1} and ampicillin decreasing from 47±3 mg·L^{-1} (1st droplet) to 0.3±0.1 (11th droplet). Next, we incubated the reaction mixtures for 5h at 37 °C and performed measurement of fluorescence using gel imager. Fig. 21 illustrates the

http://rcin.org.pl

averaged (n=5) and normalized intensity of fluorescence for each droplet. These data combined with the dilution ratio from Fig. 20 enabled to determine the MIC value for ampicillin to be equal 5.9±0.9 mg·L^{-1}. This result is in good agreement with the values obtained by classical dilution broth method (e.g. the MIC value for ampicillin and ATCC 25922 *E.coli* strain in a range of 2.0 and 8.0 mg·L^{-1} reported in the literature[137]).

We observed formation of bubbles during incubation at elevated temperature – phenomenon which is one of the most important practical challenges in biphasic microfluidic systems, particularly in the case of use of fluorocarbons that are characterized by high solubility of gases decreasing at elevated temperatures. This restriction was circumvented by performing the incubation outside the chip – e.g. during emulsion PCR[31,32] or, in single phase flows, by introduction of bubble traps.[230,231] In our chip bubbles are almost exclusively formed in the main reservoirs of the oil - delay channels (area '1' on Fig. 18a) or deposition module (area '2' in Fig. 18a). Most importantly, the architecture of the side chambers warrants that bubbles do not change the position of droplets locked in the storage wells – neither directly nor by flow of oil caused by expansion of bubble. Fig. 22 presents exemplary snapshots of the chips after incubation.

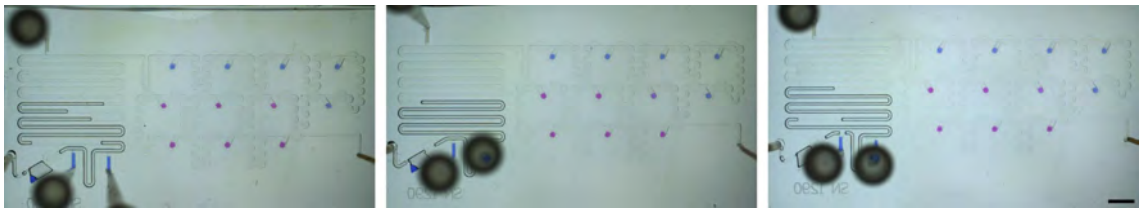


Fig. 22 Snapshots of 3 different chips depicting results of bubble formation during incubation. Scale bar is 5 mm.

4.1.6 Summary

One of the ultimate goals in droplet microfluidics is to construct inexpensive, portable and robust lab-on-chip devices for biological and chemical assays. Such simple-to-use systems will be required to perform multiple liquid handling operations in sequence, including i) preparation of the test sample, ii) generation of a gradation of concentration of reagent taken from the stock solution and subsequently iii) mixing and incubation of the reaction mixtures. The fluid actuation should ideally be simple and preferably insensitive to fluctuations. Some of these functions have already been demonstrated, as e.g. dilution,[101,102,105,106] yet without

http://rcin.org.pl

the necessary component of adding a component at constant concentration and storage for subsequent analysis and without a demonstration of operating the system with a tool as commonly available in the laboratories as an automatic pipette.

In summary the system that we presented here addresses all the above challenges as it i) precisely meters small portions of the sample, ii) prepares a concentration gradient of the reagent on the same chip, iii) can be operated with simple micropipette and iv) does not require additional moving elements or external forces to control the transport of droplets. Another advantage is stable locking of droplets after formation of the gradient. Once the simple protocol of five pipetting steps is executed the chip can be transported, shaken, incubated and the droplets safely stay in their reaction chambers kept there by capillary forces.

http://rcin.org.pl

4.2 Studies of bacterial growth and adaptation in microdroplet chemostats

In this section we describe an automated microfluidic system for the formation and long-term study of bacteria in multiple, parallel microdroplet chemostats.

The microfluidic system (Fig. 23) possesses four main features:

i) formation and monitoring of multiple microdroplets containing microbial cells, reagents, and soluble growth factors;

ii) use of an immiscible liquid as a barrier for insulating cells from the walls of channels and from other droplets, which prevents biofilm formation and the cross-contamination of reagents and cells

iii) cycling microdroplets for incubation and in-line measurements of cell growth; and

iv) splitting and merging microdroplets to control the chemical compositions of microbial cultures over time.

4.2.1 Microdroplet chemostat design

The design and operation of the system for generation of microdroplet chemostats is summarized in Fig. 23**.** The system consists of several regions where operations are performed—that we refer to as *'segments'*—for: i) on-demand generation of microdroplets containing cells, reagents, and soluble growth factors (Fig. 23a); ii) cycling microdroplet chemostats during growth and monitoring of bacteria (Fig. 23b); and iii) splitting (Fig. 23c) and fusing (Fig. 23d) microdroplets to exchange media and manipulate the concentration of chemical factors in time in each of the microdroplet chemostats.

4.2.2 Microdroplet formation

In the first step we loaded the device reservoirs with liquid samples, then we used a source of positive pressure and external electromagnetic valves to regulate the flow of oil (the carrier fluid), aqueous broth media for microbial growth, and a suspension of bacteria. We generated a sequence of aqueous microdroplets comprising bacterial cells, nutrients, and reagents. Each microdroplet in the sequence was formed by coalescing smaller microdroplets consisting of a user-defined, preprogrammed volume of different solutions.[55,56,77] The formation of microdroplets was automated using a real-time video feedback loop that enabled

http://rcin.org.pl

us to control the volume of the microdroplets and the time at which they were formed. The software used an edge detection algorithm to track the process of microdroplet formation and controlled the volume to an accuracy of ~0.3 %. Merging of droplets was facilitated by using an electrocoalescence mechanism.[55,226]

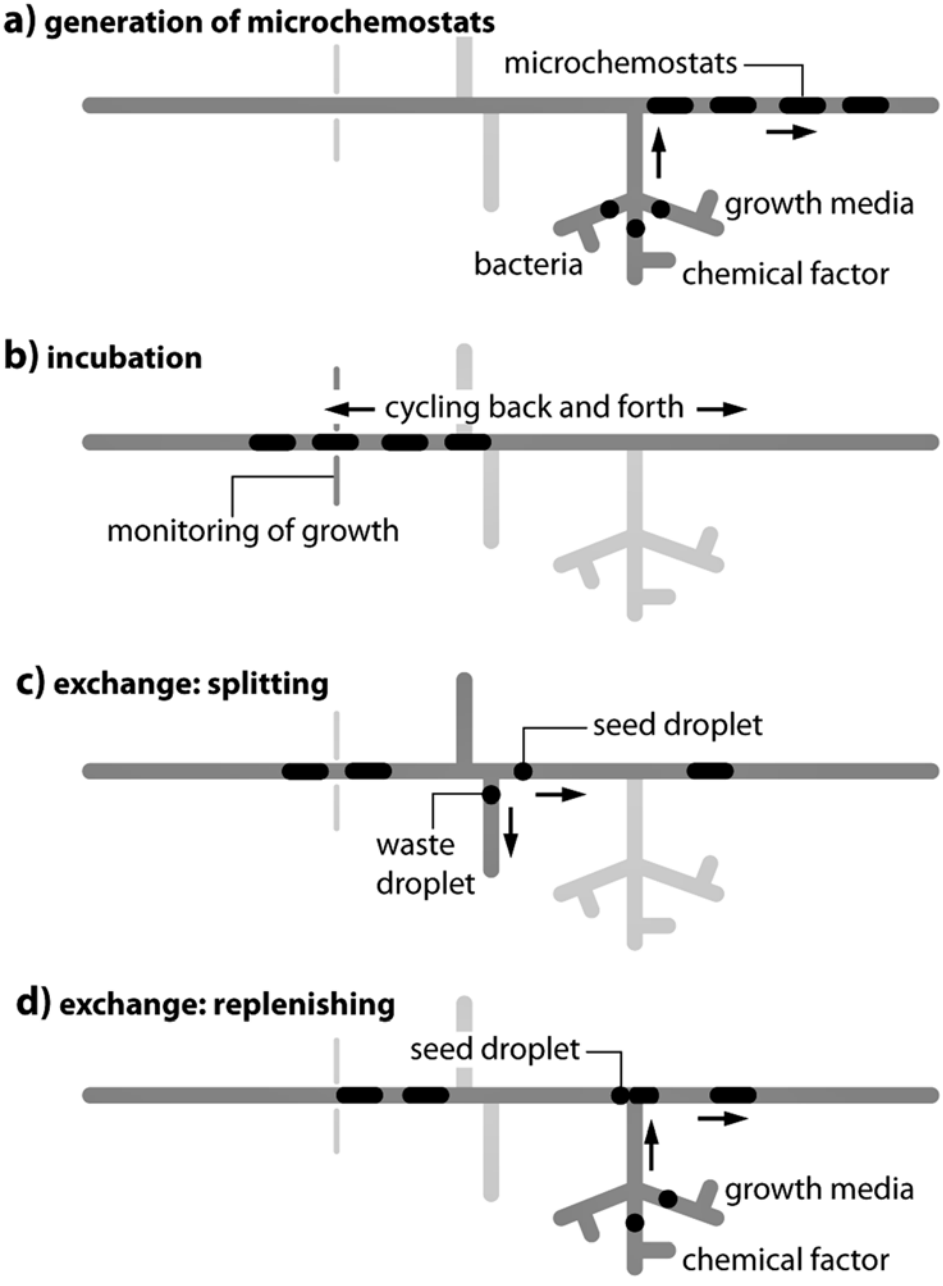


Fig. 23 Schematic diagram of the layout and operation of the microdroplet chemostat system. a) A sequence of microdroplet chemostats is created by merging droplets containing bacteria, antibiotics and growth media b) Microdroplets are cycled in the incubation segment during which cell growth is monitored. c) Each microchemostat is split into a seed droplet and a waste droplet. d) The seed droplet is merged with a microdroplet containing fresh nutrient media.

http://rcin.org.pl

4.2.3 Microdroplet incubation

After generating a sequence of microdroplet chemostats, we cycled them back and forth in the incubation segment to avoid wetting the walls of the microchannels with aqueous phase and to continuously measure cell growth in the droplets. To set up an oscillatory motion of microdroplets in the incubation segment, we used pressure driven flow controlled with two pairs of (in/out) valves at each end of the channel (Fig. 24a). As the microdroplets cycled in the channel, they periodically passed an in-situ, waveguide spectrophotometer that measured the absorbance of light passing through the droplet (Fig. 24a) at the 5-mm long optical path. The system was designed to simultaneously cycle 164 microdroplets (each with a volume of ~ 1.28 μL).

4.2.4 Controlling microdroplet chemistry

At user-defined intervals, the system performed a set of operations on each microdroplet. First, microdroplets were split (Fig. 24b) into two preprogrammed subvolumes (i.e., a waste microdroplet and a seed microdroplet). Next, the seed microdroplets were fused with microdroplets containing fresh reagents (Fig. 24c). We split microdroplets into seed and waste fractions by partitioning the droplet between the main and side channel. The waste fraction was removed through the side channel and the seed microdroplet remained in the main channel. We were able to control the volume of the seed microdroplet between 0.1 - 0.9 of the volume of the initial microdroplet with an accuracy of ~0.8 %. We merged the seed microdroplet with microdroplets containing reagents using an electrocoalescence mechanism. Using this approach, we were able to control the concentration of bacteria and reagents in microdroplets over tens of hours.

We used solutions of red and blue dye to measure the accuracy and reproducibility of multiple changes in chemical concentration within a lineage of microdroplets (Fig. 25). First, we generated a microdroplet containing a mixture of red and blue dye. At each iteration we split the microdroplet and fused the seed droplet with a new microdroplet containing an arbitrarily set composition of dyes. During this process, the concentration of each dye was changed independently. Fig. 25 shows the absorbance measured for a microdroplet at λ=450 nm and at 650 nm, which corresponds to the concentration of blue and red dye, respectively.

http://rcin.org.pl

The largest root mean square error between the measured and programmed dye concentration was 0.7 %, which reflects a high accuracy in controlling the chemical composition of microdroplets in time.

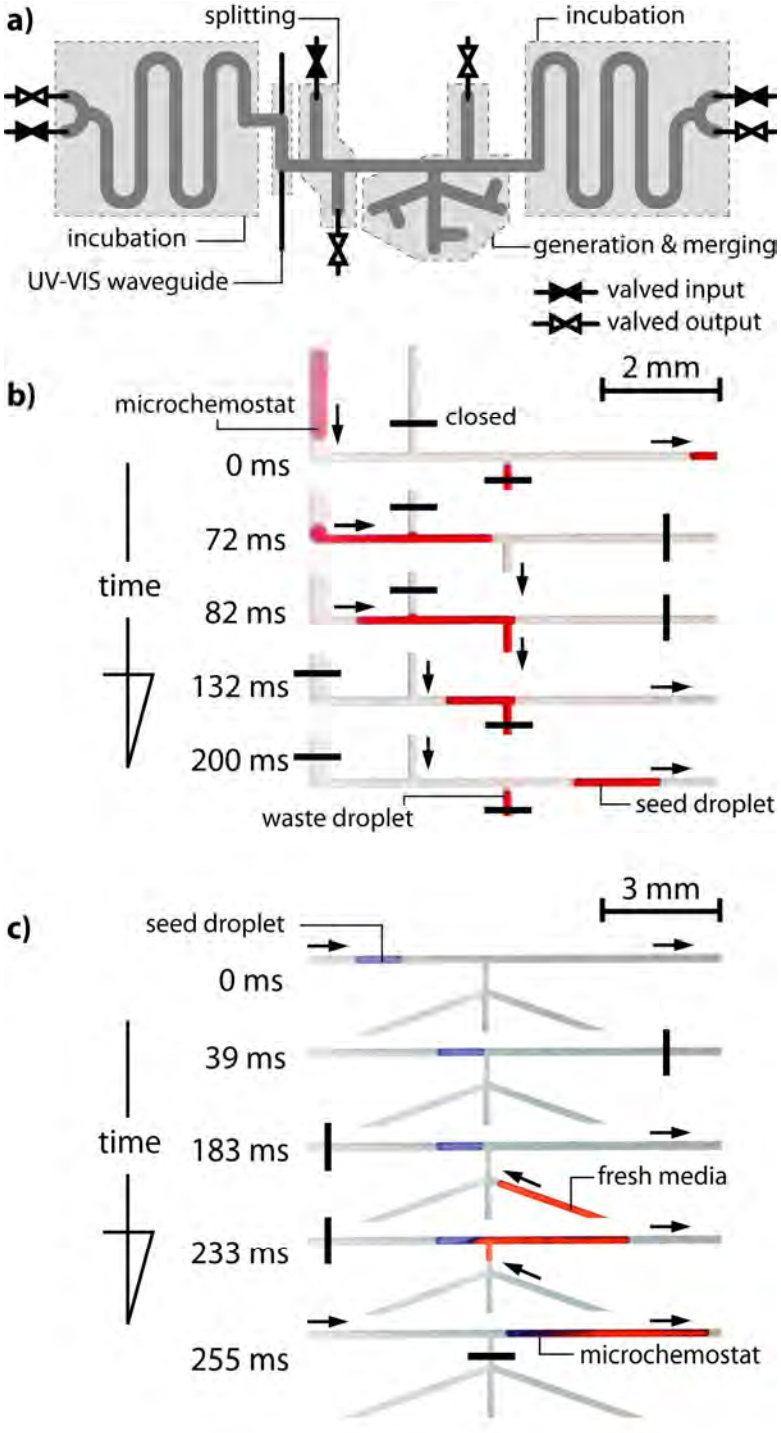


Fig. 24 a) A schematic illustration of the layout of the chip. b) A sequence of micrographs depicting the operation of splitting of a microdroplet into a seed droplet and waste droplets with pre-programmed volumes. c) A sequence of micrographs illustrating the fusion of the seed droplet with fresh media. This operation enables control over the cell density and the chemical composition in each microdroplet.

http://rcin.org.pl

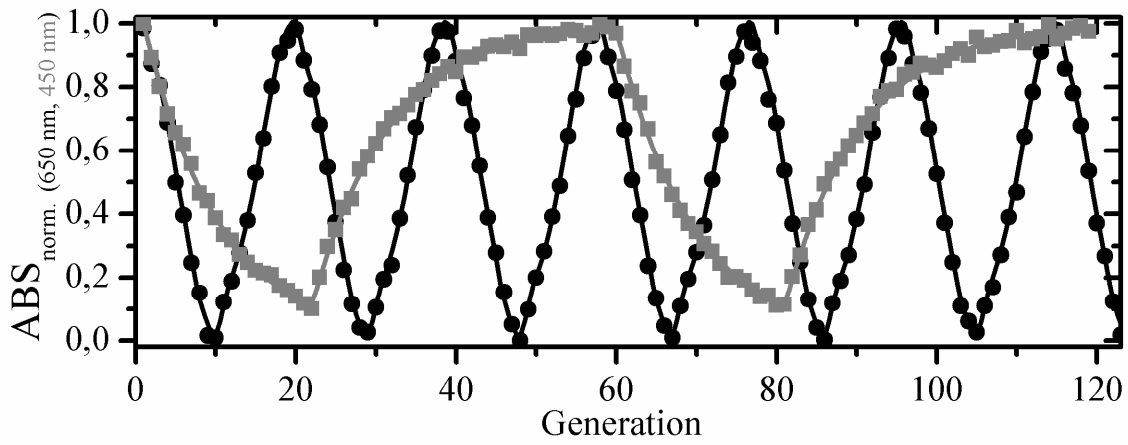


Fig. 25 A graph of the normalized absorbance at 450 and 650 nm, showing exemplary traces of the concentration of blue (light grey line) and red (black line) dyes in a chemostat droplet over 120 generations. The data points present the absorbance measurements while the lines correspond to the programmed values.

4.2.5 *E. coli* growth in microdroplet chemostats

The salient characteristics of the microdroplet system make it well suited to create and maintain cultures of microorganisms continuously. To use this technique for microchemostats, we encapsulated cells in microdroplets, periodically split the microdroplet, and fused the seed microdroplet with a droplet of liquid growth media. This approach enabled us to transfer a fraction of a growing population of microorganisms to new microdroplets containing fresh media and user-defined chemical compositions, and to perform experiments that require long-term cell bacteria growth.

We monitored the population density of bacteria (λ=600 nm) and established growth curves of cells in microchemostats. Specifically, we prepared microdroplets (volume, 1.28 μL) containing a suspension of *E. coli* cells (strain ATCC 25922) at a cell density of $(1.09\pm0.13)\cdot10^7$ CFU·mL^{-1}, that corresponds to ~14 000 cells encapsulated in a single droplet at the beginning of experiment. We cycled the drops for 600 min and monitored the cell density over time (Fig. 26a). The measured data points form a curve that comprises the classic three stages of growth: 1) initial exponential growth; 2) log phase; and 3) saturation of growth at a high cell density and can be fitted with Monod's model.[232]

http://rcin.org.pl

The number of cells in the chemostat is determined by the equation,

$$N(t) = N_0 e^{\mu(c(t))t},$$

where

- N_0 is the initial number of cells,
- $\mu(c(t)) = (\mu_{MAX}\, c(t))/(K_M + c(t))$ is the specific growth rate of bacteria [h^{-1}],
- $c(t)$ is the concentration of the rate limiting nutrient [$g \cdot ml^{-1}$],
- μ_{MAX} is the maximum growth rate [h^{-1}],
- and K_M[$g \cdot ml^{-1}$] is the saturation parameter corresponding to the substrate concentration that yields half of the maximum growth rate.

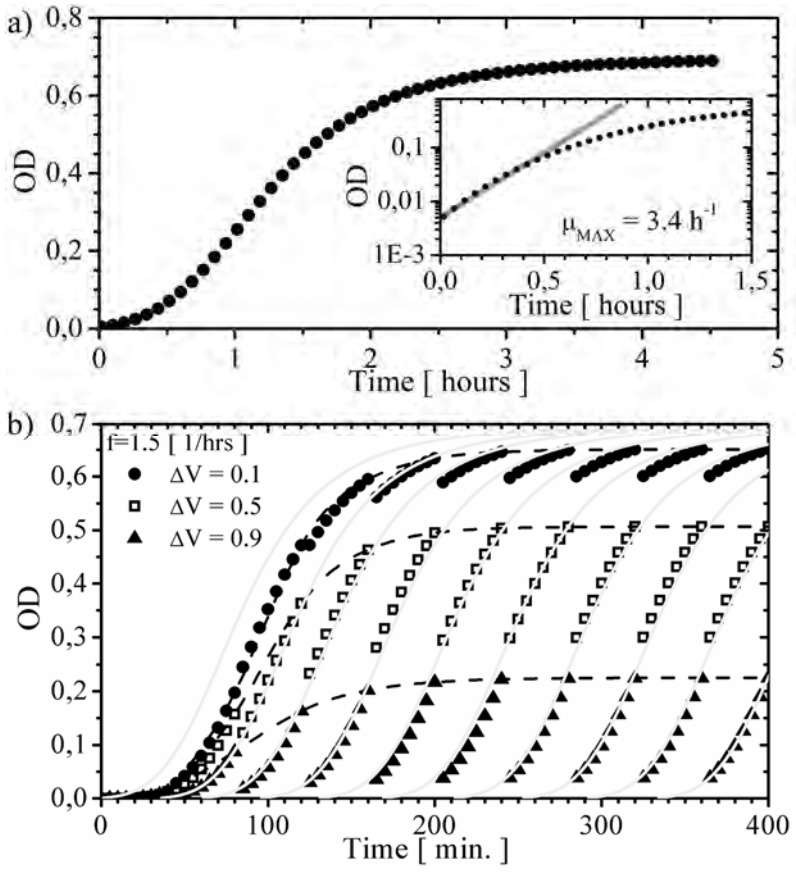


Fig. 26 a) Representative growth curve of *E coli* ATCC 25922 in a microchemostat. The inset plot depicts a calculation of the growth rate by fitting the exponential function. b) A plot illustrating three repetitive growth curves acquired for an extended period of time and with different fractions of exchanged media (either 0.1, 0.5, or 0.9 of the droplet volume). The experimental data points are in good agreement with theoretical curves depicting Monod's model (light grey lines).

http://rcin.org.pl

The conditions for cell growth in microdroplet chemostats are controlled using three parameters: 1) the chemical composition of the growth media; 2) the frequency of exchanging the culture media by splitting and fusing microdroplets; and 3) the fraction of the microdroplet volume that is exchanged at each iteration. To understand how parameters (2) and (3) affect the dynamics of bacterial growth, we created a sequence of microdroplets and iterated the steps of cycling the drops and exchanging media, while monitoring the population density in each droplet. The time-dependent concentration of cells followed the Monod's growth curve (Fig. 26b).

Initially, the concentration of cells at the moment of exchanging the media increased with every iteration. After several iterations the population of cells in the chemostat reached a periodic trajectory. The shape of the growth curves in Fig. 26b illustrate the approach of the community to a stable cell density N_{SAT} at the moment of exchange of media. The region of Monod's curve probed by the colonies in each (i-th) microchemostat and the saturation density of cells (Fig. 26b) depend on the choice of the two parameters: the interval T_i between—or frequency $f_i = T_i^{-1}$ of—exchanges, and the fraction ΔV_i of the volume V of the droplet that is exchanged. The dilution rate D for a standard chemostat is defined as $D = Q/V$, where Q is the flow rate. The analog parameter in the microdroplet chemostats is $D = f\Delta V/V$.

To test how N_{SAT} depends on D we created a sequence of 54 microdroplets, starting with, N_0 = (1.09±0.13)·10^7 CFU·mL^{-1} and tested an 9 x 6 matrix of values where $\Delta V/V \in (0.1, 0.9)$ with a step of 0.1 and $f \in (0.5, 3)$ [h^{-1}] with a step of 0.5 [h^{-1}]. Fig. 27a shows the grayscale-coded plot of N_{SAT}. Qualitatively the value of N_{SAT} is intuitive: at low values of f and $\Delta V/V$, microchemostats contain a high density of cells. A high frequency of exchanging the liquid and a large volumetric ratio of exchange decreased the density of cells; at extreme values of these parameters, the culture is unable to regrow within the interval T. Fig. 27b demonstrates a quantitative comparison of the value of N_{SAT} measured in microchemostats with the value predicted for a continually replenished (classic) chemostat.

http://rcin.org.pl

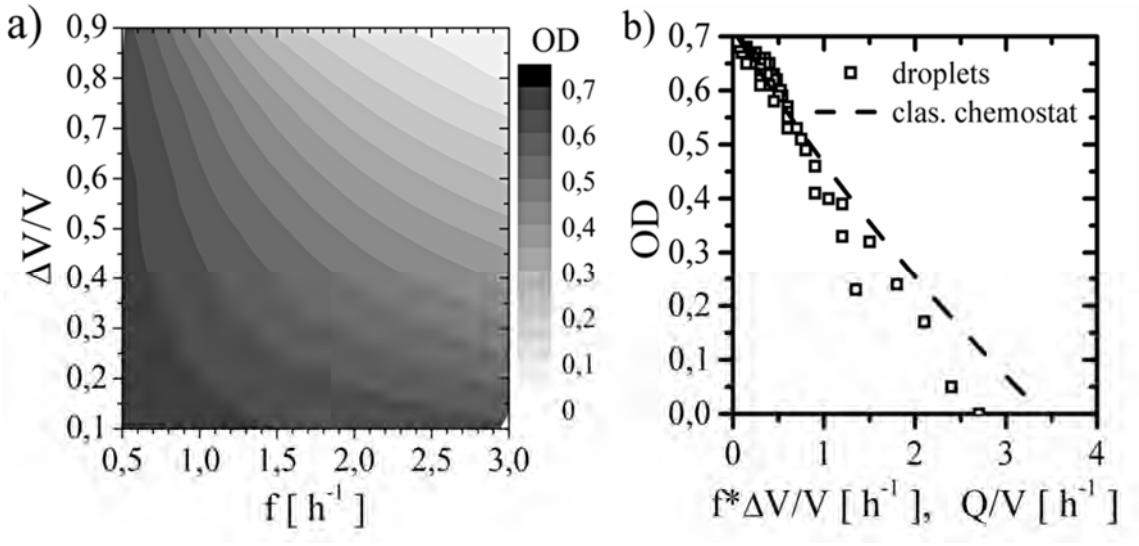


Fig. 27 (a) A heat map illustrating the bacterial cell density at the moment of exchange of media as a function of the frequency of exchanges and the fraction of the volume of liquid exchanged. (b) A graph comparing the saturation density of cells at the moment of exchange to the density of cells in a chemostat with continuous exchange of media. Explanation of abbreviations: "*droplets*" refers to microdroplet chemostats; "*clas. chemostat*" refers to classical chemostats.

4.2.6 Cell growth in microchemostats containing antibiotics

The microchemostat system is well suited for performing parallel experiments of microbial population dynamics - including studies of predator/prey and syntrophic interactions - and the response and adaptation of bacteria to chemical and environmental stress. These studies require that there is no contamination between the contents of microdroplet chemostats. We have previously demonstrated that incubation of bacteria with antibiotic in microdroplets separated by hexadecane oil containing 2 % Span 80 does not result in cross-contamination after several hours.[56] As the present system focuses on continuous cultivation over hundreds of generations, we performed additional control experiments in which we compared the growth rate and saturation density of cells in adjacent microdroplets that either contained LBK nutrient media or LBK admixed with chlormamphenicol (at a final concentration of 5 $\mu g \cdot mL^{-1}$). We did not observe any cross-contamination between the microdroplets in these experiments (Fig. 28a). We have also checked if there was noticeable transfer of antibiotic between successive droplets, but we did not detect any measurable variation in chemical composition of microchemostats after 24 exchanges of medium (Fig. 28b).

http://rcin.org.pl

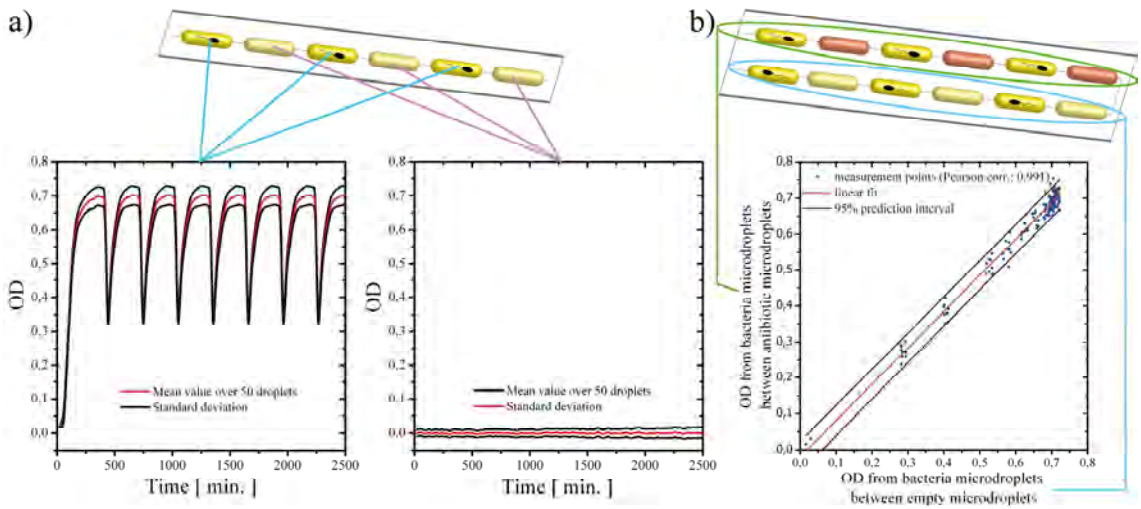


Fig. 28 Results of experiments that excluded any cross-contamination between the droplet microchemostats in our system. (a) We generated 100 microdroplets consisting of an alternating sequence of microdroplets seeded with bacteria and microdroplets only containing growth media. We did not observe cell growth in microdroplets that initially did not contain cells. (b) We also performed an experiment in which microdroplets seeded with bacteria were neighboring in the sequence with microdroplets containing high concentration of chloramphenicol (at a final concentration of 5 μg·mL^{-1}). We cycled back and forth both sequences of microdroplets for 24 h at 37 °C and performed 24 liquid exchange steps. We found a high correlation of bacterial growth in both experiments which thereby excluded the transfer of cells or antibiotic compounds between neighboring microdroplets.

4.2.7 Monitoring the response of bacterial communities to stress

The system enables the user to control the composition of microchemostats in time and makes it possible to perform experiments that test the response and adaptation of populations of microorganisms to stress and fluctuating environments. To explore this area, we studied the response of a population of *E. coli* cells to sudden increase of the concentration of chloramphenicol (Fig. 29). We grew cells to a steady state in the absence of antibiotic for four hours (*E. coli* strain ATCC 25922, LB media, f = 3 h^{-1}, ΔV = 0.5) and then applied one of three different concentrations of chloramphenicol (Fig. 29b-d). We maintained a constant concentration of chloramphenicol and monitored the dynamics of the populations of bacteria over 45 hours. The growth rate of bacteria decreased as chloramphenicol was added and continued to decrease for several generations. After a time interval that depended on the concentration of chloramphenicol, the population adapted to the stress and the growth rate increased gradually back to the initial rate. There are several possible molecular explanations for the changes in bacteria susceptibility to

http://rcin.org.pl

chloramphenicol, including changes in membrane properties,[233] drug efflux,[233] or changes in the ribosome structure.[234]

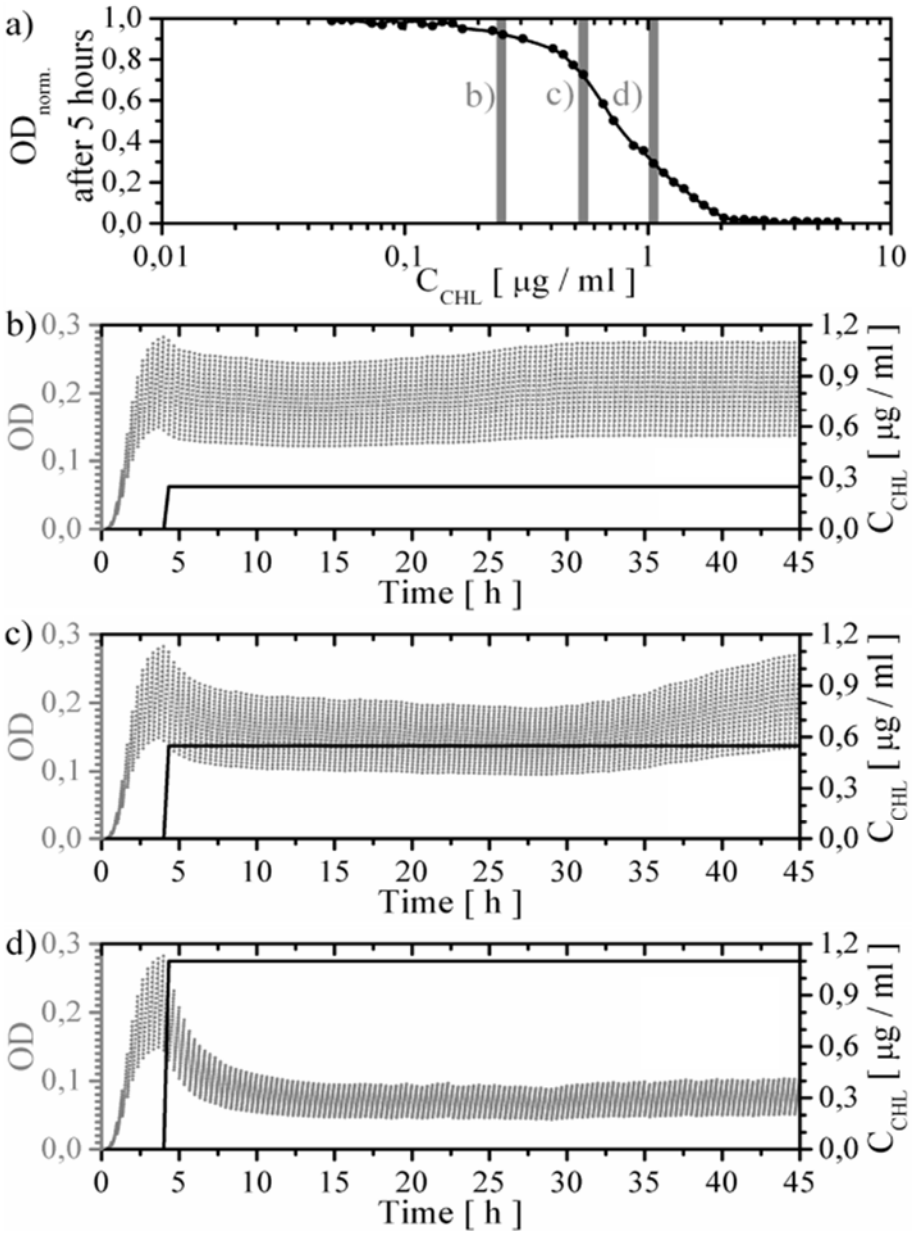


Fig. 29 a) A plot of the relationship between the normalized optical density of *E. coli* cells (λ=600 nm) and the concentration of chloramphenicol. Vertical bars mark the concentrations used in the adaptation experiments (b-d). The right axis of graphs (b-d) depicts the concentration of antibiotic (black solid line), and left axes depict the optical density recorded from the microchemostats (grey dots).

We next studied the response of populations of *E. coli* to slowly increasing concentration of chloramphenicol (Fig. 30). We prepared 15 microchemostats consisting of three groups of 5 microdroplets that were treated with increasing chloramphenicol concentration at different rates: 0.006, 0.01 and 0.015 $\mu g \cdot mL^{-1} \cdot h^{-1}$. The maximum standard deviation in the absorbance between microdroplet in each

http://rcin.org.pl

5-droplet series did not exceed 5.7% (for a rate of 0.006 $\mu g \cdot mL^{-1} \cdot h^{-1}$), 6.1% (for a rate of 0.01 $\mu g \cdot mL^{-1} \cdot h^{-1}$), and 7.1% (for a rate of 0.015 $\mu g \cdot mL^{-1} \cdot h^{-1}$) throughout the 45-hour experiment. The data suggests that higher rates of chloramphenicol addition produces more variability in growth rates in microchemostats. Our measurements are consistent with the rapid addition of chloramphenicol requiring cells to adapt rapidly compared to the slow addition of antibiotics, which provides cells with more time for mutations to accumulate.[233,235] Another possible explanation is the time scale for growth of persister cells that survive antibiotic dosing.[150]

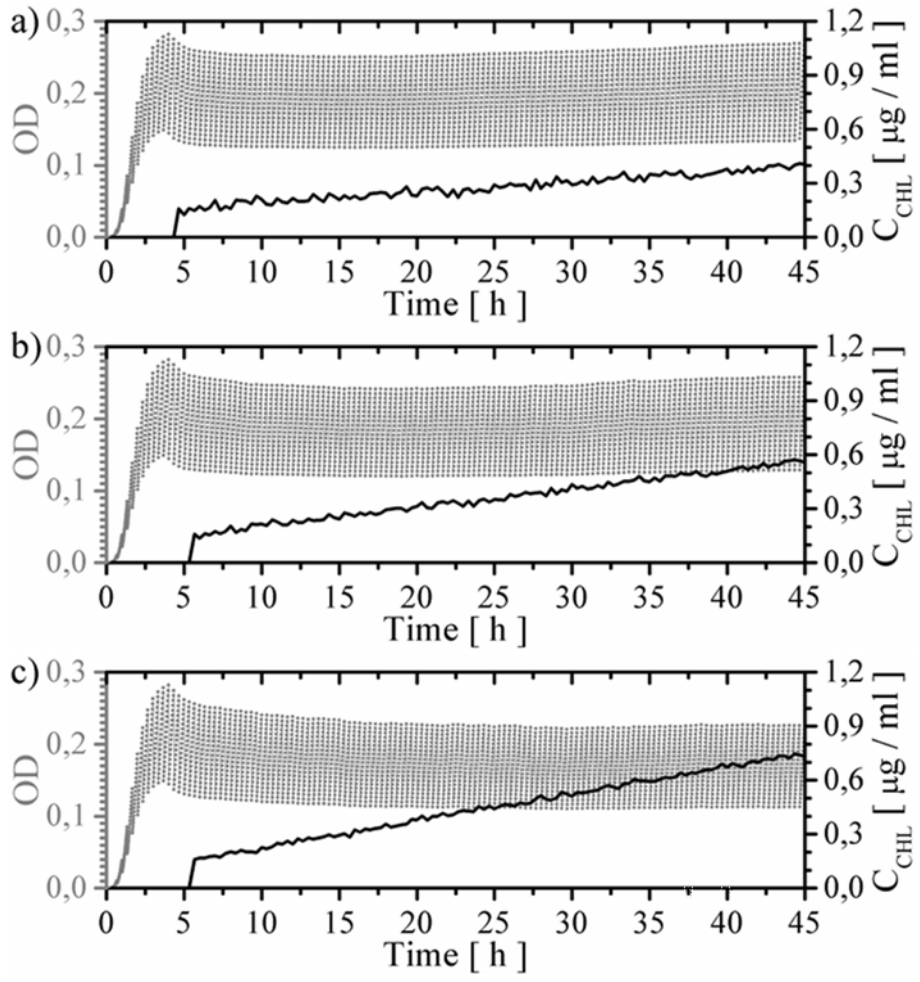


Fig. 30 Plots depicting the change of growth curves of populations of *E. coli* in microchemostats and their response to slowly increasing levels of antibiotics. We screened three rates of increasing the concentration of chloramphenicol: (a) 0.006 $\mu g \cdot mL^{-1} \cdot h^{-1}$; (b) 0.010 $\mu g \cdot mL^{-1} \cdot h^{-1}$; and (c) 0.015 $\mu g \cdot mL^{-1} \cdot h^{-1}$).

4.2.8 Summary

Microdroplet chemostat system enables long-term monitoring of cell growth in response to extracellular stress. Importantly the technology makes it possible to

http://rcin.org.pl

perform hundreds of experiments in parallel. Microdroplet technology hampers the cross-contamination between microchemostats by using oil as a continuous phase that insulates microdroplets and lubricates surfaces to prevent biofilm formation. Automated droplet microfluidic technology offers scalability of the number of microchemostats, which is limited only by the dimensions of the system and the frequency of droplet formation and manipulation.

We demonstrated the long-term cultivation of bacteria in microdroplet chemostats. Previous studies have described that the cultivation of microorganisms inside droplets is possible and can be advantageous due to several characteristics, including: 1) massive parallelization;[76,221] 2) stochastic confinement;[118,119] and 3) automation.[56,120,236] The longest cultivation times reported to-date have been only several generations due to limited nutrient availability and accumulation of secondary metabolites. The microchemostat system enables the long-term cultivation of bacteria by exchanging small volumes of liquids between microdroplets. Studies conducted in classical macroscale chemostats have demonstrated the extraordinarily rapid adaptation of bacteria to environmental changes.[233] Our approach complements this and other studies, by introducing a method for the parallel cultivation of hundreds of bacterial colonies. Importantly, the operational complexity of the system is low and the user can rapidly adjust the experimental conditions, such as phase of bacterial growth and the size and density of microbial populations. These capabilities provide new opportunities for studying the genetic and phenotypic adaptation and evolution of bacteria.

http://rcin.org.pl

4.3 Automated microfluidic system for generation of lipid bilayers and screening of membrane protein activity

This section demonstrates a microfluidic system that automates:

i) formation of a lipid bilayer at the interface between two nanoliter-sized aqueous droplets submerged in oil,
ii) reconstitution of α–hemolysin nanopore into the bilayers,
iii) electrophysiological measurements at the level of single membrane proteins, and
iv) exchange of one droplet of the pair in order to form a new bilayer and perform next recordings.

Our system takes an advantage of both:

i) active control of flow based on automation and the use of simple external valves and
ii) passive handling of droplets using dedicated microfluidic geometries - we introduce a new type of a hydrodynamic trap designed to immobilize the droplets with respect to each other and with respect to the recording electrodes.

4.3.1 Microfluidic device

The microfluidic device (depicted in Fig. 31) is composed of two polycarbonate plates, milled with a CNC drill and subsequently thermally bonded in a hydraulic press (see details of fabrication in Section 3.1.2). The width of the channels is 400 μm, excluding 200 μm-wide channels connecting the hydrodynamic trap with outlets L, R and inlet S (Fig. 31a). The depth of all channels is 400 μm. The device comprise following modules: i) a microfluidic trap N (Fig. 31b) in which droplets are locked to form a bilayer, ii) two microfluidic T-junctions (D and G) equipped with additional reservoirs for samples, and iii) an inlet port for a sequence of droplets containing various inhibitors (F). Two agarose-tipped electrodes are inserted into both of the two chambers of the trap. Preparation of electrodes is described in details in section 3.7.

http://rcin.org.pl

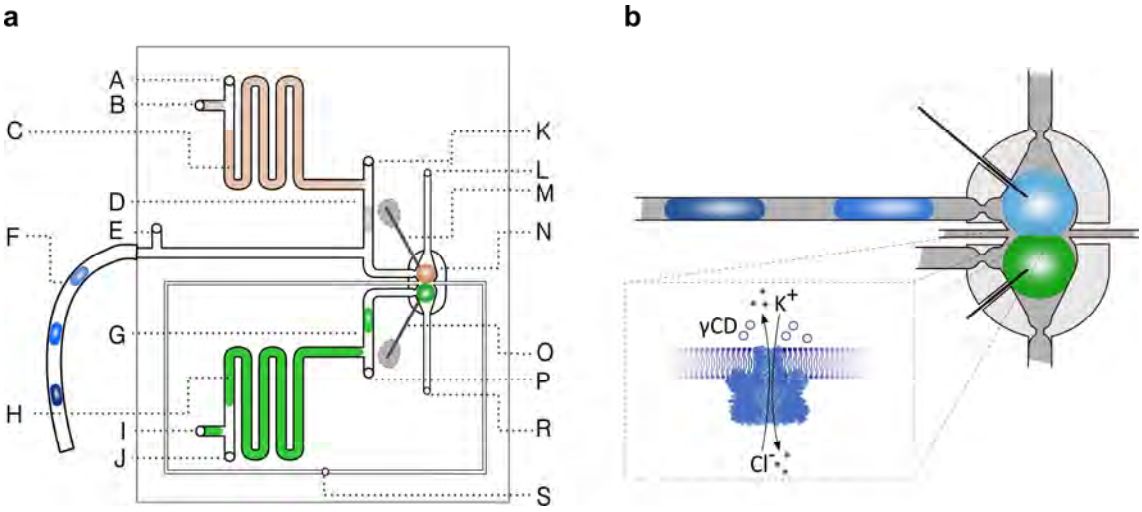


Fig. 31 The layout of the microfluidic chip:

a) A schematic diagram of the microfluidic device used in experiments: A, E, J, K, P – inlets for oil, B, I – inlets for aqueous samples, C – aspiration module with pure buffer for washing of electrodes, D, G – T-junctions, F – tubing with a sequence of droplets containing various concentration of an inhibitor, H – aspiration reservoirs with a solution of proteins, M – ground electrode, N – hydrodynamic trap, O – working electrode, S – inlet for oil in a control channel, L, R - outlets

b) A schematic picture presenting the geometry of the microfluidic trap. The DIB is formed at the interface of two droplets immobilized in the chambers filled with oil. The light-grey area represents 'bypasses' - shallow sections of channels on the sides of the trap. The dark grey area represents main 400 µm-deep channels. The continuous phase (oil with lipids) flows through the bypasses while the droplets are locked in the main chamber of the trap.

4.3.2 Operation of a chip

In the first step the whole system was filled with a continuous organic phase containing lipids (details of chemical compositions of oils and buffers are described in chapter 2.1). We then opened the inlet (B) and transferred several microliters of buffer from a glass microsyringe connected to the chip via a steel capillary. Next, we used the port (I) to introduce a small volume of the protein solution (α-hemolysin at the concentration of 0.5 $\mu g \cdot mL^{-1}$, diluted in the same buffer). After closing the deposition ports we initiated the flow of oil from inlets (A and J) into the reservoir channels (C and H) containing the sample in order to push the front of the aqueous phase to the T-junction. A sequence of droplets containing inhibitors was deposited on the chip in a similar manner (F and E). In the next step, we used external valves to generate droplets on demand in T-junctions – a defined volume of the aqueous sample was pushed into the orthogonal channel and then broken-off with the flow of oil[56] from inlets K and P (Fig. 31). Newly formed droplets were then transported into the trap N (Fig. 31b) comprising two chambers (dark grey in Fig. 31) - cavities

http://rcin.org.pl

that lock the droplets in place due to capillary forces. The shallow bypasses (marked with the light grey in Fig. 31b) allow for flow of oil around the droplets without changing their position. In the experiments, we first generated and placed in the first cavity of the trap a droplet containing α-hemolysin, then sequentially pushed droplets containing different concentrations of an inhibitor into the second cavity of the trap.

The geometry of hydrodynamic traps allows us to immobilize two droplets and observe the kinetics of formation of the DIB (Fig. 32). In parallel to tracking the process visually with a video camera we measured the capacitance of the bilayer in absence of any membrane proteins. For this purpose we applied a triangular potential (10 Hz, 50 mV peak-to-peak) and recorded the resulting square wave current at a 1 kHz sampling rate. The DIB is formed within about 60s, after the droplets are brought into the contact with each other.

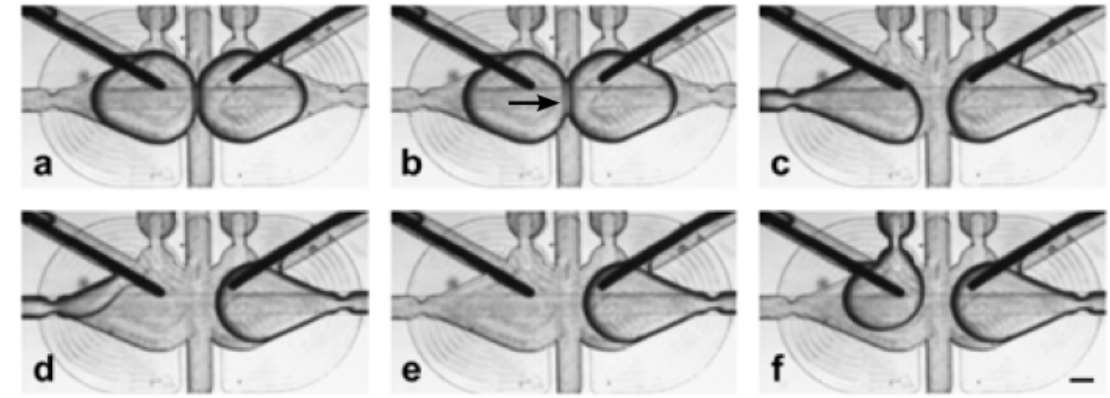


Fig. 32 Micrographs illustrating the geometry of microfluidic trap, orientation of the electrodes and the exchange of one of the droplets. a) The pair of droplets is locked in two chambers of the trap. b) Bilayer (indicated with an arrow) is formed at the interface of the droplets. c-e) One of the droplets is removed by the flow of oil. f) The new droplet is being placed in a trap. The droplet wets the electrode immediately after introduction to a trap. Scale bar is 200 μm.

4.3.3 Characterization of the bilayer

The area of the bilayer can be determined through the measurement of the capacitive current.[237] To estimate the bilayer size, we first generated pairs of droplets of five different volumes (250, 275, 300, 325 and 350 nL). For each volume we analyzed 5 pairs of droplets. For each pair a triangular potential (10 Hz, 50 mV peak-to-peak) was applied and the resulting square-wave current was recorded at a 1 kHz sampling rate. We collected and analyzed 60s-long traces.

http://rcin.org.pl

Capacitive current I_C is can be calculated from the measured value of the capacitance C_T and from the rate of change of potential dV/dt:

$$I_C = C_T \times \frac{\mathrm{d}V}{\mathrm{d}t}$$

A model cell with a known capacitance of 100 pF (MCB-1U, Molecular Devices, United States) was used to set the rate of change of potential dV/dt to 1 V·s^{-1}. Consequently, the measured value of I_C (given in pA) was equal to the value of capacitance C_T (given in pF). We calculated the average level and standard deviation of the capacitance (Fig. 33, Table 2). By using the specific capacitance of a DPhPC bilayer formed in pure hexadecane[237] (equal to 0.64 μF·cm^{-2}), we estimated the contact area between the droplets. The range of droplet volumes (250-350 nL) that can be analyzed in our system result in nearly 4-fold range in the surface area of the DIB (Fig. 33).

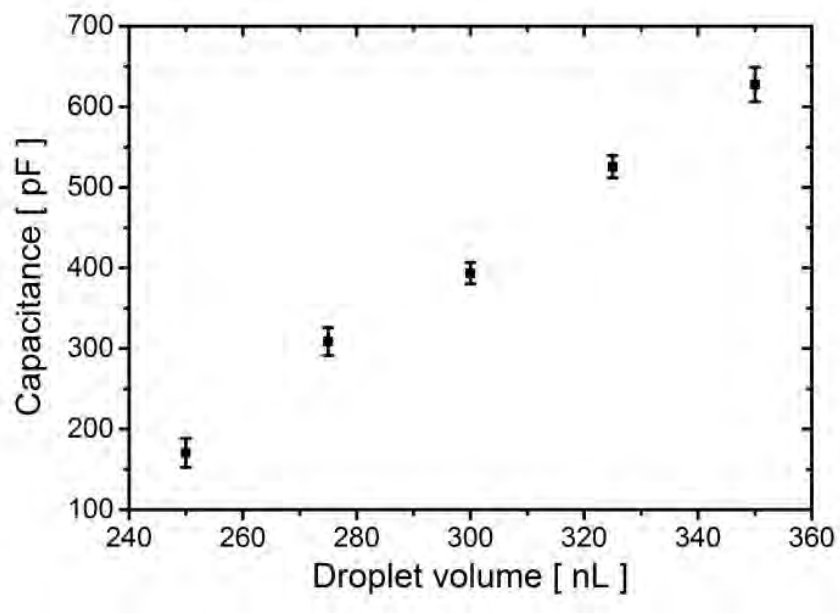


Fig. 33 Dependence of the measured bilayer capacitance on the volume of droplets. Each data point represent the average capacitance values measured for five droplet pairs; error bars represent the standard deviation (SD). The trend in the capacitance reflects the systematic dependence of the surface area of the bilayer on the volume of the droplets.

We distinguish two sources of variations. The first one refers to time-dependent fluctuations in the area of an individual bilayer, caused by internal flows of oil (e.g. convection), yet these changes are small (in the range of 1-6%). There is also variation between pairs of droplets, which may be the result of slightly different positioning of droplets in the trap during formation of bilayer. The relative

http://rcin.org.pl

standard deviation (RSD) for the bilayer area is in the range of ~5-10% in the case of smaller volumes (250 and 275 nl) and less than 5% for larger droplets. Smaller droplets, even if not positioned exactly in the middle of chambers by the confinement provided by the traps, are attracted to each other during the formation of a bilayer. Nonetheless, the position of smaller droplets in the trap is constrained to a lesser extent than for larger drops.

Droplet no	Droplet volume [nl]	Mean capacitance for a single bilayer [pF]	Time-dependent SD of capacitance for a single bilayer [pF]	Mean capacitance for a given volume [pF]	RSD of capacitance for a given volume	Bilayer area [μm^2]
1	250,00	152	9	171	10,4%	26 700 ± 2 800
2		161	5			
3		165	8			
4		176	8			
5		199	5			
6	275,00	302	9	308	7,0%	48 200 ± 3 400
7		331	19			
8		295	16			
9		292	17			
10		323	13			
11	300,00	374	8	394	4,1%	61 500 ± 2 500
12		395	11			
13		397	19			
14		411	7			
15		391	4			
16	325,00	521	26	525	4,1%	82 000 ± 3 400
17		514	16			
18		546	9			
19		534	13			
20		512	19			
21	350,00	626	21	627	3,9%	98 000 ± 3 800
22		618	13			
23		634	14			
24		601	6			
25		658	17			

Table 2 Results of measurements of capacitance and calculations of sizes of bilayers formed between droplets of various volumes.

4.3.4 α–hemolysin measurements

In order to test the functionality of the DIB we generated a pair of ~300 nL droplets and locked them in the hydrodynamic trap. One droplet contained a solution of a wild-type α–hemolysin protein nanopore and the second was

http://rcin.org.pl

composed only of the buffer. After formation of a DIB, we conducted a voltage clamp measurement at +50 mV. We observed the incorporation of single heptameric protein pores as step-wise (50 pA) increases in the current. Subsequently, we replaced the buffer droplet with a droplet containing a 5 μM γ-cyclodextrin (γCD), which is a reversible non-covalent blocker of the α-hemolysin pore. Pore blockades were observed as transient decreases in the current to ~40% of its open-pore value (Fig. 34).

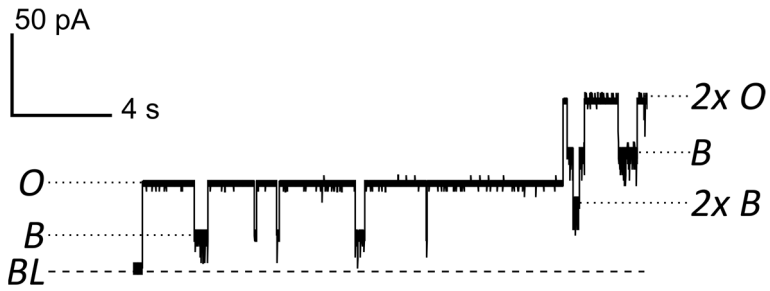


Fig. 34 A fragment of an exemplary current trace (20 s) presenting the incorporation of α-hemolysin nanopore into a DIB, clamped at + 50 mV. Stepwise increase of current from 0 to 50 pA reflects the incorporation of a single pore. The binding of inhibitor (γ-cyclodextrin, 5 μM) to the pore is observed as a decrease of current by approximately 60%. The insertion of next αHL heptamer into a lipid bilayer is seen as a further stepwise increase of current. Explanation of abbreviations: BL – baseline, O – open pore level, 2x O – 2 open pores, B – blocked pore, 2x B – 2 blocked pores.

Next, we checked whether residual inhibitor remained on the electrode. One of the generated droplets after the droplet containing very high 50-micomolar concentration of γCD. We observed intensive inhibition of the nanopores, seen as frequent events of current decrease (Fig. 35a). Next the droplet with 50 μM γCD was replaced by a droplet with buffer alone. Rare blockades (on average 1.5 events per minute compared to ~80 events per minute prior to washing) were recorded. Repetition of the exchange of the droplet completely eliminated the blockades of the nanopore (Fig. 35c). These results prove efficient washing of the electrodes.

http://rcin.org.pl

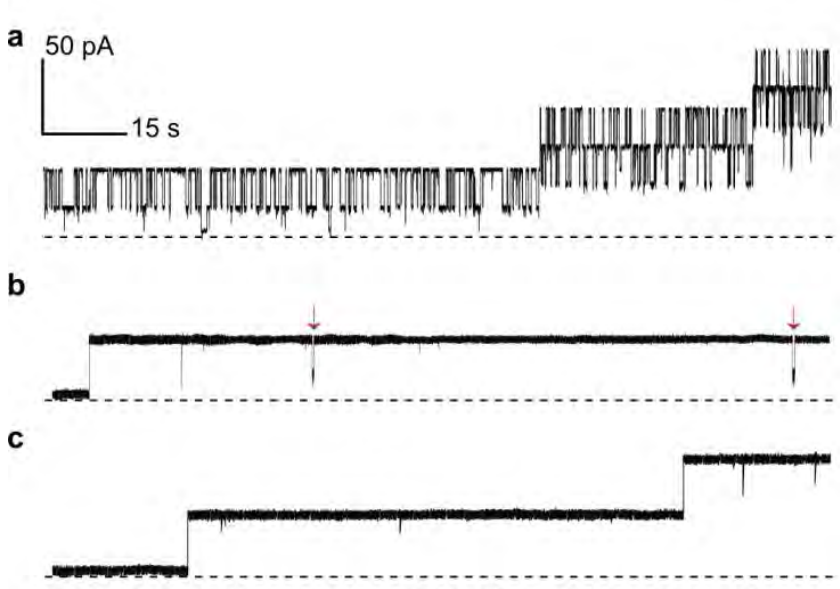


Fig. 35. Electrophysiological recordings showing the blocking events and the efficiency of the electrode washing. a) Nanopore inhibition with 50 μM γ-cyclodextrin was recorded for 10 minutes. b) The droplet containing high concentration of the inhibitor was replaced with a droplet of pure buffer (1 M KCl, 10 mM Tris-HCl, pH 7.0). Rare events of blockades (indicated with red arrows) were recorded. c) No further blockades were observed after the next round of droplet exchange.

4.3.5 Screening experiment

In the final experiment we demonstrated the ability of our system to perform automated screening. In the first step, we generated a sequence of 12 droplets containing 6 different concentrations (duplicates of 1, 10, 20, 30, 40 and 50 μM) of γ-cyclodextrin – the inhibitor of α-hemolysin nanopore. We used programmable syringe pump to form a sequence of droplets inside a 0.3 mm diameter PTFE tubing by alternating the aspiration of small volumes of aqueous solutions of different concentrations of the inhibitor (300 nL) and oil admixed with lipids (700 nL) stored in a standard 96-well plate (as described in Section 3.3 and shown in the Fig. 10). Transport of the droplets containing inhibitors on the chip was controlled by optical feedback and external valves.[77,83] In the screening experiments, we first generated a droplet containing α–hemolysin heptamers, which was subsequently locked in the trap. Then we introduced the first droplet from the sequence of droplets containing various concentrations of inhibitors. We performed measurements of the current through the pore in a bilayer that was voltage-clamped at +50 mV. In a following step we washed the electrode with the portion of pure buffer and introduced next droplet presenting different concentration of γCD. An exemplary recording of

http://rcin.org.pl

4 subsequent exchanges is shown in Fig. 36. It is important to note, that the process of droplet exchange disrupts the bilayer, and dislodges the protein. As a result, most likely different protein nanopores are studied in the measurements on successive droplet pairs. We carefully set concentration of protein to 0.5 μg·mL^{-1} in order to observe clear intervals between incorporation of the first and subsequent pores. Consequently, we were able to analyze the kinetics of inhibition at a single-pore level. After the recording, we removed the droplet containing the inhibitor and washed the electrode with a droplet comprising pure buffer alone generated automatically in a T-junction. The single cycle of removing a droplet, washing the electrode, introducing a fresh droplet with new concentration of the inhibitor and conducting the measurements took 210 s.

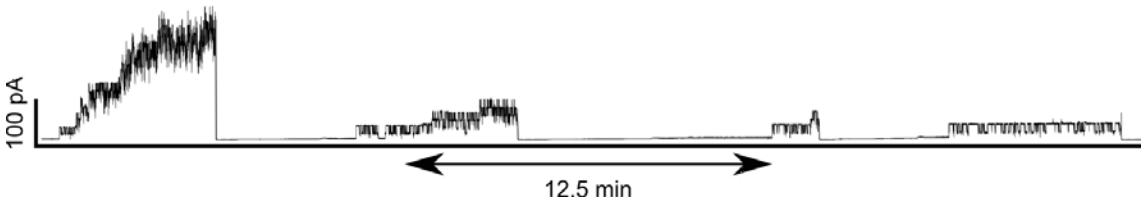


Fig. 36. Screening of various concentrations of γCD against single *α*–hemolysin pores. Continuous trace of current shows subsequent incorporation of αHL nanopores in bilayers formed between a droplet containing a protein solution and 4 successive droplets with decreasing concentrations of γ-cyclodextrin (50, 40, 30 and 20 μM).

We were able to perform two rounds of the screening with 6 concentrations of the inhibitor in each screening (Fig. 37a) by using a single droplet containing α-hemolysin. In about half of individual DIBs we observed the successful incorporation of at least one nanopore. Over time we noticed a decreased rate of pore insertion, which is consistent with the results of a previous studies.[190] We suppose that the decrease in the insertion rate is associated with aggregation of the diluted protein. After the second round of screening (40 min from the beginning of the experiment) we observed almost no insertion of pores within the arbitrarily set duration of recording equal to 210 s. However, our system allows the replacement of the droplet containing the protein with a fresh one. As a result, we were able to repeat the whole screening procedure five times, giving in total ten repetitions for each inhibitor concentration. In other words, whole procedure consisted of 60 measurements and each of them was done on a newly formed bilayer.

http://rcin.org.pl

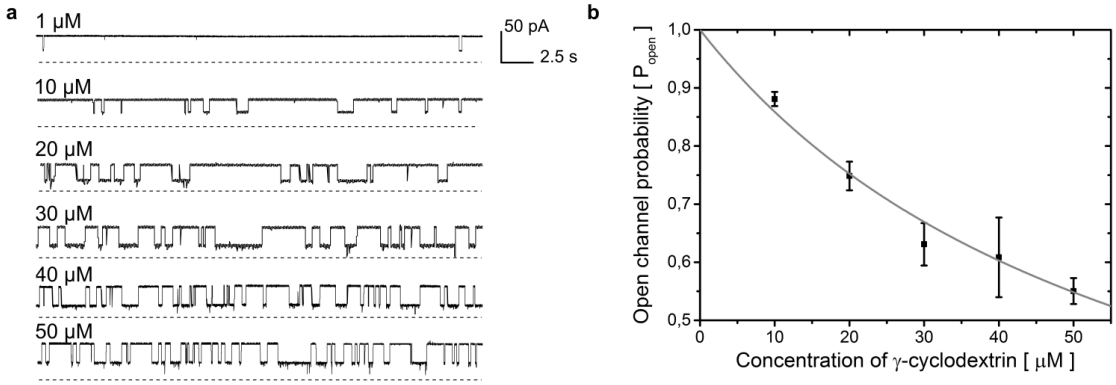


Fig. 37 a) Results of screening of inhibitors against a single α–hemolysin channel. Short segments of current traces in the presence of γ-cyclodextrin at various concentrations (1 μM - 50 μM). b) Dose-dependent inhibition of a single αHL pore by γ-cyclodextrin. Probability of open channel (P_{open}) was plotted versus the concentration of the inhibitor. The error bars represent the SD from at least three trials. The curve was plotted using the saturation function and the dissociation constant (K_d) found to be 61 ± 7 μM.

$$\mathbf{P_{open}} = \left(\mathbf{1} + \frac{c}{K_d}\right)^{-1}$$

Using the current traces obtained for 10-50 μM γCD, we analyzed the duration and frequency of blocking events and calculated the dissociation constant (K_d) in a following way:

a) We derived the rate constants using the data obtained from at least three different experiments from single channel recordings with an entire duration of at least 120 s (see Table 3). We analyzed only those fragments of traces that contain the activity of single α-HL pores.

b) We calculated the dissociation rate constants, k_{off}, for each concentration as the inverse of the mean residence time (τ_{off}) of γCD inside αHL pore.

c) We obtained the association rate constants, k_{on}, from the slope of a plot of the inverse of the mean time of inter-event interval (τ_{on}) versus the concentration of γCD. Single-channel recordings have different durations in each experiment, so we calculated the weighted mean of K_d values and the weighted mean of SDs values. The obtained value of K_d (61 ± 7 μM) compares well with the value of 47±9 μM measured in the study of Mantri *et al.*[239] for αHL heptamer (in slightly different buffer conditions: 1M KCl, 25mM Tris HCl and 50 mM EDTA, pH 8).

http://rcin.org.pl

		Concentration of γ-cyclodextrin [μM]					
		1	**10**	**20**	**30**	**40**	**50**
Round of screening	1a	x	93	x	x	24	x
	1b	x	x	57	8	x	x
	2a	x	x	106	24	44	10
	2b	x	x	x	70	x	82
	3a	22	47	x	x	27	16
	3b	x	x	82	x	92	37
	4a	25	x	x	x	66	18
	4b	x	x	20	x	x	x
	5a	62	5	13	15	x	x
	5b	92	x	x	42	34	4
	Total time	**201**	**145**	**278**	**159**	**287**	**167**

Table 3 Duration of single-channel recordings in screening experiments. The table comprises the times (in seconds) between the stochastic insertion of the first and the second nanopore to the bilayer. In some of the measurements, single-channel recording was terminated by the exchange of the droplet, according to the described protocol. The letter *'x'* indicates experiments in which there was no channel insertion into the bilayer.

4.3.6 Summary

We have developed an automated microdroplet system capable of fast, simple and reproducible screening of inhibitors against membrane proteins. Up to now, droplet microfluidics have been used to generate droplet interface bilayers very efficiently,[195,197] but without the ability to perform electrophysiological recording on the membrane formed at the interface of two droplets. In comparison to microfluidic systems relying on assay of diffusion of fluorescent dye through the pore,[194,196,198] our device is able to conduct reproducible single-pore electrophysiological recordings including the on-off kinetics of inhibition. Our method allows for automation of these measurements and for additional operations, such as washing and exchange of microdroplets containing both the inhibitor solution and the protein. The droplet microfluidic system uses a minute volume of samples, equal to several microlitres. Reduction of buffer consumption was achieved by the direct aspiration of tiny aqueous droplets (300 nL) from a 96-well microtiter plate and by design of reservoir channels that accept the microliter volumes of liquids for further operations on chip. The main advantage of our system is easy exchange of the droplets and automated execution of operations on sequences of samples, an outstanding challenge of number of studies in the recent years.[177–180,184,187,190,192] Additionally, the electrodes in our device can be used

http://rcin.org.pl

during a period of 3 weeks and they did not show loss of activity, despite their intensive use, including repetitive wetting and de-wetting of their surface with droplets. We did not observe any depletion of neither the layer of agarose gel, nor the layer of AgCl on the surface of silver wires. What is also important, there were no changes in the performance of the chip over extended periods of operation, in particular we did not observe any wetting of the walls of the channels with the aqueous content of the droplets.

The increasing number of studies on various membrane proteins (including human ion channels) incorporated into droplet interface bilayers,[175,177–180,238] suggests that DIB may constitute an alternative to methods based on formation of planar lipid membranes.

http://rcin.org.pl

4.4 Generation of libraries of nanoliter droplets and application of this technique for improved DNA quantification with digital PCR

We have developed a method for a rapid and automated generation of multiple, chemically distinct populations of ~10^3-10^4 sub-nanoliter droplets from a sequence of large, microliter samples of liquids (Fig. 38). Formation of these *'libraries of droplets'* proceeds in the following steps: i) generation of a sequence of microliter droplets of arbitraily predetermined chemical composition, ii) transport of these '*mother droplets*' from a milimeter- to a micrometer-wide channels, iii) splitting each of the parental drops with a flow-focusing junction into thousands of tightly monodisperse daughter droplets and iv) optional separation of such formed homogeneous populations with plugs of a third immiscible fluid. Our approach is compatible with various techniques of on demand generation of droplets, such as aspiration of microliter portions of liquid from a 96-well plate with a robotic station (section 3.3) or generation of microliter droplets using electromagnetic valves[55,56] or passive systems.[105]

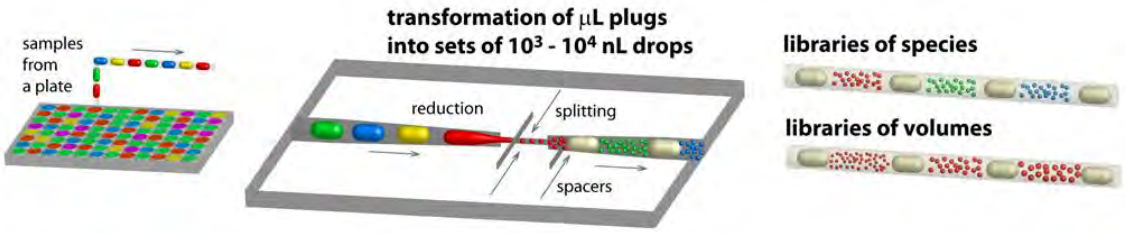


Fig. 38. A scheme of the microfluidic system for the rapid generation of droplet libraries.

The second part of this section presents application of the technique of droplet libraries to the improvement of the dynamic range of droplet digital PCR assays. The system allows for precise determination of high DNA concentration. Our approach requires only ca. 20 thousand droplets, a number reduced by up to 3 orders of magnitude in comparison to classical digital PCR assays. Importantly, our system operates on mixed libraries and does not require tracking the identities of the partitions - thus does not increase the complexity of the execution of the assay. Our approach uses a variant of the algorithm for rational design of digital assays[239] that requires small number of dilutions.

http://rcin.org.pl

The fluid handling in our system is based on 3 technologies:

a) flow control using programmable syringe pumps – described in section 3.2.2
b) merging and metering of droplets in improved hydrodynamics traps – method based on previous research of Korczyk *et al.*[105] and presented in details in section 3.3.2.
c) a novel method of splitting of droplets into monodisperse libraries of droplets using modified FF-juction.

4.4.1 Generation of droplet libraries

The challenge of transition of microliter liquid samples into populations of nanoliter droplets is complicated and demands an appropriate design of the geometry of microfluidic channels that guides the parental plugs to the FF-junction. We found that the level of monodispersity of generated micro-droplets library depends critically on the details of the geometry of the channel ahead the FF-junction. When a microliter droplet of liquid enters the FF-junction, multiple forces and parameters of the flow are changed. Most noticeably, the shape and curvature of the droplet evolve during the splitting process. Consequently, the Laplace pressure is not constant and this may introduce systematic changes in the volume of droplets produced at the beginning and at the end of the fission of the mother droplet. Another important parameter is the change of the droplet velocity during the splitting, that results from the rise of hydrodynamic resistance when the droplet enters the FF-junction. Presence of droplets in square channels increase the hydrodynamic resistance[240,241] and this effect is enhanced for elongated droplet entering FF-junction. Additionally, the speed of the droplet depends on its length[242] that changes as the droplet enters and flows through the junction - again making up for potential systematic changes of the ratio of rates of flow at the junction. All these factors can influence the monodispersity of volumes of daughter droplets.

4.4.1.1 Optimization of the geometry of the FF-junction for generation of droplet libraries

Obtaining nanoliter droplets of diameters of tens of micrometers requires a tight flow-focusing junction comprising square channels of ca. 100 μm width/height. The parental ~ 1 μL droplet in a 100 μm channel would occupy an

http://rcin.org.pl

impractical length of 10 mm, making it difficult to accommodate a long sequence of such samples and creating a very high hydrodynamic resistance to flow. It would be more reasonable to deliver microliter parental droplets via a millimetric channel. However, the change of the cross-section of the channel increases the differences in the Laplace pressures and the speed of the parental plugs relative to the flow of the continuous liquid that pushes them into the junction. Thus, the transition between the input channel and the flow-focusing junction has to be designed in such a way as to minimize the variation of size of the daughter droplets generated from a finite liquid sample. Fig. 39 shows the layout of the microfluidic chip that was used to test the optimum geometries for transformation of a microliter liquid plug into a population of monodisperse daughter droplets. The chip contained a T-junction for formation of the parental plugs. The T-junction section comprised channels of square cross-section (800 x 800 μm) and was supplied with liquids through external electromagnetic valves to allow for formation of individual droplets on demand. The outlet of the T-junction entered the transient section of the channel that led to the FF-junction of square 100 x 100 μm channels.

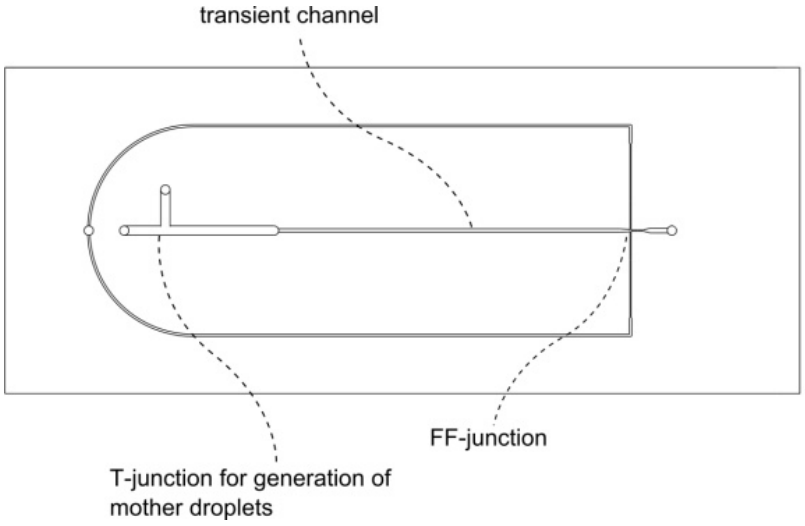


Fig. 39 A scheme of the microfluidic chip that we used to study the role of the geometry of transition between the wide inlet channel and the narrow flow-focusing junction on the quality of the volume distribution of the daughter droplets.

On the basis of multiple experiments with various geometries we selected a compromise cross-section of the transient channel of 300 x 300 μm that resulted in a ~7 fold elongation of the parental plug (as compared to the large 800 x 800 μm channel in the T-junction). Smaller cross-sections of this transient channel often resulted in an uncontrolled fragmentation of the parental plugs

http://rcin.org.pl

during elongation. As we discussed above the quality of the emulsion produced from a single parental plug depends critically on the details of the geometry of the transitions between the outlet of the T-junction and the transient channel and between the transient channel and the FF-junction. We tested in detail three geometries: a) a system equipped only with a short funnel that directly connected the wide channel with the FF-junction b) a device with a short 0.6 mm-long, transient channel that can hold only a part of a mother droplet and c) a system with a long 30 mm transient channel that is able to accommodate an entire parental microliter droplet (Fig. 40).

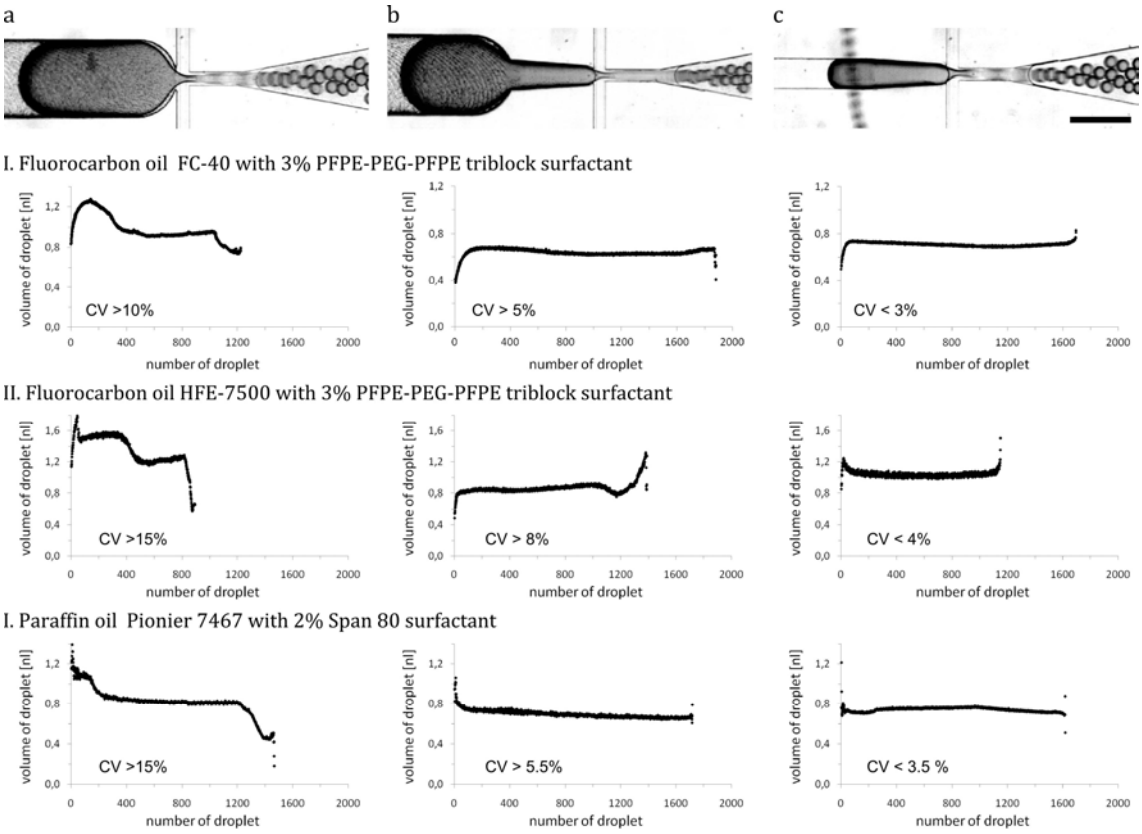


Fig. 40 Micrographs of the three geometries of the junction between the wide inlet channel for the parental plugs with the narrow flow-focusing droplet generator: a) junction without any transient channel b) junction with a short transient channel and c) junction with a long transient channel that is able to accommodate the entire parental droplet. Underneath each micrograph three graphs of the volumes of daughter nanoliter droplets produced from a single parental microliter plug in different sets of oil and surfactant. We tested the system using three different liquids as continuous phase: I – fluorocarbon oil FC-40 with 3% of PFPE-PEG-PFPE triblock surfactant. II - fluorocarbon HFE-7500 with 3% of PFPE-PEG-PFPE triblock surfactant and III - paraffin oil Pionier 7467 with 2 % Span 80.

http://rcin.org.pl

Each mother plug flowing with the velocity of 1 ml·h^{-1} was split into tiny droplets at a frequency of break-up of about 1 kHz with a 2 ml·h^{-1} cross-flow of continuous phase. The maximum rate of formation of daughter droplet was limited by a crossover to jetting regime, allowing us to safely run the experiments with rates of flow in the range of 1 mL·h^{-1} to 10 mL·h^{-1}. We measured the volume of each daughter droplet using methods of image analysis described in section 3.4. The geometry (a) that had a direct connection between the wide (800 μm) and the narrow (100 μm) channels provided a significant polydispersity described by the coefficient of variance (CV > 10 %) of volume of the daughter droplets (Fig. 40a). As shown in the graphs in the first column of the Fig. 40, at the beginning of the splitting process larger droplets were produced. We hypothesize that this phenomenon results from a release of pressure that is build-up in the inlet channel in order to overcome the Laplace capillary back-pressure when the large plug enters the small FF-junction. After this initial burst, we observed a relatively short interval of stabilization of the size of the droplets followed by the final stage within which systematically smaller droplets were formed. The decrease of the volume of the droplets in the last stage can be explained by the increasing flow of oil through corner gutters *by* the parental plug of decreasing length – resulting in a smaller rate of flow of the droplet phase. Also, at the end the rear of the droplet adopts an increasingly tighter curvature that slows down the flow of the plug through the FF-junction. Addition of a short transient channel just upstream of the FF-junction in geometry (b) (results presented in the middle column of the Fig. 40) significantly improved the tightness of the distribution of volumes of daughter droplets. The coefficient of variance of the volume of droplets produced in geometry (b) fell slightly above 8 %. Finally, in geometry (c) that completely separates the processes of squeezing the liquid plug into a tighter channel and the process of splitting the plug into nL drops we observed that less than 1.5 % of the daughter droplets had volumes significantly different than the mean. The CV of the volumes of the droplets produced in this system was smaller than 4 % (third column in the Fig. 40), thus passing the standard definition of monodispersity.

http://rcin.org.pl

4.4.1.2 Generation of exemplary libraries

Having identified the optimum geometry of the system for splitting micro-liter plugs into nL droplets, we constructed the integrated system that accepts a sequence of microliter liquid samples, splits them into daughter droplets and separates the chemically homogeneous populations with spacer bubbles or droplets of third immiscible liquid. We used the integrated system to generate two types of exemplary populations of nL droplets: i) libraries of species, and ii) libraries of volumes. As a continuous phase we used either hexadecane or fluorocarbon oil FC-40. First, we prepared the sequence of 1 μL mother droplets by aspiration of samples from microtiter plates (see details in section 3.3). To demonstrate formation of libraries of species we used aqueous solution of inks of various colors: havana, black, red, blue and green (Waterman, France). The mother droplets were generated at a frequency 0.15 Hz which was limited by the specifications of positioning system – i.e. minimum time needed for XYZ movement of automated arm from one well to another. Throughput of droplet aspiration can be increased by parallelization and use of multiple pumps. Next we transferred the sequence to the chip equipped with FF-junction for droplet splitting. We fabricated two versions of the splitting chip: i) made of polycarbonate – a material compatible with hexadecane and ii) PDMS chips for use with fluorocarbon oils. The single library was produced at a frequency of 0.14 Hz with the daughter drops formed at ca. 1 kHz (Fig. 41). The throughput of the splitting process can be improved by decreasing the volume of the mother droplet and by a decrease of the dimensions of the FF-junction. After the fission process, the daughter droplets flew into an again-wider channel (800 x 800 μm) equipped with an additional T-junction needed for formation of the spacers. We were able to produce two types of spacers: i) air bubbles or ii) 400 nL plugs composed of light mineral oil (Sigma Aldrich, Germany) saturated with dye Oil Red EGN (Sigma Aldrich, Germany). We used real time optical detection of droplets[54] using a digital camera (uEye UI-1245LE-C, IDS GmbH, Germany) connected to an image processing Lab View software that used the signal from the droplets to trigger the valves controlling the flow of the spacer fluid (air or oil). Micrographs on Fig. 41 illustrate an exemplary process of splitting of a microliter mother droplet into a population of nanoliter daughter drops and introduction of a gas spacer in a

http://rcin.org.pl

polycarbonate chip. After splitting we transferred the populations of daughter droplets into tubing of circular cross-section in order to minimize the flow of the continuous liquid passing the spacers and transfer of small droplets through the corner gutters that appear in rectangular channels.

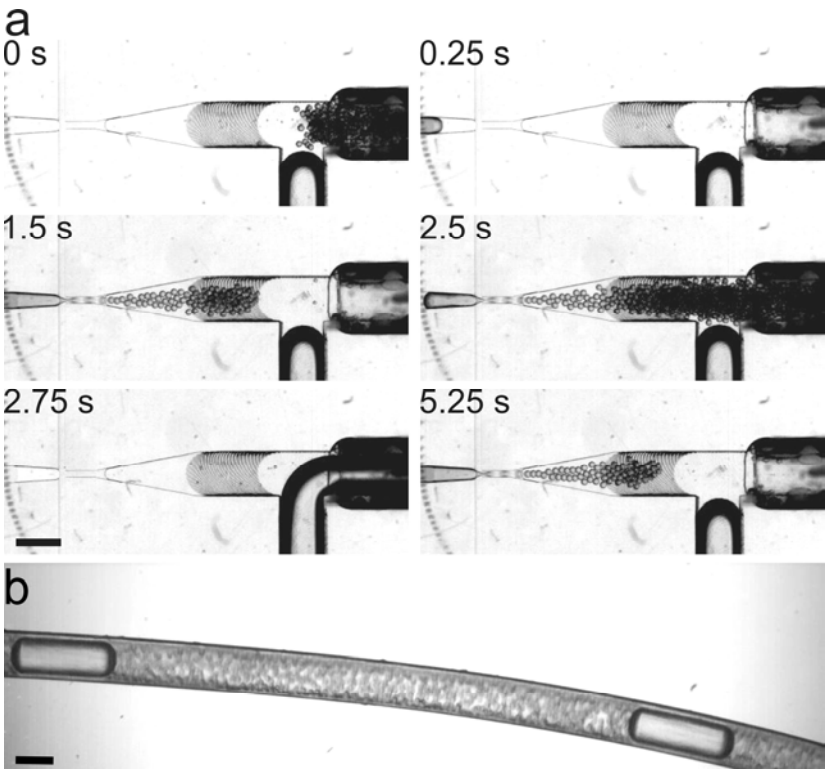


Fig. 41 Micrographs illustrating generation of an exemplary library in a polycarbonate chip. The parent microliter droplet is split into ca. 1600 daughter droplets (volume ~ 0.6 nL). Each population of daughter droplets is generated at a frequency of 0.2 Hz. Each element (daughter drop) of the library is generated at a frequency ~1 kHz. Libraries are separated by air bubbles generated on demand in the operation that is automatically synchronized with the splitting process. Inset b presents the polyethylene tubing (Becton Dickinson, United States) containing the libraries separated by bubbles. Scale bars are 800 µm.

Apart from formation of droplet libraries of distinct chemical composition (Fig. 42a), we were able to generate populations with changing volume (Fig. 42b). To this end, we first generated an array of 1 µL identical aqueous droplets containing 1 % of red ink and split them into a sequence of populations and each of them was generated with a different rate of flow of the oil through the FF-junction. The automated change of oil flow rate was possible thank to the real-time image analysis system with a Lab View control of pressure via an electronic proportional regulator (MPT40, Parker, United States). The system adjusted the rate of flow of the splitting-oil between 1.2 $ml \cdot h^{-1}$ and 3.6 $ml \cdot h^{-1}$ producing a sequence of populations of droplets of different volumes (Fig. 42c).

http://rcin.org.pl

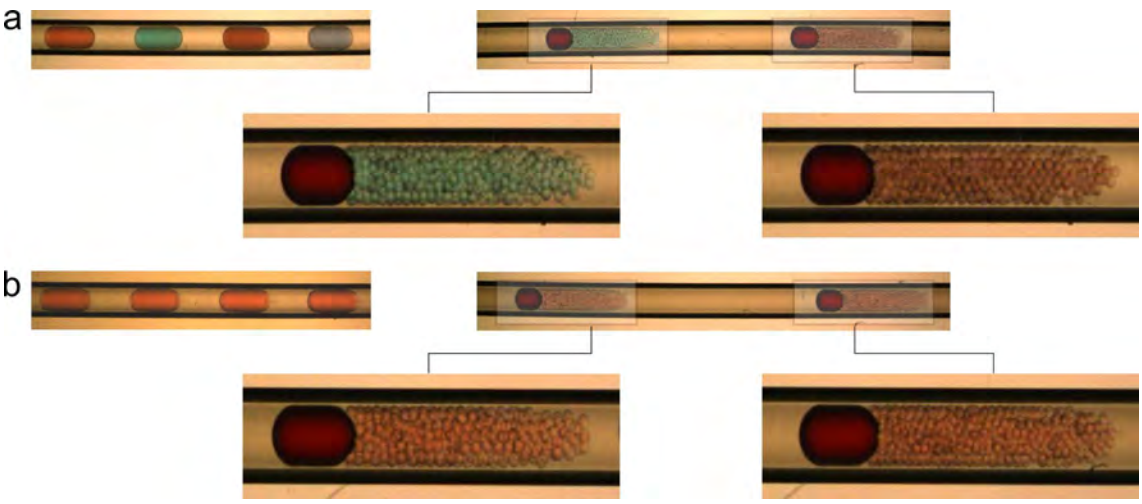


Fig. 42 Examples of two different input sequences of parental plugs and the corresponding libraries of daughter droplets. Droplet libraries are separated with spacers of immiscible third phase – in this case dyed light mineral oil. Micrograph (a) presents libraries with various compositions; micrograph (b) depicts libraries with various volumes of daughter droplets. Droplet phase used in this experiment was 1% (v/v) aqueous solution of inks of various colors. Fluorocarbon oil FC-40 with 3% of PFPE-PEG-PFPE triblock surfactant was used as continuous phase.

Besides the prevention of cross-contamination of the populations of chemically distinct droplet populations, our system can be used as a method for transport and incubation of droplets. Flow segmentation ensures equal incubation time, similarly to the previously proposed delay lines[55] or close-packed plug flow.[56] The separation of the libraries in a sequence can also be used to identify the different populations without the need for colorimetric coding.

4.4.2 Combining droplet libraries with digital PCR for quantification of high DNA concentrations

This section describes the application of the technology of generation of droplet libraries to quantification of very high DNA concentrations that are beyond the capabilities of classical digital PCR. The protocol of the technique consists of four steps (Fig. 43): i) generation of a sequence of 20 microliter droplets comprising 2-fold dilutions of a DNA sample, ii) each of these parental droplets is split into ca. thousand tightly monodisperse daughter droplets iii) all the resulting nanoliter droplets are pooled together and stored in an Eppendorf tube for an off-chip PCR, and finally iv) fluorescence of each of the ca. 20 thousand droplets is measured in high-throughput manner. The microfluidic system is composed of two separate microfluidic devices. The first one utilizes passive hydrodynamic traps to prepare

http://rcin.org.pl

dilutions of the sample and comprises FF-junction for transforming microliter droplets into libraries of nanoliter drops. The second chip is used for reinjection of the emulsion after PCR for high throughput interrogation of the fluorescent signal from each nanoliter droplet.

We used the recently published algorithm[239] to estimate the expected value of initial concentration of DNA on the basis of the dilution ratio and population of each library. Then we compared theoretical predictions with the values measured in our system.

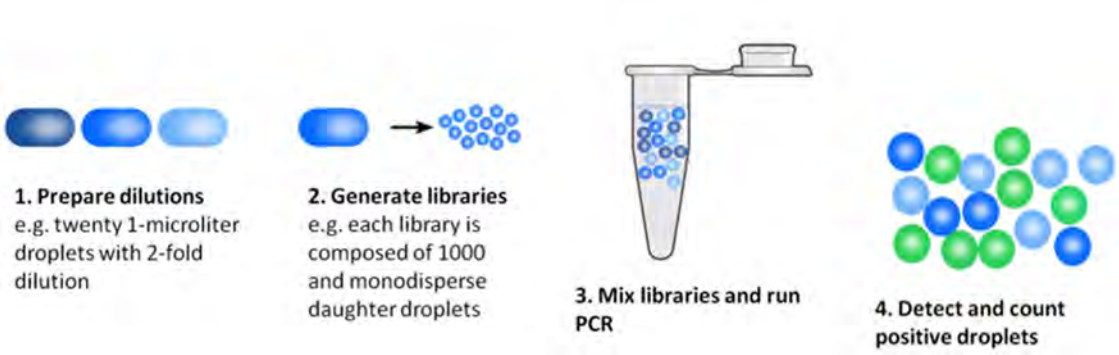


Fig. 43 A scheme depicting subsequent steps of the technique utilizing droplet libraries for digital PCR with extended dynamic range.

The first microfluidic device comprises a dilutor, a storage channel and a droplet splitter. The dimensions of microfluidic channels ranged from 100x100 µm to 800x800 µm. The dilutor module is based on the technique of hydrodynamic traps (see detailed description in the section 3.3.2) in which droplets are sequentially locked, cut and merged.[105] There are two types of traps in our system: i) the metering trap that precisely cuts and aliquots nanoliter volumes from larger droplet and ii) the merging trap that locks two droplets, fuse them and release one droplet for further operations. Geometry of the traps was optimized in order to provide efficient processing of droplets containing PCR mix that is characterized by very low values of surface tension. We also scaled up the dimensions of the traps in order to generate the dilution in 1 µL droplets. However, as a result of imperfections of micromilling process, our system was capable in formation of concentration gradient in 0.95 µL droplets. The successive steps of gradient formation are presented on Fig. 44. For the purpose of clear visualization of the process we added following dyes to the aqueous phase: 0.05 % w/v Congo Red (POCH, Poland) and 0.002 % w/v blue resazurin (Sigma Aldrich, Germany).

http://rcin.org.pl

We first on-demand generate a 1.9 μL droplet with the sample comprising reaction mix with primers, probes and DNA (Fig. 44A) in the T-junction. The droplet flows intact through the merging trap (Fig. 44B) and it is split into two equal subvolumes in the metering trap – first droplet comprised the first dilution and it is transported outside the module while the latter one stayed locked in the trap (Fig. 44C). Next, we reversed the direction of flow in order to release the droplet from the metering trap and to route it back to the merging trap (Fig. 44D). In the following step, we generated a droplet containing the buffer (reaction mix with primers, probes but without DNA) in a T-junction (Fig. 44E) and then fused the two droplets in a merging trap. The content of the merged droplet was subsequently mixed in a winding channel (Fig. 44G). We then 18 times repeated the steps of dilutions (Fig. 44D-G). The system completed generation of the sequence of 20 microliter droplets containing a gradation of concentration of a sample within ~ 8 minutes. The whole operation was conducted using programmable syringe pumps (Cetoni, Germany).

In order to assess the quality of the gradient we performed control experiments with rhodamine 110 added to the sample. We did not measure the decrease of fluorescence for all 20 droplets due to the high level of noise in the signal from the very low (less than 10 nM) concentrations of dye. We assumed that the dilution ratio is constant throughout the generation of subsequent droplets since the operation of splitting and merging were conducted with the same traps. The averaged dilution ratio equaled 2.23 ± 0.08 (RSD was 3.5 %, n=3). The ratio was higher than expected 2-fold, probably due to not complete mixing of the droplet in the winding channel. Most importantly, however, for the prospect of use of this technology, the procedure is highly reproducible (within a batch and between batches), i.e. it is precise. The accuracy can be tuned by changing the geometrical aspects of the traps.

http://rcin.org.pl

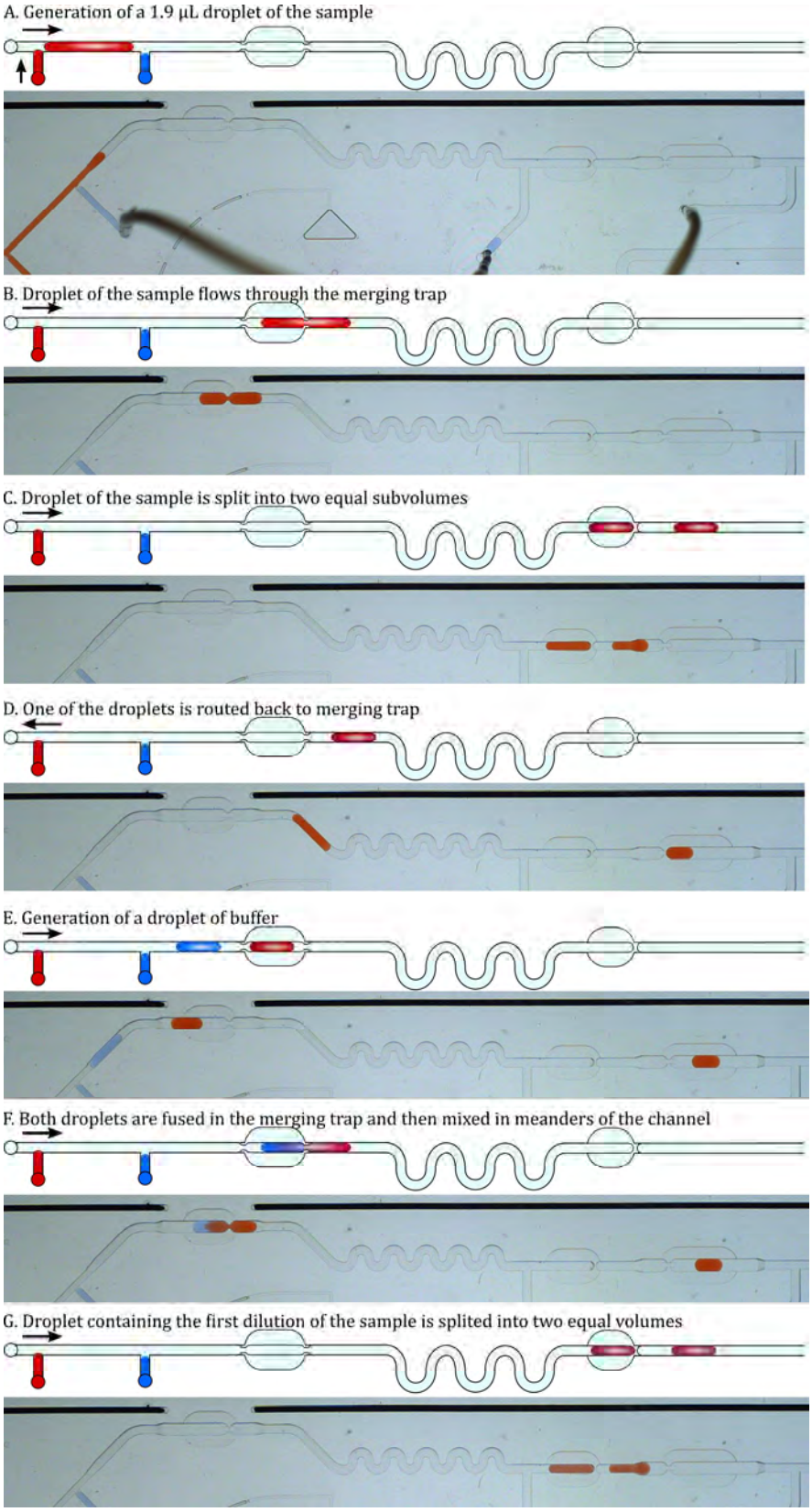


Fig. 44 A-G) Simplified schemes and corresponding pictures depicting the process of generation of serial dilution in the sequence of 20 microliter droplets. The function of the additional large hydrodynamic trap presented on the micrographs (on the right side of the picture) was to ensure that only one of the 0.95 µL droplet (generated as a result of splitting of 1.90 µL large plug) is routed back for further dilution.

http://rcin.org.pl

Next microliter parental droplets were split in a similar way (Fig. 45A, B) as in the method described in the section concerning droplet libraries (4.4.1.2). Briefly, we passed 0.95 µL droplets, initially stored in a wide channel (800x800 µm), to a transient, narrow channel (300x300 µm) which ended with FF-junction (100x100 µm). We adjusted the flow rates to 1.5 ml·h^{-1} for droplet phase and 7 ml·h^{-1} for splitting continuous phase and we obtained library comprising ca. 954±17 relatively monodisperse droplets (Fig. 46).

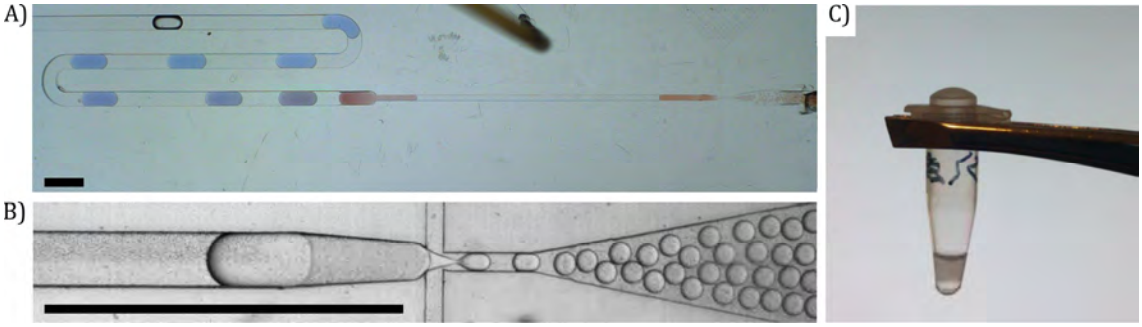


Fig. 45 A-B) Pictures depicting the process of splitting of mother droplet into the library of nanoliter droplets. At the end of the sequence of mother droplets, there is air bubble generated after formation of gradient. After splitting, the bubble pushes libraries of nanoliter droplets from the tubing to 96-well PCR plate or 0.2 mL PCR tube (C). Scale bar is 2 mm.

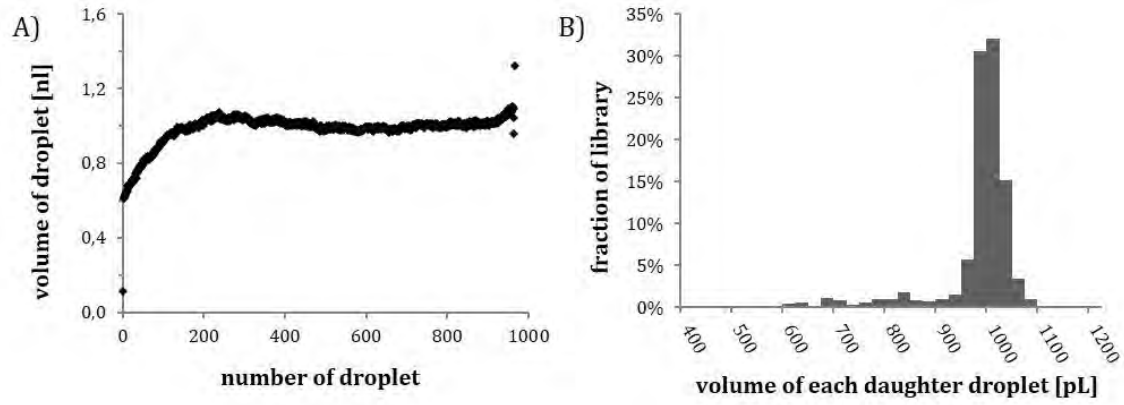


Fig. 46 A) An exemplary plot of the volumes of daughter droplets produced from a single parental plug. B) Histogram (average from 7 measurements) showing the distribution of droplet volumes in an exemplary library.

The quantity of droplets in each library and the level of polydispersity was determined by measuring volumes of each droplet in 7 different libraries. The level of polydispersity (CV of volumes was equal 8.5%) was higher than in the case of droplet libraries generated from pure aqueous solution – this phenomenon can be associated with high concentration of surfactant in both phases: aqueous PCR mix and oil used for droplet PCR. We collected the libraries in a U-shaped FEP tubing

http://rcin.org.pl

(I.D. 0.8 mm O.D. 1.6 mm, Bola Bohlender, Germany) connected to the inlet of the chip. Buoyancy of droplets led to the compact packing of the emulsion in the bended part of the tubing. After having split all the droplets the plug of air pushed the packed emulsion towards the other inlet of the tubing, assuring deposition of all the droplets into the well of 96-well plate or 0.2 mL Eppendorf tube (Fig. 45C). We used Rotaxys positioning system to control deposition of subsequent samples.

We run PCR using standard thermocycler and reaction conditions described in the section 3.8. After thermocycling we aspirated the emulsion to 0.8 mm FEP tubing using Nemezys syringe pump and Rotaxys positioning system (both from Cetoni, Germany). Next, we re-injected the emulsion into the detection chip with the flow of 0.6 $\mu l \cdot s^{-1}$ and we carried out the fluorescence readout (Fig. 47). We spaced single nanoliter droplets in the junction by pure HFE-7500 oil (3M, United States) flowing from side channels with the rate of 1.8 $\mu \cdot s^{-1}$ (Fig. 47A). We used confocal microscope to measure the intensity of fluorescence at the rate of up to ~500 droplets per second (Fig. 47B). At least 15 000 droplets out of 19 000 were aspirated and successfully measured for each sample. We did not aim at measuring all of the droplets - we assumed that the measured fraction was representative of the mixture of droplets with different concentrations of the sample since the droplets had been mixed after generation inside the wide FEP tubing and during deposition in the well of PCR plate.

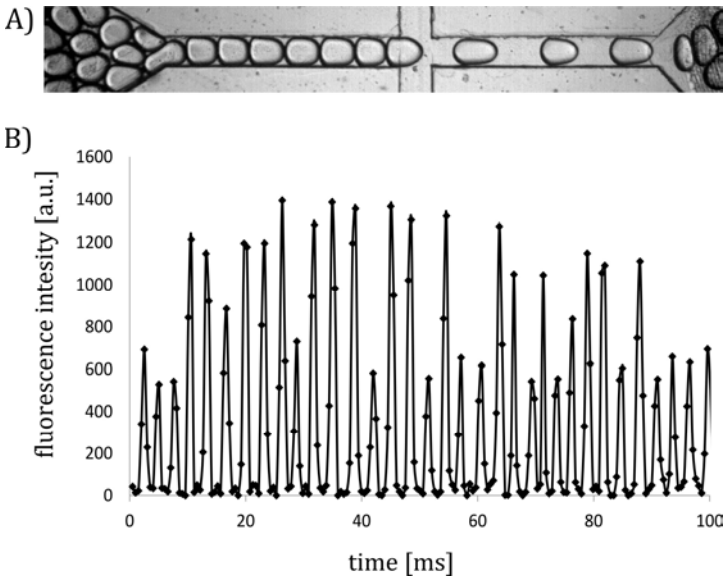


Fig. 47 A) A micrograph depicting the geometry of the chip used for optical readout droplets. The width and depth of the channels at FF-junction was 100 μm B) An exemplary 100 ms trace with the results of high throughput measurement of fluorescence. Every peak corresponds to signal from a single droplet.

http://rcin.org.pl

In order to validate the method, we performed series of PCR experiments with samples containing 3 different DNA concentration 3.3 x 10^5, 3.3 x 10^6 and 3.3 x 10^7 copies per microliter (Fig. 48). We can clearly distinguish two populations of negative (with low fluorescence) and positive (with high fluorescence) droplets. The positive droplets contained at least one strand of DNA after formation of a library.

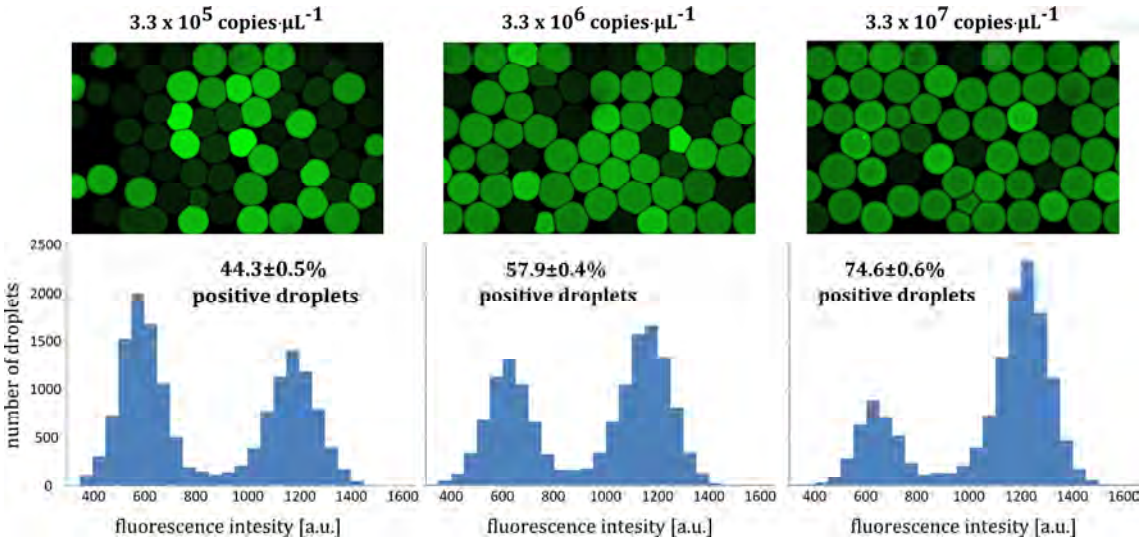


Fig. 48 Results of ddPCR based on droplet libraries: confocal images depicting the emulsions after thermocycling and corresponding plots with distribution of the values of fluorescence signals in the sample.

The experimental results were verified numerically using grand canonical Monte Carlo simulations according to recently published mathematical model.[239] Calculations were conducted by Paweł Dębski and their results are presented in the Table 4. Each run of the simulation referred to a real, independent assessment. The performance of the assay was tested for 100 values of initial concentration uniformly distributed in the range of concertation from 10^0 copies·µL^{-1} to 10^9 copies·µL^{-1}. Simulations also take into account various parameters of the assay (averaged ratio of dilutions, number of compartments in the library, volumes of compartments in one library), that were given by Gaussian distributions with expected number of droplets in the library and standard deviation determined experimentally. In the simulation, it was assumed that even a single molecule of the analyte (DNA strand) always yields positive signal.

http://rcin.org.pl

DNA concentration	Experimental results	Theoretical predictions
$3.3x10^5$ copies·μL^{-1}	44.3±0.5%	46.9±1.3%
$3.3x10^6$ copies·μL^{-1}	57.9±0.4%	61.0±1.7%
$3.3x10^7$ copies·μL^{-1}	74.6±0.6%	74.9±2.1%

Table 4. Comparison of results obtained experimentally with theoretical predictions calculated using Monte Carlo simulations.

As shown in the Table 4, the experimental results slightly deviate form predicted theoretical values, which can be explained by not complete mixing in droplets during generation of gradients. In the close future we are going to test theoretical model with a device comprising more efficient mixing module with a longer winding channel. Nevertheless, these differences do not disturb overall precision of the assay, which is acceptable for most applications of PCR in biology and diagnostics. The main advantage of our approach is extended dynamic range comparing with the classical digital PCR. For example, in order to determine the concentration of $3.3x10^7$ copies·μL^{-1}, classical dPCR[34,60,112] would require ca. 10 million droplets – a number which is not practical in terms of experimental execution of the assay and which is higher by more than ~3 orders of magnitude than the number of compartments in our approach.

4.4.3 Summary

The system for generation of droplet libraries presents the complementation of the automated systems[55,56,108] for generation of large microliter plugs of arbitrary composition with the methods for generation and high-throughput screening of small nano- and picoliter droplet libraries.[76,221] The optimal geometry that we report here offers a remarkably monodisperse population of subnanoliter droplets generated by the splitting of discrete and small, microliter liquid samples (standard variation of the volumes within a library can be smaller than 4 % of the mean). For comparison, the distribution of volumes produced in fractal cascades of T-junctions, produced CVs of the volumes of daughter droplets at the level of 10 % or higher.[59,100]

Technology of droplet libraries allows for facile transformation of sequence of microliter plugs into libraries of nanoliter droplets brings the advantages of both - previously separated - capabilities of droplet microfluidic systems, i.e. to

http://rcin.org.pl

perform systematic studies that require the elasticity of e.g. a micro-titer robot with the ability for high-throughput screens of reactions conducted in the confinement offered by pL and nL droplets. The main advantages of the technology reported here are: i) efficient and automated generation of distinct populations nL droplets, ii) possibility to avoid the necessity for additional fluorescent coding and decoding of the distinct populations, iii) minimum consumption of the samples, as the technique transforms the total volume of the microliter plugs into nanoliter daughter droplets.

We also demonstrated that the technology of droplet libraries can be used for the improvement of droplet digital PCR. Generation of the sequence of microliter plugs with gradually decreasing concentration of DNA, followed by transition into nanoliter droplets, off-chip thermocycling of the emulsion and high throughput interrogation of droplet fluorescence, allowed for quantification of very high DNA concentrations, that are beyond the capabilities of classical digital PCR.

http://rcin.org.pl

5. CONCLUSIONS AND PERSPECTIVES

http://rcin.org.pl

5.1 General conclusions

The dissertation presents automated micro-droplet technologies and passive systems capable of executing complex liquid handling protocols. With these two approaches we demonstrated the control over the chemical composition of micro-droplets ranging in volumes from just a few nano-liters to microliters e.g. generate gradations of chemical composition in droplets, actively control the chemical composition in each droplet over time, and perform liquid handling operations including splitting, merging and positioning of micro-drops on a chip. We used these technologies in academic demonstrations that provide unique experimental solutions for important challenges in microbiology and biochemistry such as: testing microbial susceptibility and providing tools for research of microbial adaptation, testing of activity of membrane proteins and quantification of molecules using digital assays. Application of microdroplet technology to this seemingly distant research problems provided not only the reduction of reagent consumption, but also brought added values such as massive parallelization, precise control of successive reaction steps and the influence of the interface by ensuring exceptional stability of bilayers and by preventing biofilm formation. We envisage that further research may comprise other possibilities of application of our microfluidic toolbox (automation, traps and droplet libraries) to microbial and biochemical assays presented here. Two feasible future perspectives may comprise i) use of the droplet libraries to measure the heterogeneity of bacterial populations at the level of single cells and ii) parallel formation and studies of lipid membranes in completely passive systems based on multiple Meter&Store modules.

Below we summarize and discuss the results presented in the dissertation.

5.2 Determination of MIC using passive microdroplet system based on the technology of passive traps

We have developed a microfluidics device that passively prepares a series of dilutions of a chemical compound and mixes them with portions of sample. The precise cutting, storing, merging and mixing of discrete microvolumes of liquid is hard-wired into the device's geometry by using hydrodynamic traps. Liquid handling does not require any syringe pumps or pressure control systems but it can be executed with a simple and commonly available manual pipette, which makes it

http://rcin.org.pl

suitable for in-field applications and as point-of-care device for third world countries.

Our system not only simplifies the operation of droplet microfluidic devices but also reduces the amount of labor needed to execute a common assay, and in comparison to standardized laboratory techniques it allows for reduction of the volume of the reagents and increases the precision of preparation of the dilution series. As an exemplary application of the device we demonstrate the determination of minimum inhibitory concentration (MIC) of ampicillin against *E. coli* ATCC 25922.

We believe that the device can be very useful for wide range of biological and chemical applications which require a fast yet precise preparation of assays and consequently mixing them with a target sample e.g. protein crystallization, formation of lipid membranes or cell assays, etc.

We used a gel imaging system equipped with fluorescence camera for optical fluorescence readout, however detections setup can be simplified, e.g. portable devices such as mobile phones can be used for the fluorescence measurement.[243] Another challenge is the limited precision of droplet metering that might be improved by more precise fabrication and use of lower flow rates of continuous phase for the operation of the device. Volumes we used here are quite large (metered droplet is ca. 450 nL) but they were determined by the characteristics of commercial pipettes. We envisage that dedicated pipettes with lower flow rates and relatively large volumes should be developed and used with systems such this presented here.

Our system comprises technical improvements that can be combined with other portable technologies such as SlipChips.[244,245] Liquids can be deposited and stored in wells and other method of flow generation can be used e.g. pumping lids[246] or oscillatory peristaltic pumps propelled by the vacuum.[247,248] Throughput of the technology can be improved by parallelization of the modules for gradient generation and use of multi-channel pipettes as a source of flow.

http://rcin.org.pl

5.3 Microdroplet chemostats

We have developed microdroplet chemostats for manipulating and monitoring the continuous growth of populations of bacteria over extended time intervals that were not previously attainable in microsystems. The system consists of an automated microfluidic network in which 10 input and output channels control the formation and composition of ~160 droplets in parallel and over several days. The microfluidic system enables the user to encapsulate cells and manipulate the composition of soluble chemical factors in each microdroplet independently over time. In this manuscript we characterize the dynamics of bacterial populations in microdroplet chemostats and study the response of bacteria to a range of antibiotic concentrations that are either stable or change predictably over time. These studies provide a foundational technology for highly parallel, long-term studies of microbial physiology, evolution, adaptation, and ecology.

Our approach complements previous chemostat and evolution studies by introducing a method for the parallel observation of bacteria growth in hundreds of individual microchemostats. Importantly, the operational complexity of the system is low and the user can rapidly adjust the phase of bacterial growth in experiments and the size and density of bacterial populations. These capabilities provide new opportunities for studying the genetic and phenotypic adaptation of bacteria and open a new window for the investigation of the process of microbial evolution.

Our technology is not free from limitations. An important hurdle will be the replacing of the material for the microfluidic system with a polymer that has better gas permeability, which will facilitate gas transport into microdroplets during their incubation and support aerobic growth of bacteria. The most commonly used material in this class of polymers is polydimethylsiloxane (PDMS). PDMS is frequently used to fabricate microfluidic systems in which organisms grow, however this polymer has a low elastic constant that prohibits precise fluidic operations on sequences of small droplets. Other polymeric materials should be implemented in order to meet these operational needs. Alternatively, better oxygenation can be achieved using fluorocarbon liquids as a continuous phase.

The system can be also improved by the introduction of the additional feedback control loop that will enable to adjust the parameters of media and reagent exchange of media ($f, \Delta V/V$) in response to measured rates of growth at user-

http://rcin.org.pl

defined time intervals. This capability will make it possible to perform long-term experiments on the trajectories of adaptation of microbial communities to environmental stresses.

Importantly, our system can be integrated with the technique for splitting large microliter droplets containing populations of bacteria into libraries of thousands of monodisperse and small picoliter droplets for further assays at the single cell level.[28,76,221] This could open new areas of study, including the measurement of distribution of fitness or gene expression in a microbial population exposed to changes in the chemical environment during cultivation.

5.4 Screening of model lipid membranes using droplet microfluidic systems

We have developed the microfluidic device that enables fast, simple and reproducible screening of the function of membrane proteins. The system automates i) formation of a lipid bilayer at the interface between a pair of nanoliter-sized aqueous droplets in oil, ii) exchange of one droplet to form a new bilayer between compartments comprising new chemistry, and iii) measurements of electrical current through single protein channels. Our work introduces a new microfluidic architecture: a trap designed to localize the droplets with respect to each other and with respect to the recording electrodes. We demonstrate formation of stable artificial lipid bilayers, incorporation of model protein into the bilayers and electrophysiological measurements.

The system might be further improved towards higher throughput. Direct protein expression in droplets using of *in vitro* transcription and translation (IVTT) may allow to avoid the steps of isolation, purification, freezing and dilution.[175] Alternatively, the implementation of on-chip dilution module[105] of protein stock will allow for more efficient screening protocols. The use of on-demand droplet screening techniques[55,56] may provide for fast screening of the composition of buffers and their effects on the function of protein pores. We hope that our device is a step towards the construction of systems for high-throughput *in vitro* tests of activity of membrane proteins, in which sequential screens might be conducted in massive parallel way.[178,249,250]

http://rcin.org.pl

5.5 Generation of droplet libraries and application of this technology for the improvement of droplet digital PCR

The system for generation of droplet libraries combines the control of flow of the input sequence of microliter droplets, the cross-flow of the oil through the FF-junction and the introduction of the third immiscible fluid for separation of droplet populations. The details of the architecture of the chip and of the automated protocol can be further improved e.g. for reduction of the volume of the continuous liquid in the final emulsions, for generation of smaller droplets (in a range of several picoliters) or for lower polydispersity of droplet within a single library, especially in case of solutions rich in surfactants, such as mixtures and oils used for PCR.

We envision that the technology of droplet libraries can be useful in a number of microfluidic assays, including single cell or single molecule screening. For example, in microbiology, this system makes it possible to perform systematic screens of the effect of various concentration of antibiotics or nutrients on the distribution of individual responses of cells in the population. This capability can be useful in e.g. isolation and characterization of rare cells or individuals with unique properties from heterogeneous populations, investigation of stochastic processes, such as bimodal gene expression or screening of activity of single enzyme molecules.[28,251]

In exemplary application, we showed that droplet libraries can be useful in digital PCR systems for extension of dynamic range of the DNA quantification. The technology facilitates integrated protocols for dilution and generation of multiple populations of monodisperse compartments and enables for precise determination of high concentration of nucleic acids. System can be used for quantification of other biologically relevant objects e.g. microorganisms[119,252] or proteins.[253,254] Detection of proteins using ELISA would require smaller droplets[253,254] because of linear amplification of the signal in the enzymatic reaction. Alternatively other strategies can be used, such as immuno-PCR[255] or other assays based on amplification of DNA attached to antibodies.[256–258]

http://rcin.org.pl

Literature

1 A. K. Yetisen, L. R. Volpatti, A. F. Coskun, S. Cho, E. Kamrani, H. Butt, A. Khademhosseini and S. H. Yun, *Lab Chip*, 2015, **15**, 3638–3660.

2 W. Aspray, *Ieee Ann. Hist. Comput.*, 1997, **19**, 4–15.

3 J. Warnock, C. Berry, M. H. Wood, L. Sigal, Y. Chan, G. Mayer, M. Mayo, Y. Chan, F. Malgioglio, G. Strevig, C. Nagarajan, S. Carey, G. Salem, F. Schroeder, H. H. Smith, D. Phan, R. H. Nigaglioni, T. Strach, M. M. Ziegler, N. Fricke, K. Lind, J. L. Neves, S. H. Rangarajan, J. P. Surprise, J. M. Isakson, J. Badar, D. Malone, D. W. Plass, A. Aipperspach, D. F. Wendel, R. M. Averill and R. Puri, *IBM J. Res. Dev.*, 2015, **59**, 15:1–15:15.

4 E. K. Sackmann, A. L. Fulton and D. J. Beebe, *Nature*, 2014, **507**, 181–189.

5 D. Harrison, K. Fluri, K. Seiler, Z. Fan, C. Effenhauser and A. Manz, *Science*, 1993, **261**, 895–897.

6 A. Persat, R. D. Chambers and J. G. Santiago, *Lab. Chip*, 2009, **9**, 2437–2453.

7 A. Persat, M. E. Suss and J. G. Santiago, *Lab. Chip*, 2009, **9**, 2454–2469.

8 T. Thorsen, S. J. Maerkl and S. R. Quake, *Science*, 2002, **298**, 580–584.

9 E. A. Ottesen, J. W. Hong, S. R. Quake and J. R. Leadbetter, *Science*, 2006, **314**, 1464–1467.

10 L. Warren, D. Bryder, I. L. Weissman and S. R. Quake, *Proc. Natl. Acad. Sci. U. S. A.*, 2006, **103**, 17807–17812.

11 C. Hansen and S. R. Quake, *Curr. Opin. Struct. Biol.*, 2003, **13**, 538–544.

12 C. L. Hansen, E. Skordalakes, J. M. Berger and S. R. Quake, *Proc. Natl. Acad. Sci. U. S. A.*, 2002, **99**, 16531–16536.

13 C. L. Hansen, M. O. A. Sommer and S. R. Quake, *Proc. Natl. Acad. Sci. U. S. A.*, 2004, **101**, 14431–14436.

14 P. Dalerba, T. Kalisky, D. Sahoo, P. S. Rajendran, M. E. Rothenberg, A. A. Leyrat, S. Sim, J. Okamoto, D. M. Johnston, D. Qian, M. Zabala, J. Bueno, N. F. Neff, J. Wang, A. A. Shelton, B. Visser, S. Hisamori, Y. Shimono, M. van de Wetering, H. Clevers, M. F. Clarke and S. R. Quake, *Nat. Biotechnol.*, 2011, **29**, 1120–1127.

15 T. Kalisky and S. R. Quake, *Nat. Methods*, 2011, **8**, 311–314.

16 H. C. Fan, J. Wang, A. Potanina and S. R. Quake, *Nat. Biotechnol.*, 2011, **29**, 51–57.

17 J. Wang, H. C. Fan, B. Behr and S. R. Quake, *Cell*, 2012, **150**, 402–412.

18 T. M. Squires and S. R. Quake, *Rev. Mod. Phys.*, 2005, **77**, 977–1026.

19 X. Casadevall i Solvas and A. deMello, *Chem. Commun.*, 2011, **47**, 1936–1942.

20 H. Song, D. L. Chen and R. F. Ismagilov, *Angew. Chem.-Int. Ed.*, 2006, **45**, 7336–7356.

21 F. K. Balagadde, L. C. You, C. L. Hansen, F. H. Arnold and S. R. Quake, *Science*, 2005, **309**, 137–140.

http://rcin.org.pl

22 K. J. Regehr, M. Domenech, J. T. Koepsel, K. C. Carver, S. J. Ellison-Zelski, W. L. Murphy, L. A. Schuler, E. T. Alarid and D. J. Beebe, *Lab. Chip*, 2009, **9**, 2132–2139.

23 S. Tay, J. J. Hughey, T. K. Lee, T. Lipniacki, S. R. Quake and M. W. Covert, *Nature*, 2010, **466**, 267–271.

24 R. A. Kellogg and S. Tay, *Cell*, 2015, **160**, 381–392.

25 R. A. Kellogg, R. Gomez-Sjoeberg, A. A. Leyrat and S. Tay, *Nat. Protoc.*, 2014, **9**, 1713–1726.

26 R. Gomez-Sjoeberg, A. A. Leyrat, D. M. Pirone, C. S. Chen and S. R. Quake, *Anal. Chem.*, 2007, **79**, 8557–8563.

27 L. Mazutis, J.-C. Baret, P. Treacy, Y. Skhiri, A. F. Araghi, M. Ryckelynck, V. Taly and A. D. Griffiths, *Lab. Chip*, 2009, **9**, 2902–2908.

28 J. J. Agresti, E. Antipov, A. R. Abate, K. Ahn, A. C. Rowat, J.-C. Baret, M. Marquez, A. M. Klibanov, A. D. Griffiths and D. A. Weitz, *Proc. Natl. Acad. Sci. U. S. A.*, 2010, **107**, 4004–4009.

29 A. Zinchenko, S. R. A. Devenish, B. Kintses, P.-Y. Colin, M. Fischechner and F. Hollfelder, *Anal. Chem.*, 2014, **86**, 2526–2533.

30 M. Fischlechner, Y. Schaerli, M. F. Mohamed, S. Patil, C. Abell and F. Hollfelder, *Nat. Chem.*, 2014, **6**, 791–796.

31 B. J. Hindson, K. D. Ness, D. A. Masquelier, P. Belgrader, N. J. Heredia, A. J. Makarewicz, I. J. Bright, M. Y. Lucero, A. L. Hiddessen, T. C. Legler, T. K. Kitano, M. R. Hodel, J. F. Petersen, P. W. Wyatt, E. R. Steenblock, P. H. Shah, L. J. Bousse, C. B. Troup, J. C. Mellen, D. K. Wittmann, N. G. Erndt, T. H. Cauley, R. T. Koehler, A. P. So, S. Dube, K. A. Rose, L. Montesclaros, S. Wang, D. P. Stumbo, S. P. Hodges, S. Romine, F. P. Milanovich, H. E. White, J. F. Regan, G. A. Karlin-Neumann, C. M. Hindson, S. Saxonov and B. W. Colston, *Anal. Chem.*, 2011, **83**, 8604–8610.

32 D. Pekin, Y. Skhiri, J.-C. Baret, D. Le Corre, L. Mazutis, C. Ben Salem, F. Millot, A. El Harrak, J. B. Hutchison, J. W. Larson, D. R. Link, P. Laurent-Puig, A. D. Griffiths and V. Taly, *Lab. Chip*, 2011, **11**, 2156–2166.

33 Q. Zhong, S. Bhattacharya, S. Kotsopoulos, J. Olson, V. Taly, A. D. Griffiths, D. R. Link and J. W. Larson, *Lab. Chip*, 2011, **11**, 2167–2174.

34 M. Baker, *Nat. Methods*, 2012, **9**, 541–544.

35 J. D. Tice, H. Song, A. D. Lyon and R. F. Ismagilov, *Langmuir*, 2003, **19**, 9127–9133.

36 J. D. Tice, A. D. Lyon and R. F. Ismagilov, *Anal. Chim. Acta*, 2004, **507**, 73–77.

37 G. Taylor, *Proc. R. Soc. Lond. Ser. -Math. Phys. Sci.*, 1953, **219**, 186–203.

38 R. Aris, *Proc. R. Soc. Lond. Ser. -Math. Phys. Sci.*, 1956, **235**, 67–77.

39 C. Holtze, A. C. Rowat, J. J. Agresti, J. B. Hutchison, F. E. Angile, C. H. J. Schmitz, S. Koster, H. Duan, K. J. Humphry, R. A. Scanga, J. S. Johnson, D. Pisignano and D. A. Weitz, *Lab. Chip*, 2008, **8**, 1632–1639.

40 T. Thorsen, R. W. Roberts, F. H. Arnold and S. R. Quake, *Phys. Rev. Lett.*, 2001, **86**, 4163–4166.

http://rcin.org.pl

41 S. L. Anna, N. Bontoux and H. A. Stone, *Appl. Phys. Lett.*, 2003, **82**, 364–366.

42 C. Cramer, P. Fischer and E. J. Windhab, *Chem. Eng. Sci.*, 2004, **59**, 3045–3058.

43 P. Guillot, A. Colin, A. S. Utada and A. Ajdari, *Phys. Rev. Lett.*, 2007, **99**, 104502.

44 A. S. Utada, A. Fernandez-Nieves, H. A. Stone and D. A. Weitz, *Phys. Rev. Lett.*, 2007, **99**, 094502.

45 G. F. Christopher, N. N. Noharuddin, J. A. Taylor and S. L. Anna, *Phys. Rev. E*, 2008, **78**, 036317.

46 P. Garstecki, M. J. Fuerstman, H. A. Stone and G. M. Whitesides, *Lab. Chip*, 2006, **6**, 437–446.

47 M. De Menech, P. Garstecki, F. Jousse and H. A. Stone, *J. Fluid Mech.*, 2008, **595**, 141–161.

48 V. van Steijn, C. R. Kleijn and M. T. Kreutzer, *Phys. Rev. Lett.*, 2009, **103**, 214501.

49 B. Dollet, W. van Hoeve, J.-P. Raven, P. Marmottant and M. Versluis, *Phys. Rev. Lett.*, 2008, **100**, 034504.

50 P. Garstecki, H. A. Stone and G. M. Whitesides, *Phys. Rev. Lett.*, 2005, **94**, 164501.

51 Z. Nie, M. Seo, S. Xu, P. C. Lewis, M. Mok, E. Kumacheva, G. M. Whitesides, P. Garstecki and H. A. Stone, *Microfluid. Nanofluidics*, 2008, **5**, 585–594.

52 N. Bremond, A. R. Thiam and J. Bibette, *Phys. Rev. Lett.*, 2008, **100**, 024501.

53 X. Niu, S. Gulati, J. B. Edel and A. J. deMello, *Lab. Chip*, 2008, **8**, 1837–1841.

54 K. Ahn, J. Agresti, H. Chong, M. Marquez and D. A. Weitz, *Appl. Phys. Lett.*, 2006, **88**, 264105.

55 K. Churski, P. Korczyk and P. Garstecki, *Lab. Chip*, 2010, **10**, 816–818.

56 K. Churski, T. S. Kaminski, S. Jakiela, W. Kamysz, W. Baranska-Rybak, D. B. Weibel and P. Garstecki, *Lab. Chip*, 2012, **12**, 1629–1637.

57 M. Sesen, T. Alan and A. Neild, *Lab. Chip*, 2014, **14**, 3325–3333.

58 C. N. Baroud, M. R. de Saint Vincent and J.-P. Delville, *Lab. Chip*, 2007, **7**, 1029–1033.

59 A. R. Abate and D. A. Weitz, *Lab. Chip*, 2011, **11**, 1911–1915.

60 A. C. Hatch, J. S. Fisher, A. R. Tovar, A. T. Hsieh, R. Lin, S. L. Pentoney, D. L. Yang and A. P. Lee, *Lab. Chip*, 2011, **11**, 3838–3845.

61 D. J. Eastburn, A. Sciambi and A. R. Abate, *Anal. Chem.*, 2013, **85**, 8016–8021.

62 H. Song and R. F. Ismagilov, *J. Am. Chem. Soc.*, 2003, **125**, 14613–14619.

63 L. Frenz, K. Blank, E. Brouzes and A. D. Griffiths, *Lab. Chip*, 2009, **9**, 1344–1348.

64 C. H. J. Schmitz, A. C. Rowat, S. Koester and D. A. Weitz, *Lab. Chip*, 2009, **9**, 44–49.

65 A. Huebner, D. Bratton, G. Whyte, M. Yang, A. J. deMello, C. Abell and F. Hollfelder, *Lab. Chip*, 2009, **9**, 692–698.

http://rcin.org.pl

66 Y. Bai, X. He, D. Liu, S. N. Patil, D. Bratton, A. Huebner, F. Hollfelder, C. Abell and W. T. S. Huck, *Lab. Chip*, 2010, **10**, 1281–1285.

67 L. Mazutis, A. F. Araghi, O. J. Miller, J.-C. Baret, L. Frenz, A. Janoshazi, V. Taly, B. J. Miller, J. B. Hutchison, D. Link, A. D. Griffiths and M. Ryckelynck, *Anal. Chem.*, 2009, **81**, 4813–4821.

68 D. R. Link, S. L. Anna, D. A. Weitz and H. A. Stone, *Phys. Rev. Lett.*, 2004, **92**, 054503.

69 S. Koester, F. E. Angile, H. Duan, J. J. Agresti, A. Wintner, C. Schmitz, A. C. Rowat, C. A. Merten, D. Pisignano, A. D. Griffiths and D. A. Weitz, *Lab. Chip*, 2008, **8**, 1110–1115.

70 L. Mazutis and A. D. Griffiths, *Appl. Phys. Lett.*, 2009, **95**, 204103.

71 A. R. Abate, J. J. Agresti and D. A. Weitz, *Appl. Phys. Lett.*, 2010, **96**, 203509.

72 M. Chabert and J.-L. Viovy, *Proc. Natl. Acad. Sci. U. S. A.*, 2008, **105**, 3191–3196.

73 J.-C. Baret, O. J. Miller, V. Taly, M. Ryckelynck, A. El-Harrak, L. Frenz, C. Rick, M. L. Samuels, J. B. Hutchison, J. J. Agresti, D. R. Link, D. A. Weitz and A. D. Griffiths, *Lab. Chip*, 2009, **9**, 1850–1858.

74 T. Franke, S. Braunmueller, L. Schmid, A. Wixforth and D. A. Weitz, *Lab. Chip*, 2010, **10**, 789–794.

75 J. Shemesh, A. Bransky, M. Khoury and S. Levenberg, *Biomed. Microdevices*, 2010, **12**, 907–914.

76 E. Brouzes, M. Medkova, N. Savenelli, D. Marran, M. Twardowski, J. B. Hutchison, J. M. Rothberg, D. R. Link, N. Perrimon and M. L. Samuels, *Proc. Natl. Acad. Sci. U. S. A.*, 2009, **106**, 14195–14200.

77 M. E. Dolega, S. Jakiela, M. Razew, A. Rakszewska, O. Cybulski and P. Garstecki, *Lab. Chip*, 2012, **12**, 4022–4025.

78 S. Makulska, S. Jakiela and P. Garstecki, *Lab. Chip*, 2013, **13**, 2796–2801.

79 S. E. Barnes, Z. T. Cygan, J. K. Yates, K. L. Beers and E. J. Amis, *Analyst*, 2006, **131**, 1027–1033.

80 G. Cristobal, L. Arbouet, F. Sarrazin, D. Talaga, J.-L. Bruneel, M. Joanicot and L. Servant, *Lab. Chip*, 2006, **6**, 1140–1146.

81 F. Sarrazin, J.-B. Salmon, D. Talaga and L. Servant, *Anal. Chem.*, 2008, **80**, 1689–1695.

82 D. Chen, W. Du, Y. Liu, W. Liu, A. Kuznetsov, F. E. Mendez, L. H. Philipson and R. F. Ismagilov, *Proc. Natl. Acad. Sci. U. S. A.*, 2008, **105**, 16843–16848.

83 J. Guzowski, P. M. Korczyk, S. Jakiela and P. Garstecki, *Lab. Chip*, 2011, **11**, 3593–3595.

84 G. T. Roman, M. Wang, K. N. Shultz, C. Jennings and R. T. Kennedy, *Anal. Chem.*, 2008, **80**, 8231–8238.

85 L. M. Fidalgo, G. Whyte, B. T. Ruotolo, J. L. P. Benesch, F. Stengel, C. Abell, C. V. Robinson and W. T. S. Huck, *Angew. Chem.-Int. Ed.*, 2009, **48**, 3665–3668.

http://rcin.org.pl

86 R. T. Kelly, J. S. Page, I. Marginean, K. Tang and R. D. Smith, *Angew. Chem.-Int. Ed.*, 2009, **48**, 6832–6835.

87 J. Pei, Q. Li, M. S. Lee, G. A. Valaskovic and R. T. Kennedy, *Anal. Chem.*, 2009, **81**, 6558–6561.

88 C. Luo, X. Yang, O. Fu, M. Sun, Q. Ouyang, Y. Chen and H. Ji, *Electrophoresis*, 2006, **27**, 1977–1983.

89 Z. Han, W. Li, Y. Huang and B. Zheng, *Anal. Chem.*, 2009, **81**, 5840–5845.

90 A. B. Theberge, G. Whyte and W. T. S. Huck, *Anal. Chem.*, 2010, **82**, 3449–3453.

91 N. Damean, L. F. Olguin, F. Hollfelder, C. Abell and W. T. S. Huck, *Lab. Chip*, 2009, **9**, 1707–1713.

92 J. Wegrzyn, A. Samborski, L. Reissig, P. M. Korczyk, S. Blonski and P. Garstecki, *Microfluid. Nanofluidics*, 2013, **14**, 235–245.

93 O. J. Miller, A. El Harrak, T. Mangeat, J.-C. Baret, L. Frenz, B. El Debs, E. Mayot, M. L. Samuels, E. K. Rooney, P. Dieu, M. Galvan, D. R. Link and A. D. Griffiths, *Proc. Natl. Acad. Sci. U. S. A.*, 2012, **109**, 378–383.

94 A. R. Abate, T. Hung, P. Mary, J. J. Agresti and D. A. Weitz, *Proc. Natl. Acad. Sci. U. S. A.*, 2010, **107**, 19163–19166.

95 F. Gielen, T. Buryska, L. Van Vliet, M. Butz, J. Damborsky, Z. Prokop and F. Hollfelder, *Anal. Chem.*, 2015, **87**, 624–632.

96 R. Dangla, E. Fradet, Y. Lopez and C. N. Baroud, *J. Phys. -Appl. Phys.*, 2013, **46**, 114003.

97 R. Dangla, S. C. Kayi and C. N. Baroud, *Proc. Natl. Acad. Sci. U. S. A.*, 2013, **110**, 853–858.

98 V. van Steijn, P. M. Korczyk, L. Derzsi, A. R. Abate, D. A. Weitz and P. Garstecki, *Biomicrofluidics*, 2013, **7**, 024108.

99 N. Mittal, C. Cohen, J. Bibette and N. Bremond, *Phys. Fluids*, 2014, **26**, 082109.

100 J. Clausell-Tormos, A. D. Griffiths and C. A. Merten, *Lab. Chip*, 2010, **10**, 1302–1307.

101 S. S. Bithi, W. S. Wang, M. Sun, J. Blawzdziewicz and S. A. Vanapalli, *Biomicrofluidics*, 2014, **8**, 034118.

102 M. Sun, S. S. Bithi and S. A. Vanapalli, *Lab. Chip*, 2011, **11**, 3949–3952.

103 P. Abbyad, R. Dangla, A. Alexandrou and C. N. Baroud, *Lab. Chip*, 2011, **11**, 813–821.

104 E. Fradet, P. Abbyad, M. H. Vos and C. N. Baroud, *Lab. Chip*, 2013, **13**, 4326–4330.

105 P. M. Korczyk, L. Derzsi, S. Jakiela and P. Garstecki, *Lab. Chip*, 2013, **13**, 4096–4102.

106 X. Niu, F. Gielen, J. B. Edel and A. J. deMello, *Nat. Chem.*, 2011, **3**, 437–442.

http://rcin.org.pl

107 M. Chabert, K. D. Dorfman, P. de Cremoux, J. Roeraade and J.-L. Viovy, *Anal. Chem.*, 2006, **78**, 7722–7728.

108 M. Sun and Q. Fang, *Lab. Chip*, 2010, **10**, 2864–2868.

109 L.-F. Cai, Y. Zhu, G.-S. Du and Q. Fang, *Anal. Chem.*, 2012, **84**, 446–452.

110 A. R. Abate, T. Hung, R. A. Sperling, P. Mary, A. Rotem, J. J. Agresti, M. A. Weiner and D. A. Weitz, *Lab. Chip*, 2013, **13**, 4864–4869.

111 R. Tewhey, J. B. Warner, M. Nakano, B. Libby, M. Medkova, P. H. David, S. K. Kotsopoulos, M. L. Samuels, J. B. Hutchison, J. W. Larson, E. J. Topol, M. P. Weiner, O. Harismendy, J. Olson, D. R. Link and K. A. Frazer, *Nat. Biotechnol.*, 2009, **27**, 1025–U94.

112 C. M. Hindson, J. R. Chevillet, H. A. Briggs, E. N. Gallichotte, I. K. Ruf, B. J. Hindson, R. L. Vessella and M. Tewari, *Nat. Methods*, 2013, **10**, 1003–1005.

113 M. M. Kiss, L. Ortoleva-Donnelly, N. R. Beer, J. Warner, C. G. Bailey, B. W. Colston, J. M. Rothberg, D. R. Link and J. H. Leamon, *Anal. Chem.*, 2008, **80**, 8975–8981.

114 J. E. Kreutz, T. Munson, T. Huynh, F. Shen, W. Du and R. F. Ismagilov, *Anal. Chem.*, 2011, **83**, 8158–8168.

115 F. Shen, B. Sun, J. E. Kreutz, E. K. Davydova, W. Du, P. L. Reddy, L. J. Joseph and R. F. Ismagilov, *J. Am. Chem. Soc.*, 2011, **133**, 17705–17712.

116 J. Lederberg, *J. Bacteriol.*, 1954, **68**, 258–259.

117 G. Nossal and J. Lederberg, *Nature*, 1958, **181**, 1419–1420.

118 J. Q. Boedicker, M. E. Vincent and R. F. Ismagilov, *Angew. Chem.-Int. Ed.*, 2009, **48**, 5908–5911.

119 J. Q. Boedicker, L. Li, T. R. Kline and R. F. Ismagilov, *Lab. Chip*, 2008, **8**, 1265–1272.

120 J. Cao, D. Kuersten, S. Schneider, A. Knauer, P. M. Guenther and J. M. Koehler, *Lab. Chip*, 2012, **12**, 474–484.

121 L. Baraban, F. Bertholle, M. L. M. Salverda, N. Bremond, P. Panizza, J. Baudry, J. A. G. M. de Visser and J. Bibette, *Lab. Chip*, 2011, **11**, 4057–4062.

122 S. P. Damodaran, S. Eberhard, L. Boitard, J. G. Rodriguez, Y. Wang, N. Bremond, J. Baudry, J. Bibette and F.-A. Wollman, *Plos One*, 2015, **10**, e0118987.

123 B. L. Wang, A. Ghaderi, H. Zhou, J. Agresti, D. A. Weitz, G. R. Fink and G. Stephanopoulos, *Nat. Biotechnol.*, 2014, **32**, 473–U194.

124 L. Boitard, D. Cottinet, C. Kleinschmitt, N. Bremond, J. Baudry, G. Yvert and J. Bibette, *Proc. Natl. Acad. Sci. U. S. A.*, 2012, **109**, 7181–7186.

125 M. Huang, Y. Bai, S. L. Sjostrom, B. M. Hallstrom, Z. Liu, D. Petranovic, M. Uhlen, H. N. Joensson, H. Andersson-Svahn and J. Nielsen, *Proc. Natl. Acad. Sci. U. S. A.*, 2015, **112**, E4689–96.

126 J. Clausell-Tormos, D. Lieber, J.-C. Baret, A. El-Harrak, O. J. Miller, L. Frenz, J. Blouwolff, K. J. Humphry, S. Koster, H. Duan, C. Holtze, D. A. Weitz, A. D. Griffiths and C. A. Merten, *Chem. Biol.*, 2008, **15**, 427–437.

http://rcin.org.pl

127 M. E. Vincent, W. Liu, E. B. Haney and R. F. Ismagilov, *Chem. Soc. Rev.*, 2010, **39**, 974–984.

128 M. Weitz, A. Mueckl, K. Kapsner, R. Berg, A. Meyer and F. C. Simmel, *J. Am. Chem. Soc.*, 2014, **136**, 72–75.

129 J. Shim, S. N. Patil, J. T. Hodgkinson, S. D. Bowden, D. R. Spring, M. Welch, W. T. S. Huck, F. Hollfelder and C. Abell, *Lab. Chip*, 2011, **11**, 1132–1137.

130 D. J. Collins, A. Neild, A. deMello, A.-Q. Liu and Y. Ai, *Lab. Chip*, 2015, **15**, 3439–3459.

131 E. W. M. Kemna, R. M. Schoeman, F. Wolbers, I. Vermes, D. A. Weitz and A. van den Berg, *Lab. Chip*, 2012, **12**, 2881–2887.

132 J. F. Edd, D. Di Carlo, K. J. Humphry, S. Koster, D. Irimia, D. A. Weitz and M. Toner, *Lab. Chip*, 2008, **8**, 1262–1264.

133 S. Huang, J. K. Srimani, A. J. Lee, Y. Zhang, A. J. Lopatkin, K. W. Leong and L. You, *Biomaterials*, 2015, **61**, 239–245.

134 M. Najah, R. Calbrix, I. P. Mahendra-Wijaya, T. Beneyton, A. D. Griffiths and A. Drevelle, *Chem. Biol.*, 2014, **21**, 1722–1732.

135 T. Beneyton, F. Coldren, J.-C. Baret, A. D. Griffiths and V. Taly, *Analyst*, 2014, **139**, 3314–3323.

136 D.-K. Kang, M. M. Ali, K. Zhang, S. S. Huang, E. Peterson, M. A. Digman, E. Gratton and W. Zhao, *Nat. Commun.*, 2014, **5**, 5427.

137 Clinical and Laboratory Standards Institute, 2012, **32**, 136.

138 I. Wiegand, K. Hilpert and R. E. W. Hancock, *Nat. Protoc.*, 2008, **3**, 163–175.

139 C. H. Chen, Y. Lu, M. L. Y. Sin, K. E. Mach, D. D. Zhang, V. Gau, J. C. Liao and P. K. Wong, *Anal. Chem.*, 2010, **82**, 1012–1019.

140 I. Peitz and R. van Leeuwen, *Lab. Chip*, 2010, **10**, 2944–2951.

141 Z. Hou, Y. An, K. Hjort, K. Hjort, L. Sandegren and Z. Wu, *Lab. Chip*, 2014, **14**, 3409–3418.

142 Y.-J. Eun, A. S. Utada, M. F. Copeland, S. Takeuchi and D. B. Weibel, *Acs Chem. Biol.*, 2011, **6**, 260–266.

143 N. J. Cira, J. Y. Ho, M. E. Dueck and D. B. Weibel, *Lab. Chip*, 2012, **12**, 1052–1059.

144 M. W. Toepke and D. J. Beebe, *Lab. Chip*, 2006, **6**, 1484–1486.

145 K. Leung, H. Zahn, T. Leaver, K. M. Konwar, N. W. Hanson, A. P. Page, C.-C. Lo, P. S. Chain, S. J. Hallam and C. L. Hansen, *Proc. Natl. Acad. Sci. U. S. A.*, 2012, **109**, 7665–7670.

146 T. U. Berendonk, C. M. Manaia, C. Merlin, D. Fatta-Kassinos, E. Cytryn, F. Walsh, H. Buergmann, H. Sorum, M. Norstrom, M.-N. Pons, N. Kreuzinger, P. Huovinen, S. Stefani, T. Schwartz, V. Kisand, F. Baquero and J. Luis Martinez, *Nat. Rev. Microbiol.*, 2015, **13**, 310–317.

147 A. Novick and L. Szilard, *Science*, 1950, **112**, 715–716.

http://rcin.org.pl

148 A. Novick and L. Szilard, *Proc. Natl. Acad. Sci. U. S. A.*, 1950, **36**, 708–719.

149 T. James, *Annu. Rev. Microbiol.*, 1961, **15**, 27–&.

150 N. Q. Balaban, J. Merrin, R. Chait, L. Kowalik and S. Leibler, *Science*, 2004, **305**, 1622–1625.

151 A. Groisman, C. Lobo, H. J. Cho, J. K. Campbell, Y. S. Dufour, A. M. Stevens and A. Levchenko, *Nat. Methods*, 2005, **2**, 685–689.

152 S. H. Au, S. C. C. Shih and A. R. Wheeler, *Biomed. Microdevices*, 2011, **13**, 41–50.

153 U. Lehnert, Y. Xia, T. E. Royce, C. S. Goh, Y. Liu, A. Senes, H. Y. Yu, Z. L. Zhang, D. M. Engelman and M. Gerstein, *Q. Rev. Biophys.*, 2004, **37**, 121–146.

154 F. M. Ashcroft, *Nature*, 2006, **440**, 440–447.

155 O. Hamill, A. Marty, E. Neher, B. Sakmann and F. Sigworth, *Pflugers Arch.-Eur. J. Physiol.*, 1981, **391**, 85–100.

156 E. Neher, B. Sakmann and J. Steinbach, *Pflugers Arch.-Eur. J. Physiol.*, 1978, **375**, 219–228.

157 T. Gutsmann, T. Heimburg, U. Keyser, K. R. Mahendran and M. Winterhalter, *Nat. Protoc.*, 2015, **10**, 188–198.

158 J. L. Gornall, K. R. Mahendran, O. J. Pambos, L. J. Steinbock, O. Otto, C. Chimerel, M. Winterhalter and U. F. Keyser, *Nano Lett.*, 2011, **11**, 3334–3340.

159 B. Sakmann and E. Neher, *Annu. Rev. Physiol.*, 1984, **46**, 455–472.

160 F. Sigworth and E. Neher, *Nature*, 1980, **287**, 447–449.

161 S. Stoelzle, A. Obergrussberger, A. Brueggemann, C. Haarmann, M. George, R. Kettenhofen and N. Fertig, *Front. Pharmacol.*, 2011, **2**, UNSP 76.

162 A. Bruggemann, C. Haarmann, T. Stengel, M. Vogel, J. Steindl, M. Mueller, J. Stiehler, M. George and N. Fertig, *Biophys. J.*, 2014, **106**, 132A–132A.

163 H. Bayley, B. Cronin, A. Heron, M. A. Holden, W. L. Hwang, R. Syeda, J. Thompson and M. Wallace, *Mol. Biosyst.*, 2008, **4**, 1191–1208.

164 T. J. Dale, C. Townsend, E. C. Hollands and D. J. Trezise, *Mol. Biosyst.*, 2007, **3**, 714–722.

165 M. Montal, *Methods Enzymol.*, 1974, **32**, 545–54.

166 M. Montal and P. Mueller, *Proc. Natl. Acad. Sci.*, 1972, **69**, 3561–3566.

167 P. Mueller, D. Rudin, H. Tien and W. Wescott, *Nature*, 1962, **194**, 979–&.

168 E. T. Castellana and P. S. Cremer, *Surf. Sci. Rep.*, 2006, **61**, 429–444.

169 L. K. Tamm and H. M. McConnell, *Biophys. J.*, 1985, **47**, 105–113.

170 G. J. Schutz, H. Schindler and T. Schmidt, *Biophys. J.*, 1997, **73**, 1073–1080.

171 L. Tsofina, E. Liberman and A. Babakov, *Nature*, 1966, **212**, 681–&.

172 M. A. Holden, D. Needham and H. Bayley, *J. Am. Chem. Soc.*, 2007, **129**, 8650–8655.

http://rcin.org.pl

173 W. L. Hwang, M. A. Holden, S. White and H. Bayley, *J. Am. Chem. Soc.*, 2007, **129**, 11854–11864.

174 K. Funakoshi, H. Suzuki and S. Takeuchi, *Anal. Chem.*, 2006, **78**, 8169–8174.

175 R. Syeda, M. A. Holden, W. L. Hwang and H. Bayley, *J. Am. Chem. Soc.*, 2008, **130**, 15543–15548.

176 L. Z. Song, M. R. Hobaugh, C. Shustak, S. Cheley, H. Bayley and J. E. Gouaux, *Science*, 1996, **274**, 1859–1866.

177 S. Aghdaei, M. E. Sandison, M. Zagnoni, N. G. Green and H. Morgan, *Lab. Chip*, 2008, **8**, 1617–1620.

178 R. Kawano, Y. Tsuji, K. Sato, T. Osaki, K. Kamiya, M. Hirano, T. Ide, N. Miki and S. Takeuchi, *Sci Rep*, 2013, **3**.

179 S. A. Acharya, A. Portman, C. S. Salazar and J. J. Schmidt, *Sci Rep*, 2013, **3**.

180 A. M. El-Arabi, C. S. Salazar and J. J. Schmidt, *Lab. Chip*, 2012, **12**, 2409–2413.

181 S. A. Portonovo, C. S. Salazar and J. J. Schmidt, *Biomed. Microdevices*, 2013, **15**, 255–259.

182 J L Poulos and S A Portonovo and H Bang and J J Schmidt, *J. Phys. Condens. Matter*, 2010, **22**, 454105.

183 M. Lein, J. Huang and M. A. Holden, *Lab. Chip*, 2013, **13**, 2749–2753.

184 N. Malmstadt, M. A. Nash, R. F. Purnell and J. J. Schmidt, *Nano Lett.*, 2006, **6**, 1961–1965.

185 J. L. Poulos, W. C. Nelson, T.-J. Jeon, C.-J. 'CJ' Kim and J. J. Schmidt, *Appl. Phys. Lett.*, 2009, **95**, -.

186 S. A. Sarles and D. J. Leo, *Lab. Chip*, 2010, **10**, 710–717.

187 V. C. Stimberg, J. G. Bomer, I. van Uitert, A. van den Berg and S. Le Gac, *Small*, 2013, **9**, 1076–1085.

188 M. Takinoue, H. Onoe and S. Takeuchi, *Small*, 2010, **6**, 2374–2377.

189 T. Thapliyal, J. L. Poulos and J. J. Schmidt, *Biosens. Bioelectron.*, 2011, **26**, 2651–2654.

190 Y. Tsuji, R. Kawano, T. Osaki, K. Kamiya, N. Miki and S. Takeuchi, *Anal. Chem.*, 2013, **85**, 10913–10919.

191 M. Zagnoni, M. E. Sandison, P. Marius, A. G. Lee and H. Morgan, *Lab. Chip*, 2007, **7**, 1176–1183.

192 M. Zagnoni, M. E. Sandison and H. Morgan, *Biosens. Bioelectron.*, 2009, **24**, 1235–1240.

193 M. Zagnoni, M. E. Sandison, P. Marius and H. Morgan, *Anal. Bioanal. Chem.*, 2009, **393**, 1601–1605.

194 O. K. Castell, J. Berridge and M. I. Wallace, *Angew. Chem.-Int. Ed.*, 2012, **51**, 3134–3138.

195 Y. Elani, A. J. deMello, X. Niu and O. Ces, *Lab. Chip*, 2012, **12**, 3514–3520.

http://rcin.org.pl

241 M. J. Fuerstman, P. Garstecki and G. M. Whitesides, *Science*, 2007, **315**, 828–832.

242 S. Jakiela, S. Makulska, P. M. Korczyk and P. Garstecki, *Lab. Chip*, 2011, **11**, 3603–3608.

243 H. Zhu, O. Yaglidere, T.-W. Su, D. Tseng and A. Ozcan, *Lab. Chip*, 2011, **11**, 315–322.

244 L. Li, W. Du and R. F. Ismagilov, *J. Am. Chem. Soc.*, 2010, **132**, 112–119.

245 W. Du, L. Li, K. P. Nichols and R. F. Ismagilov, *Lab. Chip*, 2009, **9**, 2286–2292.

246 S. Begolo, D. V. Zhukov, D. A. Selck, L. Li and R. F. Ismagilov, *Lab. Chip*, 2014, **14**, 4616–4628.

247 P. N. Duncan, T. V. Nguyen and E. E. Hui, *Proc. Natl. Acad. Sci. U. S. A.*, 2013, **110**, 18104–18109.

248 M. Rhee and M. A. Burns, *Lab. Chip*, 2009, **9**, 3131–3143.

249 B. Le Pioufle, H. Suzuki, K. V. Tabata, H. Noji and S. Takeuchi, *Anal. Chem.*, 2007, **80**, 328–332.

250 B. Lu, G. Kocharyan and J. J. Schmidt, *Biotechnol. J.*, 2014, **9**, 446–451.

251 B. M. Paegel and G. F. Joyce, *Chem. Biol.*, 2010, **17**, 717–724.

252 M. Najah, A. D. Griffiths and M. Ryckelynck, *Anal. Chem.*, 2012, **84**, 1202–1209.

253 J. Shim, R. T. Ranasinghe, C. A. Smith, S. M. Ibrahim, F. Hollfelder, W. T. S. Huck, D. Klenerman and C. Abell, *Acs Nano*, 2013, **7**, 5955–5964.

254 H. N. Joensson, M. L. Samuels, E. R. Brouzes, M. Medkova, M. Uhlen, D. R. Link and H. Andersson-Svahn, *Angew. Chem.-Int. Ed.*, 2009, **48**, 2518–2521.

255 M. Adler, R. Wacker and C. M. Niemeyer, *Analyst*, 2008, **133**, 702–718.

256 S. Fredriksson, M. Gullberg, J. Jarvius, C. Olsson, K. Pietras, S. M. Gustafsdottir, A. Ostman and U. Landegren, *Nat. Biotechnol.*, 2002, **20**, 473–477.

257 S. Fredriksson, W. Dixon, H. Ji, A. C. Koong, M. Mindrinos and R. W. Davis, *Nat. Methods*, 2007, **4**, 327–329.

258 E. Assarsson, M. Lundberg, G. Holmquist, J. Bjoerkesten, S. B. Thorsen, D. Ekman, A. Eriksson, E. R. Dickens, S. Ohlsson, G. Edfeldt, A.-C. Andersson, P. Lindstedt, J. Stenvang, M. Gullberg and S. Fredriksson, *Plos One*, 2014, **9**, e95192.

B. 484/16

Instytut Chemii Fizycznej PAN BIBLIOTEKA

http://rcin.org.pl

218 P. Sykes, S. Neoh, M. Brisco, E. Hughes, J. Condon and A. Morley, *Biotechniques*, 1992, **13**, 444–449.

219 K. A. Heyries, C. Tropini, M. VanInsberghe, C. Doolin, O. I. Petriv, A. Singhal, K. Leung, C. B. Hughesman and C. L. Hansen, *Nat. Methods*, 2011, **8**, 649–U64.

220 R. A. White, S. R. Quake and K. Curr, *J. Virol. Methods*, 2012, **179**, 45–50.

221 J.-C. Baret, Y. Beck, I. Billas-Massobrio, D. Moras and A. D. Griffiths, *Chem. Biol.*, 2010, **17**, 528–536.

222 S. Dube, J. Qin and R. Ramakrishnan, *Plos One*, 2008, **3**, e2876.

223 A. S. Whale, J. F. Huggett, S. Cowen, V. Speirs, J. Shaw, S. Ellison, C. A. Foy and D. J. Scott, *Nucleic Acids Res.*, 2012, **40**, e82.

224 J. N. Lee, C. Park and G. M. Whitesides, *Anal. Chem.*, 2003, **75**, 6544–6554.

225 S. Cheley, L.-Q. Gu and H. Bayley, *Chem. Biol.*, 2002, **9**, 829–838.

226 T. Szymborski, P. M. Korczyk, R. Holyst and P. Garstecki, *Appl. Phys. Lett.*, 2011, **99**, 094101.

227 W. Li, E. W. K. Young, M. Seo, Z. Nie, P. Garstecki, C. A. Simmons and E. Kumacheva, *Soft Matter*, 2008, **4**, 258–262.

228 H. Song, M. R. Bringer, J. D. Tice, C. J. Gerdts and R. F. Ismagilov, *Appl. Phys. Lett.*, 2003, **83**, 4664–4666.

229 *http://www.eppendorf.com/int/index.php?l=211&pb=307f5fcfc3cfee65&action=products&contentid=1&catalognode=67026&productpage=3*.

230 A. M. Skelley and J. Voldman, *Lab. Chip*, 2008, **8**, 1733–1737.

231 C. Lochovsky, S. Yasotharan and A. Guenther, *Lab. Chip*, 2012, **12**, 595–601.

232 J. Monod, *Ann. Inst. Pasteur (Paris)*, 1950, **79**, 390–410.

233 E. Toprak, A. Veres, J.-B. Michel, R. Chait, D. L. Hartl and R. Kishony, *Nat. Genet.*, 2012, **44**, 101–U140.

234 O. Pongs, R. Bald and V. Erdmann, *Proc. Natl. Acad. Sci. U. S. A.*, 1973, **70**, 2229–2233.

235 H. H. Lee, M. N. Molla, C. R. Cantor and J. J. Collins, *Nature*, 2010, **467**, 82–U113.

236 J. R. Moffitt, J. B. Lee and P. Cluzel, *Lab. Chip*, 2012, **12**, 1487–1494.

237 L. C. M. Gross, A. J. Heron, S. C. Baca and M. I. Wallace, *Langmuir*, 2011, **27**, 14335–14342.

238 N. Rojko, B. Cronin, J. S. H. Danial, M. A. B. Baker, G. Anderluh and M. I. Wallace, *Biophys. J.*, 2014, **106**, 1630–1637.

239 P. R. Debski, K. Gewartowski, M. Sulima, T. S. Kaminski and P. Garstecki, *Anal. Chem.*, 2015, **87**, 8203–8209.

240 M. J. Fuerstman, A. Lai, M. E. Thurlow, S. S. Shevkoplyas, H. A. Stone and G. M. Whitesides, *Lab. Chip*, 2007, **7**, 1479–1489.

http://rcin.org.pl

241 M. J. Fuerstman, P. Garstecki and G. M. Whitesides, *Science*, 2007, **315**, 828–832.

242 S. Jakiela, S. Makulska, P. M. Korczyk and P. Garstecki, *Lab. Chip*, 2011, **11**, 3603–3608.

243 H. Zhu, O. Yaglidere, T.-W. Su, D. Tseng and A. Ozcan, *Lab. Chip*, 2011, **11**, 315–322.

244 L. Li, W. Du and R. F. Ismagilov, *J. Am. Chem. Soc.*, 2010, **132**, 112–119.

245 W. Du, L. Li, K. P. Nichols and R. F. Ismagilov, *Lab. Chip*, 2009, **9**, 2286–2292.

246 S. Begolo, D. V. Zhukov, D. A. Selck, L. Li and R. F. Ismagilov, *Lab. Chip*, 2014, **14**, 4616–4628.

247 P. N. Duncan, T. V. Nguyen and E. E. Hui, *Proc. Natl. Acad. Sci. U. S. A.*, 2013, **110**, 18104–18109.

248 M. Rhee and M. A. Burns, *Lab. Chip*, 2009, **9**, 3131–3143.

249 B. Le Pioufle, H. Suzuki, K. V. Tabata, H. Noji and S. Takeuchi, *Anal. Chem.*, 2007, **80**, 328–332.

250 B. Lu, G. Kocharyan and J. J. Schmidt, *Biotechnol. J.*, 2014, **9**, 446–451.

251 B. M. Paegel and G. F. Joyce, *Chem. Biol.*, 2010, **17**, 717–724.

252 M. Najah, A. D. Griffiths and M. Ryckelynck, *Anal. Chem.*, 2012, **84**, 1202–1209.

253 J. Shim, R. T. Ranasinghe, C. A. Smith, S. M. Ibrahim, F. Hollfelder, W. T. S. Huck, D. Klenerman and C. Abell, *Acs Nano*, 2013, **7**, 5955–5964.

254 H. N. Joensson, M. L. Samuels, E. R. Brouzes, M. Medkova, M. Uhlen, D. R. Link and H. Andersson-Svahn, *Angew. Chem.-Int. Ed.*, 2009, **48**, 2518–2521.

255 M. Adler, R. Wacker and C. M. Niemeyer, *Analyst*, 2008, **133**, 702–718.

256 S. Fredriksson, M. Gullberg, J. Jarvius, C. Olsson, K. Pietras, S. M. Gustafsdottir, A. Ostman and U. Landegren, *Nat. Biotechnol.*, 2002, **20**, 473–477.

257 S. Fredriksson, W. Dixon, H. Ji, A. C. Koong, M. Mindrinos and R. W. Davis, *Nat. Methods*, 2007, **4**, 327–329.

258 E. Assarsson, M. Lundberg, G. Holmquist, J. Bjoerkesten, S. B. Thorsen, D. Ekman, A. Eriksson, E. R. Dickens, S. Ohlsson, G. Edfeldt, A.-C. Andersson, P. Lindstedt, J. Stenvang, M. Gullberg and S. Fredriksson, *Plos One*, 2014, **9**, e95192.

B. 484/16

Instytut Chemii Fizycznej PAN BIBLIOTEKA

http://rcin.org.pl

Biblioteka Instytutu Chemii Fizycznej PAN
F-B.484/16
90000000192784

http://rcin.org.pl